NORTHWESTERN UNIVERSITY

Bioadhesion of Mussels and Geckos: Molecular Mechanics, Surface Chemistry, and Nanoadhesives

A DISSERTATION

SUBMITTED TO THE GRADUATE SCHOOL
IN PARTIAL FULFILLMENT OF THE REQUIREMENTS

for the degree

DOCTOR OF PHILOSOPHY

Field of Biomedical Engineering

By

Haeshin Lee

EVANSTON, ILLINOIS

June 2008

ABSTRACT

Bioadhesion of Mussels and Geckos: Molecular Mechanics, Surface Chemistry, and Nanoadhesives

Haeshin Lee

The adhesive strategies of living creatures are diverse, ranging from temporary to permanent adhesions with various functions such as locomotion, self-defense, communication, colony formation, and so on. The classic example of temporary adhesion is the gecko, which is known for its ability to walk along vertical and even inverted surfaces; this remarkable adhesion arises from the interfacial weak interactions of van der Waals and capillary forces. In contrast, a celerbrated example of permanent adhesion is found in marine mussels which secrete protein adhesives that function in aqueous environments without mechanical failure against turbulent conditions on the seashore. In addition, mussel adhesives stick to virtually all inorganic and organic surfaces. However, most commonly used man-made adhesives lack such unique adhesion properties compared to their natural counterparts. For example, many commercial adhesives quickly lose their adhesive strength when exposed to solvents, particularly water.

The first part of this thesis focused on adhesion mechanics of mussels at a single-molecule level, in which the adhesive molecule showed surprisingly strong yet reversible adhesion on inorganic surfaces but exhibited irreversible covalent bond formation on organic surfaces. Strong and reversible adhesion on mucin surfaces was found, indicating potential application for drug delivery via mucus layers. Next, inspired by the mussel's versatile adhesion on a wide variety of material surfaces, a material-independent surface modification chemistry called 'polydopamine coating' is described. This concept was subsequently adapted to develop a

surface-independent polymeric primer for layer-by-layer assembly of multifunctional coatings. Finally, a new bio-hybrid adhesive ‘geckel’ was developed by the functional combination of adhesion strategies of geckos and mussels.

The new bio-inspired adhesive and material-independent surface chemistry can revolutionize the research areas such as medical devices, adhesives, and diagnostics, nanotechnology, biointerface, and catalysis.

To my wife, Wanjeon Lim,
without her endless and selfless support
this could not have been achieved

"A patient man has great understanding,
but a quick-tempered man displays folly"
Proverbs 14:29

ACKNOWLEDGEMENTS

My Ph.D. degree cannot be accomplished without advices and discussions with my thesis advisor, other faculty members and research colleagues (post-docs, graduate students, and the staff at a variety of user facilities). Reflecting my science-driven, five-year 'sticky' life at the Evanston campus, Northwestern University won't be forgettable forever.

First of all, I thank my thesis advisor Professor Phillip B. Messersmith who is always a pleasant scientist and willing to discuss any topics reminiscent of not only science but also life. I greatly appreciate him first from the bottom of my heart. As a graduate student, I have learned a lot about bio/nano-materials, fabrications, a variety of analytical tools, communication skills, and the most important one, 'motivation' which has been the endless source for new ideas. I am also thankful for giving me opportunities to attend many conferences; Material Research Society Meeting at San Francisco and Boston, Society for Biomaterials Meeting at Memphis, ACS annual meeting, Gordon Research Conferences at Switzerland and Newport, Drug Delivery Symposium at Utah, Self-assembly Meeting at Crete (thank Ms. Sherri Messersmith for everything you did for me at Crete and Athens!!) etc. From those meetings, I have been able to understand recent trends of science that also served as invaluable sources for new ideas.

I appreciate my thesis committee members, Professor Norbert F. Scherer, Kenneth Shull, David Kelso. Without their support, many challenging tasks such as single-molecule experiments and contact mechanics cannot be performed. In particular, I thank Prof. Scherer and his wife, Dr. Susan Choi for the generous thanksgiving invitations and laboratory lunch meetings, Shull for stimulating motivation to study contact mechanics, and Kelso for his warm welcome and insightful comments from his experiences.

I thank Professor Tae Gwan Park in Department of Biological Science at KAIST whom I first met in November 1996 (undergraduate senior year). He re-directed my life direction to academia at the time when I had no vision for my future life. I appreciate his mentoring in many aspects not only when I was in Korea but also currently in Evanston. This recalls Mr. Yuhan Lee, a graduate student in his research group who called himself as 'a visiting scholar' (technically his title should be a 'visiting student') which confused Professor Chad Mirkin, inviting Yuhan as a guest for a dinner after the International Nanotechnology Symposium in 2006 (funny). I wish the best in Yuhan's academic carrier.

I would like to thank my former and current laboratory members. First, Dr. Jeffrey L. Dalsin for his supports of all aspects of experiments and laboratory life, Dr. Bruce P. Lee for his patient teaching on synthesis of polymeric materials and generous donation of many priceless chemicals for my experiments (and the cookies!!), and Dr. Marsha Ritter-Jones for her insightful comments upon my questions. I am very grateful to my same year graduate colleague, Andrea R. Statz whom I have shared lots of time with. My graduate life would have been much more difficult without her help. Thank you for everything particularly for snack and sailing!! Excellent post-docs in Messersmith group deepened my scientific knowledge; I thank Dr. Bi-Huang Hu, Zhongqiang Liu, Rico Gunawan, Simonida Grubjesic, Xiaowu Fan, Kanika Chawla, Hermona K. Pandya, Jing Su, and Trung Nguyen for their discussions and guidance as academic seniors. I am glad to spend much time with graduate students joined after me: Lesley Meade, Carrie Brubaker, Dominic Fullenkamp, Kvar Black, and Hyun-Ok Ham who are all very talented and ready to take risks for studying the unexplored world of science. Also, it was very lucky for me to work with two excellent undergraduate students, Junsung Rho and Kyle Holmberg. They

quickly adapted to the lab environment and atmosphere and performed their own projects independently. I would like to say best wishes for their future carriers.

The essential part of graduate research is collaboration. It is due in part to the interdisciplinary nature of most current projects. Meeting good collaborators is important which can determine when the day for one's final exam is going to be. In this sense, I have been very lucky to work with Professor William M. Miller and graduate student Shara M. Dellatore. Their hematopoietic research was the breakthrough when I had trouble finding a biological model for the application of newly developed dopamine surface chemistry. Thank you very much! I tremendously enjoyed performing research with you. In addition, NUANCE staff scientists are my excellent collaborators: Dr. Xinqi Chen for XPS and ToF SIMS, Dr. Gajendra Shekhawat for AFM, Ben Myers for e-beam lithography, and Dr. Shuyou Li for TEM, and I would like to thank Dr. William Russin at Biological Imaging Facility (NU) for general advice for imaging techniques. Furthermore, Dr. Justin Jureller in NanoBio facility at The University of Chicago, Institute for Biological Dynamics was my great teacher regarding various imaging techniques.

I am grateful to my friends and the former employer in academia for their consistent advices upon my questions. They did not hesitate to give their valuable opinions about my projects and any topics; Professor Wouter D. Hoff who was my first employer in the US (currently Oklahoma State University) and who taught me a lot about protein biophysics. Thank you for giving me the opportunity for biophysical research. Professor Rongchao Jin at Department of Chemistry, Carnegie Melon University; Professor Sungho Park at Department of Chemistry, SungKyunKwan University (Korea); and Dr. Sung-Wook Chung at Lawrence Livermore National Laboratory gave me advices for nanotechnology aspects, and Dr. Jason Ming Zhao at Johns Hopkins University who taught me AFM and provided many insightful

comments. Thank you Ming!! Dr. Duhee Bang in Department of Genetics at Harvard University, Professor Jihoon Jeong at SungKyunKwan University broadened my knowledge for polymeric gene delivery and synthetic biology respectively, and finally Dr. Seung-Hee Yoo at Department of Neurobiology and Physiology, center for functional genomics, Northwestern University, resumed my interest in pure biological problems particularly for circadian rhythm (thank you for the lunch, dinner, and your time).

Finally, I would like to dedicate this thesis to my wife, Wanjeon Lim, and parents - particularly to my father who passed away when I was a second-year student. Without their endless help (especially for my wife and mother), this thesis could have not been achieved. I would like to say ‘thank you’ from the bottom of my heart.

TABLE OF CONTENTS

List of Figures

List of Tables

LIST OF ABBREVIATIONS AND SYMBOLS

AFM	atomic force microscopy
DOPA	3,4-dihydroxyphenylalanine
DMA	dopamine methacrylamide
ELM	spectroscopic ellipsometry
HA	hyaluronic acid
HA-C	hyaluronic acid-catechol
HAp	hydroxyapatite
LB	langmuir-blodgett
LbL	layer-by-layer
MAP	mussel adhesive protein
MEA	methoxy ethylacrylate
Mefp	*Mytilus edulis* foot protein
NTA	N-nitro-triacetic acid
mPEG	methoxy–poly(ethylene glycol)
OEG	oligo(ethylene glycol)
OWLS	optical waveguide lightmode spectroscopy
PDMS	poly(dimethylsiloxane)
PEG	poly(ethylene glycol)
PEI	polyethylenimine
PEI-C	polyethylenimine-catechol
PEEK	poly(etheretherketone)
PBS	phosphate-buffered saline
PS	poly(styrene)
PET	poly(ethylene terephthalate)
PE	poly(ethylene)
PC	poly(carbonate)
PTFE	poly(tetrafluoroethylene)
PU	poly(urethane)
PMMA	poly(methyl metacrylate)
PHEMA	poly(2-hydroxyethyl methylacrylate)
PMEA	poly(2-methoxyethyl acrylate)
PPO	poly(propylene oxide)
SAM	self-assembled monolayer
TOF-SIMS	time-of-flight secondary ion mass spectrometry
XPS	x-ray photoelectron spectroscopy

Chapter 1: Introduction

1.1 Motivation and Objective

Living creatures rely on adhesion using many different types of adhesives. During the last decade, scientists and engineers from various disciplines of biology, physics, materials, and chemistry have been studying the remarkable features of biological adhesion. Beetles, flies, frogs, and larger animals such as lizards and geckos utilize temporary (i.e. reversible) adhesion for locomotion in which their feet rapidly attach to and detach from surfaces repeatedly throughout life (*1, 2*). This type of reversible adhesion is different from the conventional pressure-sensitive adhesives, which can stick to surfaces by applying slight pressure, but which are difficult to reattach because of contamination or cohesive failure.

A great challenge for most adhesives is to achieve strong interfacial adhesion in the presence of water. In general, intermolecular forces in adhesion have an inverse relationship between surface energy of opposing dissimilar materials and the dielectric constant of a surrounding medium. For exmaple the dielectric constant in vacuum is about one but is dramatically increased to ~ 80 in water(*3*). Interestingly, mussels, one of nature's promiscuous

marine foulers, remain strongly attached on a wide variety of substrates under water. In contrast to temporary adhesion of insects and geckos, the mussel adhesion is considered to be a permanent and is achieved by the sequential events of secretion followed by rapid curing of the secreted mussel adhesive proteins.

Despite recent extensive studies of mussels and geckos, many aspects of these natural bioadhesives remain poorly understood; the molecular ariginds of adhesion (i.e. single adhesive molecule and single nanostructure) are largely unknown, the chemical and molecular factors that give rise to substrate-independent adhesion of mussels remain an open question, and rational design followed by fabrication and/or synthesis of biomimetic adhesives is difficult. This thesis has tried to address some of these fundamental questions, and further attempts to exploit an enhanced understanding of these natural bioadhesives toward development of novel biomimetic adhesives.

1.2 Thesis Outline

The thesis is composed of five major parts: (1) an introduction of bioadhesive strategies of mussels and geckos and a brief review of mechanochemistry (chapter 2), (2) measurement of mussel adhesive force at a single-molecule level on inorganic and organic surfaces (chapter 3), (3) development of two new surface chemistries that can be applied to any type of material surface: polydopamine coating (chapter 4) and surface-independent layer-by-layer assembly (chapter 5), (4) development of a new hybrid adhesive called ‘Geckel’ inspired by the adhesive strategies of geckos and mussels (chapter 6), and finally (5) a summary and discussions of future directions based on the achievements in this thesis (chapter 7).

1.3 Specific Aims

The work described in great detail from chapter 3 to 6 is based on the following three broadly defined specific aims.

Specific Aim 1: Address the adhesion mechanism of mussel adhesive proteins (MAPs).

Hypothesis 1: Atomic force microscopy can probe binding strength of the adhesion molecule at a single-molecule level.

Hypothesis 2: The measured adhesion strength can explain the adhesion mechanisms of mussel adhesion as a function of substrates.

Specific Aim 2: Development of new surface chemistry that can tailor properties of virtually all types of material surfaces.

Hypothesis 3: The characteristic amino acid motif of DOPA-lysine found in the specialized mussel adhesive proteins called Mefp-5 (*Mytilus edulis* foot protein-5) might be critical for versatile surface adhesion.

Hypothesis 4: Molecular building blocks mimicking the chemical functionality of DOPA-Lys can modify virtually all types of materials.

Specific Aim 3: Development of a reversible hybrid adhesive that is inspired by gecko and mussel adhesion

Hypothesis 5: The dry adhesion mechanism of geckos can be combined with the wet adhesion strategy of mussels, resulting in a new reversible adhesive that performs under dry/wet conditions.

Chapter 2: Background

2.1 Mussel Adhesive Proteins

2.1.1 Mytilus edulis foot protein-1 (Mefp-1)

Mefp-1 is perhaps the most well studied protein among the MAP family. It has 75-80 repeats of a decapeptide with amino acid sequence of Ala-Lys-Pro-Ser-Tyr-Hyp-Hyp-Thr-DOPA-Lys (molecular weight = ~ 110 kDa), which was obtained by extensive tryptic digest (*4*). Further analysis revealed variations of post-translational modifications in the repetitive sequence. For example, some peptide fragments contain DOPA instead of tyrosine in fifth position and hydroxyproline in third position rather than proline (*5*). Nearly a decade after its discovery, another type of post-translational modification of proline, *trans*-2,3-*cis*-3,4-dihydroxyproline in sixth position was discovered in Mefp-1 (*6*). Therefore, the revised primary sequence of Mefp-1 decapeptide is N-Ala-Lys-Pro-Ser-Tyr-Hyp-**diHyp**-Thr-DOPA-Lys-C.

In contrast to the initial belief that Mefp-1's biological role was as a potent adhesive protein, immunohistochemistry results using antibody raised against recombinant *Dreissena*

polymorpha foot protein-1 (Dpfp-1), a close homologue of Mefp-1, showed unexpected tissue distributions of Mefp-1. The antibody specifically bound to nascent threads not adhesive plaques (Figure 2-1), suggesting that the role of Mefp-1 was more likely to be as a waterproof, hydrophobic outer coating of byssal thread (*7*).

Structural analysis also supported the coating functionality of Mefp-1. Two studies showed structural variations: bent right-handed α-helix (*8*) and left-handed type II polyproline helix (*9*). Despite their difference, both structural models share the α-helical motif as a common structural denominator which can support the suggested biological role of Mefp-1 as hydrophobic outer coatings of byssal threads. Tandem repeats of Mefp-1 (approximately eighty times) can form a long rod-like structure, coating along the long, thin byssal threads. Therfore, considering all structural and biochemical evidence, the biological function of Mefp-1 appear to be a water-resistant, stiff coatings on surfaces of byssal threads.

Recently, ultrastructural examination of coating structures of Mfp-1s, structural analogue proteins found in different marine mussels, revealed a distinctive granular morphology (*10*). The comparative morphological and mechanical studies of Mgfp-1 coating found in two marine mussels *Mytilus galloprovincialis* and *Perna canaliculus* showed similar hardness (~20 MPa) and Young's modulus (~0.4 GPa), but exhibited remarkably different extensibility; tensile failure at 30% strain for *P. canaliculus* and 70% for *M. galloprovincialis*. This difference was attributed to the presence of microphase-separated granules within the cuticles of *M. galloprovincialis*.

2.1.2 Mefp-3

Although the role of DOPA in Mefp-1 appears to be more related to coating rather than adhesives, the widespread belief of DOPA's function as a molecular adhesive remained due in

part to the adhesive property of synthetic DOPA-containing polymers in the presence of water(*11*). In fact, DOPA content increases from ~10% (Mefp-1) to ~20% in Mefp-3, a protein localized at interfaces between pads and opposing substrates. The characterization of this protein, however, has been extremely difficult due to poor solubility. This problem was solved by a surprisingly simple technique called 'cold curing', which dramatically increases the amount of extractable proteins by transferring newly secreted soft plaques into low temperature sea water (4-8 ^{o}C) (*12*). Waite and colleagues found that the extracted protein gave four distinct bands in acid-urea PAGE experiments and characterized the lowest molecular weight protein. Amino acid sequencing revealed that the protein had 48 amino acids (6 kDa) with 20% DOPA content, and another post-translationally modified amino acid, hydroxyarginine, was unexpectedly identified (*13*). Due to the bio-distribution, DOPAs in Mefp-3

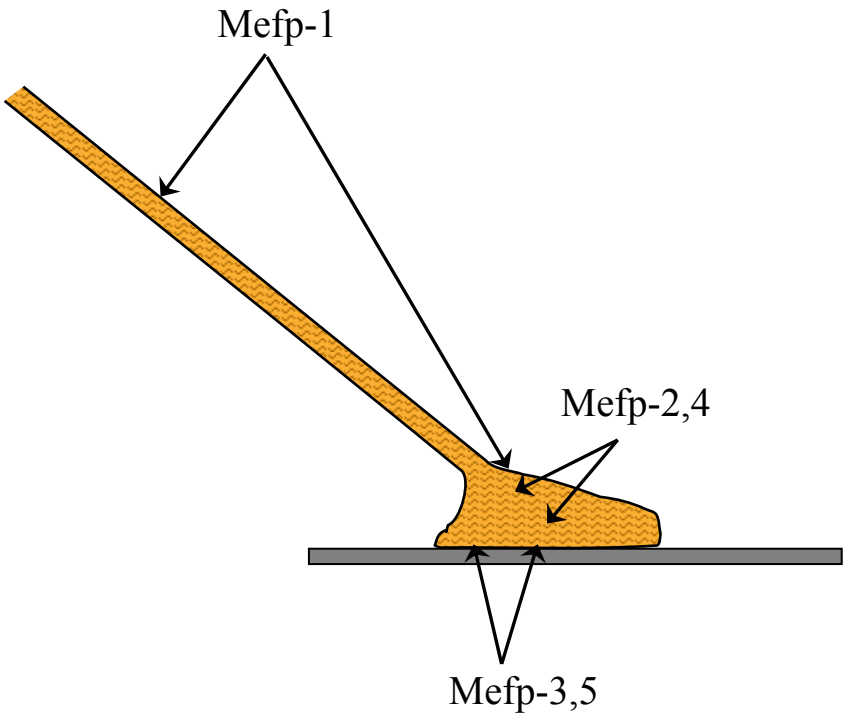

Figure 2-1. Schematic illustration of bio-distribution of mussel adhesive proteins in byssal threads and pads

are considered to serve an adhesive role (Figure 2-1) rather than purely a crosslinking amino acid. In addition, a different type of post-translationally modified amino acid, hydroxyarginine, was found. Currently, the biological role of hydroxyarginine remains unknown. The additional hydroxyl moiety can result in forming up to six hydrogen bonds, potentially enhancing adhesion strength on oxide surfaces.

A recent comparative study of Mefp-1 and -3 using a surface forces apparatus directly revealed Mefp-3's role as an adhesive protein at interfaces. The adhesion energy of fp-3 was measured to be about 0.3 mJ/m^2, which is equivalent to the force holding 100 g-m per plaque. In contrast, no adhesion was detected from Mefp-1 even under highly compressive loading (*14*).

2.1.3 Mefp-5

Mefp-5 is a relatively small 74 amino acid protein (9.5 kD) co-localized with Mefp-3 (Figure 2-1). It has the highest level of DOPA content (27 mol %) among all known MAPs, is highly basic due to enrichment in lysine, and also contains phosphoserine (*15*).

Mefp-5 and Mefp-3 have common characteristics that are distinct from other MAPs. Inspection of their amino acid sequences showed that a basic residue such as lysine is located next to (Lys-DOPA or DOPA-Lys) or adjacent to DOPA with glycine as an amino acid spacer. These lysine-containing amino acid motifs (DOPA-Lys or DOPA-Gly-Lys) might have benefits in adhesion in that the lysine 1) increases solubility of the proteins and 2) enhances interfacial adhesion via electrostatic force. The phosphoserine is also expected to contribute some degree of interfacial adhesion especially on calcium-based mineralized substrates. In fact, the mussel shell is primarily calcium carbonate (*16*). In summary, it is believed that Mefp-5 has three adhesive amino acids, DOPA, lysine, and phosphoserine, but the detailed interaction mechanisms with opposing surfaces remain largely unknown.

2.1.4 Mefp-2 and Mefp-4

Mefp-2 and 4 are less characterized proteins compared to other MAPs, partly due to their low DOPA contents: ~3 % for Mefp-2 and 4% for Mefp-4. However, they exist as the highest amount in mass (> 30%), suggesting a structural role in adhesive plaques(*17*).

Mefp-2 is a relatively large 40 kDa protein. Similar to Mefp-1, it has 11 repeats of a 35 - 40 amino acid sequence. Unlike to other Mefp proteins, it has three disulfide bonds from six cysteine residues. Cysteine is the amino acid found at extremely low frequency in other Mefp-family proteins except for Mcfp-6 (section *2.1.5*). Extensive proteolysis using a protease cocktail did not result in a complete digestion, indicating that Mefp-2 has a well-defined three dimensional structure although the atomic resolution remains to be solved (*18*). However, an important structural discovery was made by Inoue *et al*. (*19*). They cloned cDNA encoding Mgfp-2 (*Mytilus galloprovincialis* foot protein-2), another species very close to *Mytilus edulis* foot proteins and found that it encodes a ~ 40 amino acid repeat and contatins three disulfide bonds that is homologous to epidermal growth factor (EGF)-like domain. Another interesting characteristic of Mefp-2 is the distribution of the six DOPA residues in its primary sequence; they are found only at the N- (#23, 31, 36, and 43) and C-terminus (#468 and 473) not in the middle of the protein, suggesting that DOPA may play a critical role in inter- or intra-protein crosslinking.

2.1.5 Mcfp-6

A new adhesive protein, mcfp-6 (a homologous protein of Mefp-6), was identified during the study of a different marine mussel species, *Mytilus californianus*. It is a basic protein (pI ~ 9) with mass of 11.6 kDa (99 amino acids) found at the footprint of *M. californianus*, suggesting its bio-distribution near to substrates (*20*). Mcfp-6 has several distinctive features that have not been

found in other mussel adhesive proteins. First, it has a high cysteine content (~ 10 mol %) and most cysteines are in the form of thiols rather than disulfides. Second, tyrosine is largely unmodified to DOPA. Matrix-assisted laser desorption ionization (MALDI) mass spectrometry data suggest that formation of four disulfides, three DOPAs, and one phosphoserine provided the best match in mass: 11,595.8 Da from the calculated mass (3 DOPAs, 1 phosphoserine, and 4 disulfide bonds) and 11,596 Da from the observed mass. Thus, the mass result indicates that only 5% of tyrosine is post-translationally modified to DOPA. Third, an oxidative crosslinking product, 5-S-cysteinyldopa, was found (~ 1 mol %), presumably suggesting that mcfp-6 provides a cohesive link between the surface-coupling DOPA-rich proteins such as fp-3/-5 and the bulk of plaque proteins such as fp-2/-4.

2.1.6 Fusion Proteins

Engineered adhesives of fusion proteins produced from *E.coli* have been reported (*21, 22*). The fusion protein called fp-151 has a molecular configuration similar to triblock-copolymer consisting of Mefp-5 as a mid-block terminated with Mefp-1 at each end. Advantages of the fp-151 fusion protein include large quantity production from *E.coli* with high yield (1g of protein from an 11-pilot scale fed-batch bioreactor) and good aqueous solubility (~ 300 g/L). Using the fusion protein, cell adhesion peptide such as Arg-Gly-Asp (GRD) was able to be immobilized on surfaces. Tensile strength of fp-151 was stronger than that of fibrin glue: ~1.7 MPa for fp-151 and ~0.4 MPa for fibrin glue (*23*).

2.1.7 Catechol Oxidation

The redox chemistry of catechol, the side chain of DOPA, plays an important role in biosynthesis of water-insoluble materials. Two major pathways have been characterized: (1) amine (or thiol) reaction to the aryl ring of DOPA (Michael addition) and (2) aryl-aryl coupling

between DOPA residues. *In vitro* crosslinking experiments clearly showed aryl coupling reactions (diDOPA) detected in both solid-state ^{13}C NMR and MALDI-TOF mass spectrometry (*24*, *25*). In addition, mass spectrometry data suggested intermolecular Michael-addition reactions between Lys2 (or Lys10) and DOPA9, although this conclusion awaits further confirmation by other techniques because of interfering adjacent mass signals (*25*). This extensive DOPA-mediated intermolecular crosslinking produces tough waterproof proteinaceous materials. It was demonstrated that oxidation by periodate or mushroom tyrosinase increased film stiffness made from Mefp-1 (*26*).

2.2 Mechanochemistry

The tools for force measurement such as optical tweezers, AFM, and surface force apparatus, have allowed chemists and biologists to measure a wide variety of chemical and biochemical interactions. In particular, AFM and optical tweezer techniques can probe force at a resolution of individual molecule interactions. A large amount of information about biological force has been accumulated using these methods, and this field is now referred collectively as 'mechanochemistry'. There are three categories of chemical and biological interactions in mechanochemistry: reversible weak bonds, reversible strong bonds, and irreversible strong bonds. Reversible weak bonds include hydrogen bonds and van der Waals interactions. Chemical and biological metal-organic complexes such as heme, metal chelateors, and organometallic self-assembled materials are considered to be forces that are strong yet reversible. Finally, a wide variety of covalent bonds are examples of strong and irreversible bonds.

2.2.1 Reversible Weak Bonds

Most interactions in biology such as ligand-receptor interactions, DNA base pairings, and protein foldings are reversible, in which hydrogen bonds and hydrophobic interactions are two major driving forces that form stable three-dimensional structures of proteins, DNAs, RNAs as well as complexes of these components.

The first model system for studying individual receptor-ligand binding was the streptavidin-biotin interaction, and results from the experiments were independently reported by both Gaub and Colton (*27, 28*). The studies revealed that the individual biotin-streptavidin binding force is about 200 pN, and specificity of the observed single-molecule interactions was confirmed by blocking biotin-binding sites of streptavidin by the addition of excess free biotin molecules. A wide variety of other protein-ligand binding forces have been reported subsequent to these studies: 100 pN of ICAM-1/anti-ICAM antibody (*29*), 111.5 pN of goat IgG/biotinylated BSA (*30*), 50 pN of single-chain Fv (*31*), and 240 pN of human serum albumin(HSA)/anti-HAS (*32*).

Intramolecular weak interactions in a single protein molecule can also be measured by the same type of pulling experiments, which have become a popular technique in protein biophysics. The first protein investigated at a single-molecule level using AFM was titin, a globular subunit of muscle fibers structurally homologous to immunoglobulin domains (*33*). The unfolding of each structural domain resulted in a saw-tooth pattern of force-extension curves, indicating individual protein unfolding with an unfolding force range of 100-200 pN (*34*).

2.2.2 Reversible Strong Bonds

The first metal-organic coordination system studied at a single-molecule level involved N-nitro-triacetic acid (NTA), imidazole (the side chain of histidine), and Ni^{2+} coordination. Histidine has been extensively used as an affinity tag in protein purifications in which imidazole

coordinates with NTA via divalent ion-mediated hexagonal coordination (Ni, Cu, Co, or Zn). At least two histidine residues are required to form a stable coordination bond with NTA, but a typical length of the affinity tag is six consecutive histidien residues. Three independent studies were reported to addres this issue (*35-37*). Although the experimental approaches in those studies differed, a common denominator was the use of polymers such as dextran or poly(ethylene) glycol (PEG) for NTA or histidine conjugations. Conti et al. (*36*) and Schmitt et al. (*37*) used a commercially available Biacore chip on which dextran-NTA conjugates were immobilized. Interaction force was monitored by AFM cantilevers on which the surface was modified with histidine peptide. Kienberger et al. took a different approach (*35*). They synthesized PEG-histidine conjugates, which were subsequently immobilized and cantilever surfaces and measured interaction forces on NTA-immobilized gold substrates. The number of histidine amino acid was different between experiments: Kienberger and Schmitt used only six histidines, but Conti studied two and six histidines. Thus, the force values reported those studies were not consistent, ranging from 38 to 500 pN. This might be due to (1) unknown pulling speed (not available in (*36, 37*)), (2) ambiguous number of histidine-NTA interactions, (3) different configurations of molecules used in the studies: N-terminal (*35*) vs. C-terminal tags (*36, 37*), and (4) ambiguous pH values. Despite the differences, the general conclusions from these studies reveal that the coordination bond is stronger than hydrogen bonds, but with preserved reversibility.

2.2.3 Irreversible Strong Bonds

The covalent bond is a building block of all organic materials, and measuring the breakageof a single covalent bond has been considered as an extremely difficult task from both technical and analytical standpoints. Thus, few studies have been published so far, and this

section only focuses on the breakage of a linear organic chain as reported by Grandbois et al (*38*). The study used amine-functionalized tips engaged onto glass substrates which were modified with amylose polymers. During tip approach onto the substrate, ethyl-dimethylaminopropyl-carbodiimide (EDC) and N-hydroxysuccinimide (NHS) reaction was used to capture a single amylose chain. To minimize multiple bond formations, a technique called 'fly-fishing' was used, in which partial engagement and retraction of the tip was continuously performed in a stepwise manner until a single polymer stretching signal is detected. Another experimental confirmation of the individual polysaccharide chain stretching was that amylose undergoes the chair-boat structural transition of furanose rings, exhibiting a pronounced plateau at 275 pN in a force-distance curve. They observed an average bond-rupture force of ~ 2.0 nN (loating rate = 10 nN/sec). A control experiment performed in the absence of EDC and NHS showed no bond rupture around 2.0 nN force range. To determine which specific chemical bond was ruptured, the experimental results were compared to theoretical calculations based on density functional theory (DFT) of Si-C bonds. This comparison resulted in a calculated force of 2.0 nN in agreement with the experimental data.

2.3 Gecko Adhesion

The gecko, nature's remarkable climber, can adhere to and traverse vertical and even inverted surfaces. A study showed that, in the case of the tokay gecko (*Gekko gecko*), the two front feet (227 mm^2 of pad area) can withstand 20.1 N of force parallel to a surface with. In other words, an approximately 1 cm^2 area of gecko foot can support a shear force up to 10 N (*39, 41*). The gecko foot's adhesive strength arises from an array of keratinous hairs, called setae, which branch further into circular pads called spatulae that intimately contact surfaces (Figure 2-2). A

seta is approximately 100 μm in length and 4.2 μm in diameter, and a spatula is about 200 nm in diameter (*39, 40*). The long-debated potential mechanisms for adhesion include chemical glue, suction, interlocking, friction, electrostatic force, capillary force, and van der Waals force. The cooperative contributions of van der Waals (*41*) and capillary forces (*42, 43*) have recently been the most convincing mechanisms used to explain gecko adhesion. However, considering the hydrophobic nature of setae, van der Waals force is the primary adhesion mechanism.

A gecko typically has approximately 14,400 setae per mm^2, and the two front feet with the surface area of 227 mm^2 can withstand 20.1 N parallel to surfaces. Therefore, a single seta produces an adhesive force of about 6.15 μN (20.1 N / (14,400 x 227 setae) = 6.15 μN). However, experiments revealed that the isolated setae did not exhibit such a strong adhesive strength. Setal adhesion only appears with a mechanical program: orientation, preload, and drag (*41*). When performing the appropriate mechanical program, a seta revealed up to 100 μN shear force and exhibited 40 μN adhesive force (*44*).

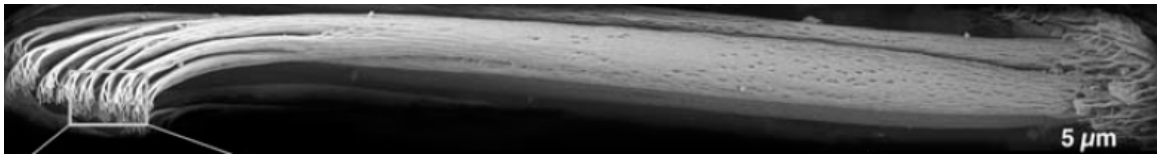

Figure 2-2. Scanning electron microscopy image of individual seta of gecko's feet (*1*).

2.3.1 Frictional Adhesion

Recently, a new model called 'frictional adhesion' was suggested as a better explanation of gecko adhesion (*45*). The mechanism of setal detachment primarily relies on creating an angle between the substrate and setae by leg movement, which results in peeling of toe pads from the substrate. This explanation raised a question: how do geckos maintain attachment to inverted surfaces like ceilings, where body weight gradually causes toe peeling by creating an angle between setae and substrates? To answer this question, Autumn et al. hypothesized that the adhesion could be increased by applying a shear force in the setal arrays, and the authors demonstrated that the adhesion force was a linear function of shear force: $F_{adh} = -0.487 \times F_{shear} + 0.002$ (in N), ($R^2 = 0.89$) (*45*). This relationship holds only when the setal array was dragged along the natural curvature of setae (Figure 2-2). In other words, when the setal array was dragged against the natural curvature, the setae remained compressed and did not adhere to the substrate. Therefore, frictional adhesion develops only when a gecko uses an appropriate loading direction (i.e. walking). An important implication of the frictional adhesion concept is that the detachment of toe pads of geckos can require nearly zero force by reducing the shear load.

2.3.2 Synthetic Gecko Adhesive Mimetics

Synthetic efforts for developing new adhesives by mimicking gecko's feet have been published by many research groups (*46-49*). One of the first attempts was reported by Geim et al (*46*). This study utilized a nanostructured aluminum mold fabricated by electron-beam lithography. The pattern of aluminum mold was transferred into a polyimide film by oxygen plasma etching and the resulting nanoadhesive exhibited 3 N in adhesion from the area of 1 cm^2. However, the polyimide pillars were collapsed after only a few cycles of attach- and detachment, which dramatically decreased the adhesion. This study suggested that gecko mimetic adhesives

are feasible but that it is of considerable importance to select materials for fabrication with suitable mechanical properties such as relatively low modulus. This result immediately suggests that mimicking the gecko foot structure using stiff materials such as polystyrene nanotubes is unlikely to be functional (*50*).

Carbon nanotube-based flexible synthetic gecko tape was fabricated (*49*). The nanotube adhesive mimicked hierarchical structures of setae (microscale) - spatulae arrays by the spatial distribution of nanotube bundles, similar to the setae array. This adhesive exhibited good shear stress up to 36 N/cm^2 on various substrates including Teflon. This shear stress is nearly four times higher than that measured in a gecko foot. However, the adhesive force of the carbon nanotube tape was not reported (shear information is only available) in the study. Due to the unique mechanical properties of carbon nanotubes, it is likely to experience interfacial failure between substrate and carbon nanotubes as well as to attenuate adhesion force during repetitive measurement.

To study the effect of the terminal geometries of pillars on adhesion, the tip geometry was engineered by modifying conventional soft-lithography techniques. Pillar arrays terminated with flat, spherical, spatular, concave, and tubal tips were fabricated (*51*). Indentation experiments revealed significant change in adhesion as a function of tip geometry, in which pillars with spatula-like structures exhibited far better performance in adhesion than any other pillars with different terminal shapes. For example, a pull-off force (P_c) of 3 mN was measured from pillars with a spatula shape, which far exceeded P_c of 0.75 mN for flat-topped pillars and 0.2 mN for sphere-topped pillars (the diameter of force probe = 5 mm). Interestingly, concave shape tips exhibited preload-dependent adhesion up to 2 mN. This study demonstrated that the

control of terminal pillar shapes contributes adhesion. However, no study has been reported to demonstrate such effects in adhesion at the nanoscale.

Chapter 3: Single-molecule DOPA Adhesion on Inorganic and Organic Surfaces

3.1 Objectives

Numerous living creatures rely on physical adhesion to biotic and abiotic objects for essential activities such as movement, protection and self-defense (*41, 52, 53*). From a purely functional point of view, bioadhesion can be of two major types: temporary and permanent. A characteristic example of a temporary bioadhesive strategy is given by the specialized foot hairs used by geckos for climbing sheer surfaces(*41*). A classic example of permanent bioadhesion is exemplified by mussels,(*54*) which secrete holdfasts essential for stability within the tidal marine environment. Remarkable features of mussel adhesion include the ability to achieve long-lasting adhesion in a wet environment (*53*), and adherence to virtually all types of inorganic and organic surfaces (*55*). The adhesive apparatus of the mussel consists of a series of byssal threads that tether the organism to a substrate (Figure 3-1A). At least 5 specialized adhesive protein subtypes

known to contain DOPA at concentrations ranging from a few to 27 mole % (Figure 3-1B) are found within the distal adhesive pad of the widely studied blue mussel, *Mytilus edulis* (*56*). The highest DOPA content occurs in the proteins Mefp-3 (Mefp = *Mytilus edulis* foot protein) (21 mole%) and Mefp-5 (27 mole%)(*13, 15*), both of which are localized near the interface between the adhesive pad and the substrate (Figure. 3-1C).

The role of DOPA in mussel adhesive proteins is not fully understood, although there is general acceptance that oxidized DOPA residues play important roles in crosslinking reactions leading to solidification of the secreted liquid protein adhesive(*11, 25, 57, 58*). The particularly high concentration of DOPA at the adhesive/substrate interface has led to much speculation regarding its role in adhesive bonding. However, the physicochemical details of DOPA-surface interactions remain elusive. Byssal thread pull-off experiments (*59*) and macroscopic lap shear bond strength measurements using DOPA-containing polypeptides(*60*) failed to clearly distinguish between cohesive and adhesive behavior and yielded little information at the molecular level. Previous atomic force microscopy (AFM) measurements of whole mussel adhesive proteins (MAPs) interacting with surfaces (*21, 61*) were complicated by the presence of other amino acids, an unknown number of proteins on the tip, and multiple DOPA residues interacting with the surface. For this paper, we employed the single-molecule method of Hinterdorfer et al.,(*62*) to isolate the contribution of DOPA toward mussel adhesion.

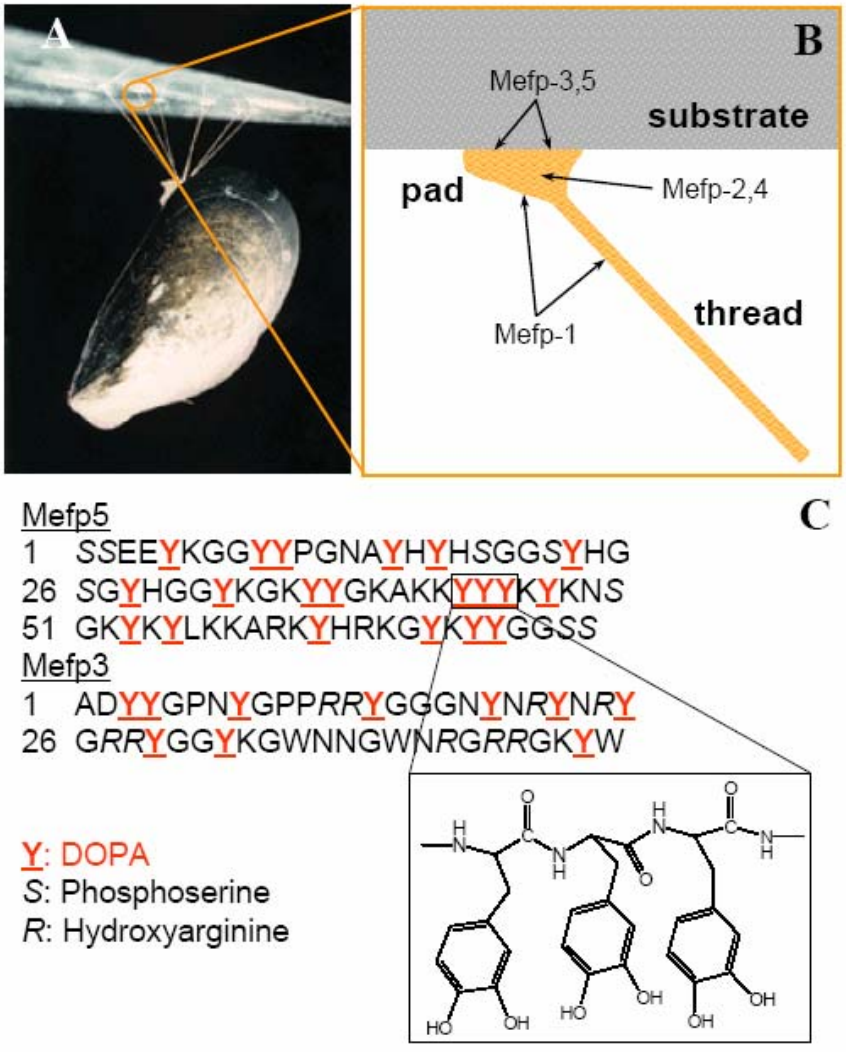

Figure 3-1. Biodistribution and amino acid composition of mussel adhesive proteins of *Mytilus edulis* A. Photograph of a mussel attached to a glass surface, showing the byssal threads and adhesive pads. B. The biodistribution of *Mytilus edulis* foot proteins (Mefps). Mefp-3 and Mefp-5 are found at the pad-substrate interface. C. The amino acid sequences of Mefp-3 and Mefp-5, which have the highest known DOPA contents, at 21 and 27 mole %, respectively. Inset: the chemical structure of DOPA as it appears in the tri-DOPA sequence in residues 43-45 of Mefp-5.

3.2 Materials and Methods

3.2.1 Tip Modification

Before surface modification, silicon nitride (Si_3N_4) tips were cleaned in an O_2 plasma (Harrick Scientific, Ossining, USA) for 3 min and then subsequently transferred to a piranha solution (sulfuric acid:H_2O_2 = 8:2) for 30 min. After extensive rinsing with nanopure H_2O, they were transferred into 20% (v/v) 3-aminopropyltrimethoxysilane (APTMS) in toluene for 30 to 60 min, resulting in an aminosilane functionalized tip. The aminated AFM tips were then functionalized with a mixture of methoxy-PEG-N-hydroxy succinimide (mPEG-NHS, Mw=2000, Nektar Inc.) and Fmoc-PEG-N-hydroxy succinimide (Fmoc-PEG-NHS, Mw 3400, Nektar Inc.) at a ratio of Fmoc-PEG-NHS:mPEG-NHS = 1:5-10. The PEG functionalization was performed at a total PEG concentration of 5mM in 50 mM sodium phosphate buffer, 0.6 M K_2SO_4, pH 7.8 at 40 ^oC and subsequently repeated in chloroform at room temperature for 3 hrs. Fmoc protecting groups were then cleaved by treatment of the tips in 20% piperidine (v/v in NMP) for 5 min, followed by coupling of *N*-Boc-DOPA to the liberated amine in (BOP/HOBt/DOPA molar ratio of 1:1:1, 8mM in NMP) solution with 10 μL DIPEA. The use of excess mPEG-NHS during PEG functionalization of the tip served to limit the number of DOPA residues on the tip, facilitating single- molecule force measurements. The same procedure was used for preparation of Boc-tyrosine functionalized tips.

3.2.2 Surface Preparation and Characterization

A 20-50 nm thin layer of Ti on Si(100) wafer surfaces was prepared using an Edwards FL400 e-beam evaporator (Boc Edwards, Sussex, UK). Before use all surfaces were sonicated (Branson 3214) in hexane, 2-propanol, and acetone and subsequently in piranha solution to

generate an oxide layer. Amine containing organic surfaces were prepared by functionalization of unmodified silicon wafers with APTMS in anhydrous toluene after the cleaning process just described. The presence of surface amines was confirmed by x-ray photoelectron spectroscopy (XPS) (Figure 3-2). Unmodified and APTMS modified Si surfaces were analyzed by X-ray photoelectron microscopy (XPS), (Omicron, Taunusstein Germany) equipped with a monochromatic Al Kα (1486.8 eV) 300 W X-ray source and an electron gun to eliminate charge build-up. The iron oxide surface was prepared by chemical vapor deposition through the reaction of iron chloride with water at a temperature range of 800-1000 ^{o}C(*63*).

3.2.3 AFM Experiment

All data were collected on an Asylum Mfp-1D AFM instrument (Asylum Research, Santa Barbara, CA). Spring constants of individual cantilevers (Veeco nanoprobes, Santa Barbara and Bio-Levers, Olympus, Japan) were calibrated by applying the equipartition theorem to the thermal noise spectrum (*64*). All AFM experiments were conducted in millipore water or Tris-HCl (20 mM, pH 9.7) buffered water at room temperature. The progress of tip functionalization with APTMS and PEG was confirmed by the appearance of characteristic force signals at each step in the modification procedure (Figure 3-3). The vast majority of DOPA functionalized AFM tips yielded force-distance curves with only a single DOPA adhesion event, although on one occasion a tip generated two spatially resolved adhesion events during pull-off (Figure 3-4). Control experiments performed with AFM tips modified as described above with Boc-tyrosine revealed only weak interactions with Ti surfaces (Figure 3-5, top panel). The presence of tyrosine was confirmed by force measurements on gold evaporated surfaces (Figure 3-5, bottom panel).

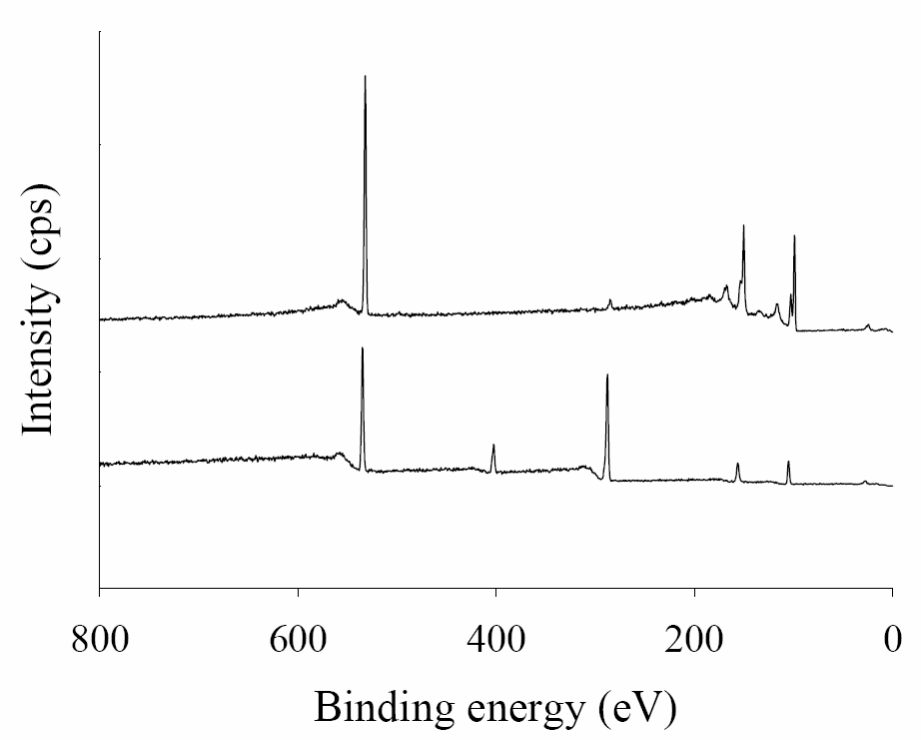

Figure 3-2. XPS characterization of amine functionalized Si surfaces.
A clean unmodified Si surface (above) and after modification with APTMS (below). The appearance of nitrogen 1s (400 eV) and increase in carbon 1s signal (284.5 eV) in the spectrum indicates successful modification by the aminosilane compound.

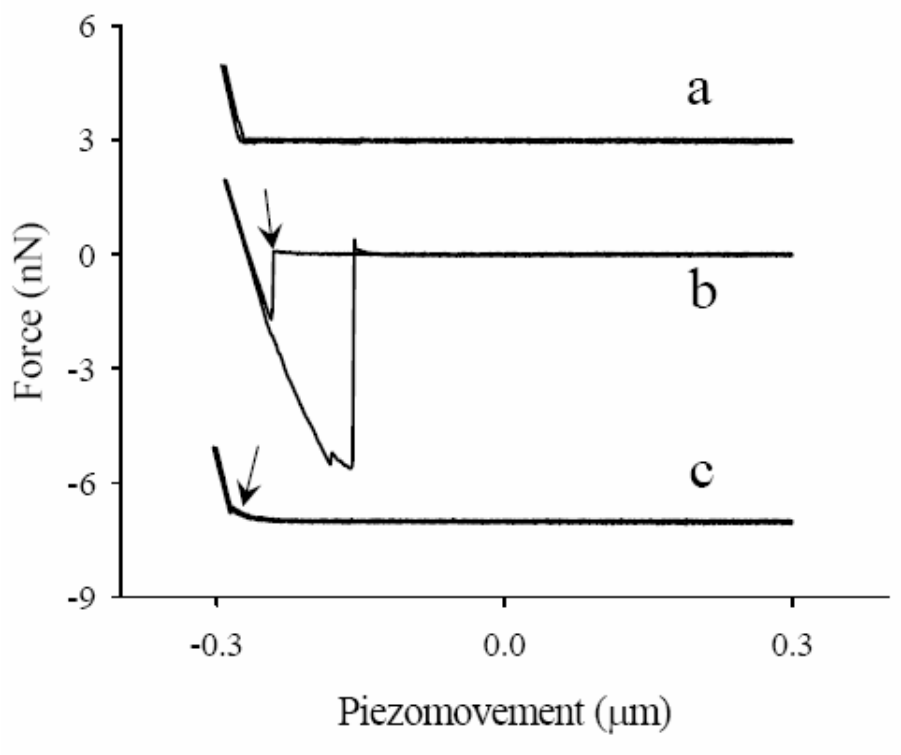

Figure 3-3. AFM force-distance traces of chemically modified silicon nitride AFM tips on Ti. a. A representative force-distance trace of a clean tip without chemical modification. Adhesion was not detected during cantilever retraction. b. A representative force-distance trace from an amine functionalized tip. Snap-on (arrow) during cantilever approach as well as a large force (~6 nN) on pull-off are suggestive of electrostatic interaction between the positively charged amine functionalized tip and negatively charged oxide surface. c. A representative force-distance trace from a PEG modified tip (no DOPA). The electrostatic interactions were attenuated by inert grafted PEG layers, resulting in a low intensity physical resistive force characteristic of a grafted PEG layer (arrow).

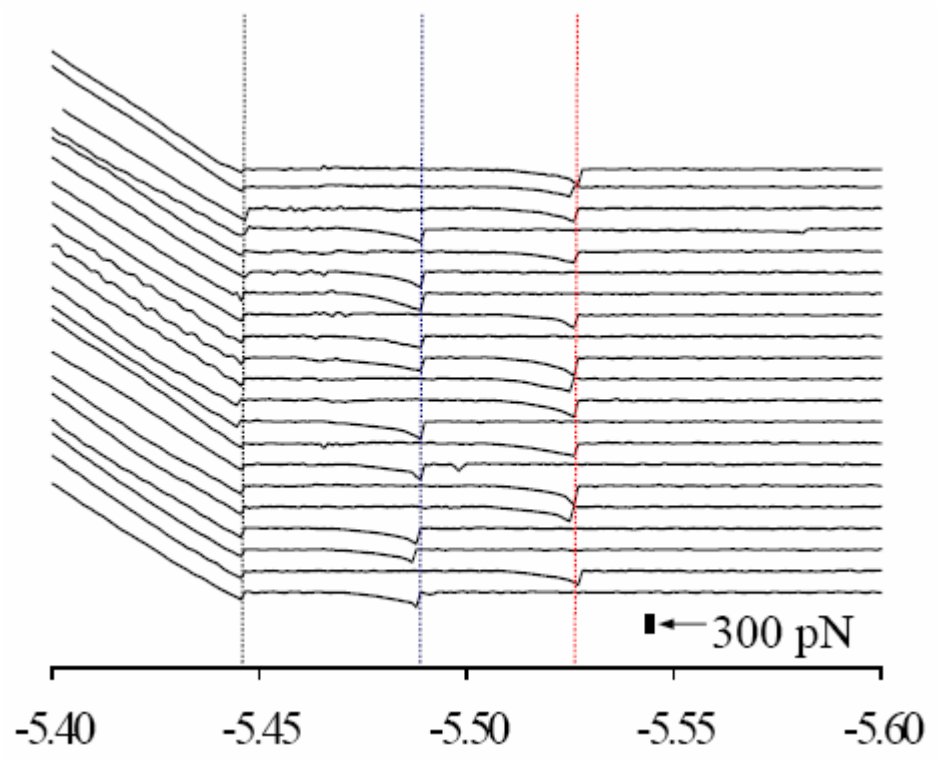

Figure 3-4. Multiple force traces of single molecule binding of DOPA.
The black vertical line represents the contact between tip and substrate. The blue and the red vertical lines (red) were spatially resolved multiple DOPA binding events. The curve indicated by the arrow exhibited two DOPA binding events in the same experiment.

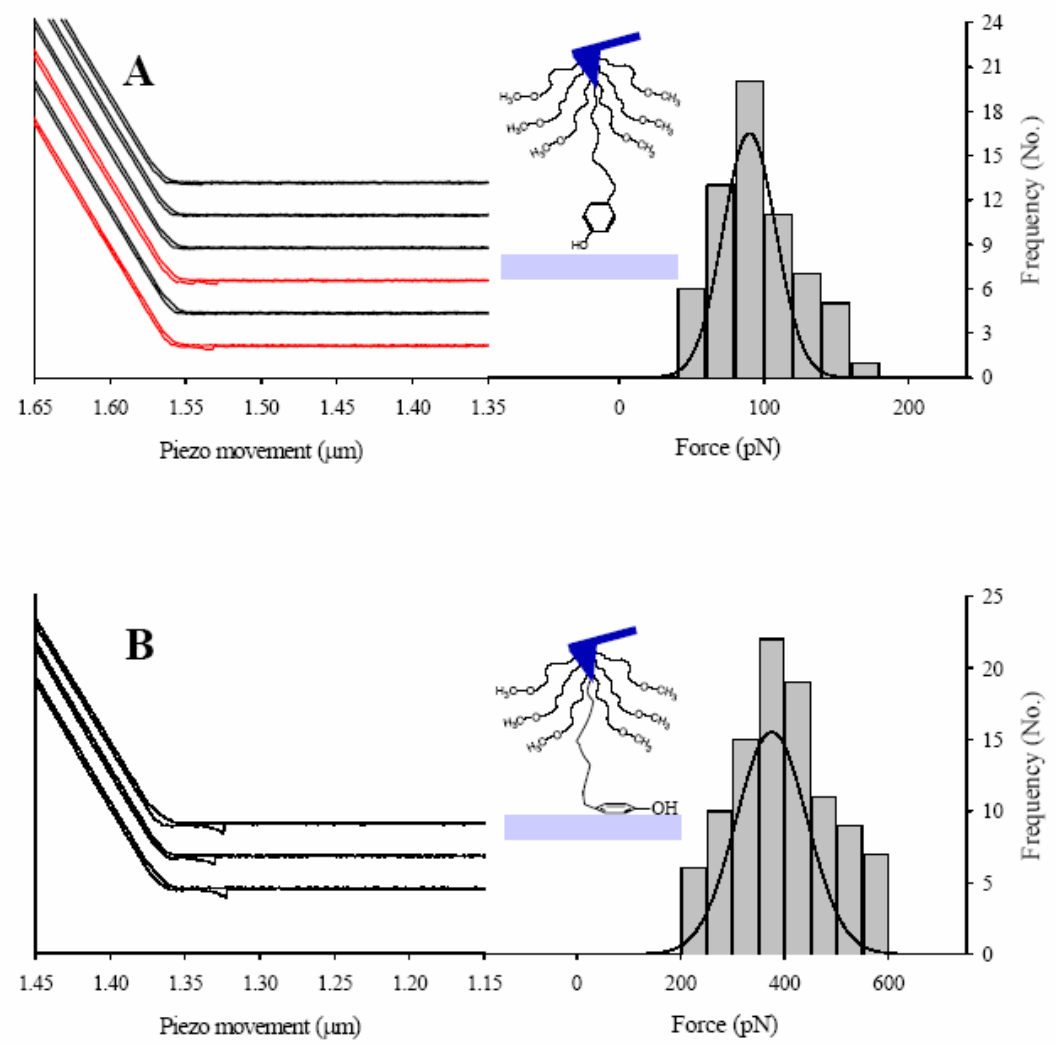

Figure 3-5. AFM force-distance traces of tyrosine modified silicon nitride AFM tips: tyrosine interacts weakly to Ti surfaces. A. Representative force-distance traces of a tyrosine modified tip on Ti. Most scans showed no detectable binding signal (black), and <10% of scans showed weak signals (red). The histogram on the right represents the statistical analysis of the weak force signals (63 events). B. Representative force-distance traces of tyrosine modified tip on Au. To eliminate the possibility that the tip used in part A did not contain tyrosine, force-distance curves using the same tip were obtained on Au. The presence of tyrosine on the tip was confirmed by the presence of interaction forces centered at 397 ± 91 pN (99 events). This observation is consistent with π-electron interactions between the tyrosine phenyl group and the Au surface.

3.2.4 Dynamic Force Experiments

AFM experiments were performed as described above at several loading rates achieved through variation of the tip spring constant and the pulling rate. Silicon nitride AFM cantilevers (Bio-Levers, Olympus, Japan) with spring constants of ~5 pN/nm, ~28 pN/nm and ~300 pN/nm were used. The lowest loading rate of 2 nN/sec was achieved with a pulling rate of 400 nm/sec and the low stiffness cantilever (~5 pN/nm). The highest loading rate (1500 nN/sec) was achieved with a pulling rate of 5 μm/sec and the stiffest cantilever (300 pN/nm, Veeco).

3.3 Results and Discussion

3.3.1 Single-Molecule Adhesion Force of DOPA.

We used chemically modified Si_3N_4 AFM cantilevers to investigate the interaction of single DOPA residues with organic and inorganic surfaces. Poly(ethylene glycol) (PEG) was used as a linker and inert back-filling molecule to isolate the contribution of DOPA(*62*). *N*-Boc-DOPA was end-tethered to PEG and the Boc protecting group remained in place to avoid electrostatic interactions. In a typical experiment, a DOPA functionalized AFM tip was lowered at constant rate onto a wet surface to a maximum load of 15-20 nN and then retracted at the same rate while the force versus extension response was recorded. Force-distance (F-D) curves exhibit the characteristic point of separation of the tip from the surface and single- molecule adhesion events.

Figure 3-6A shows representative F-D curves for approach and retraction of a DOPA-modified cantilever from a Ti surface. The initial portion of the retraction curves exhibits an

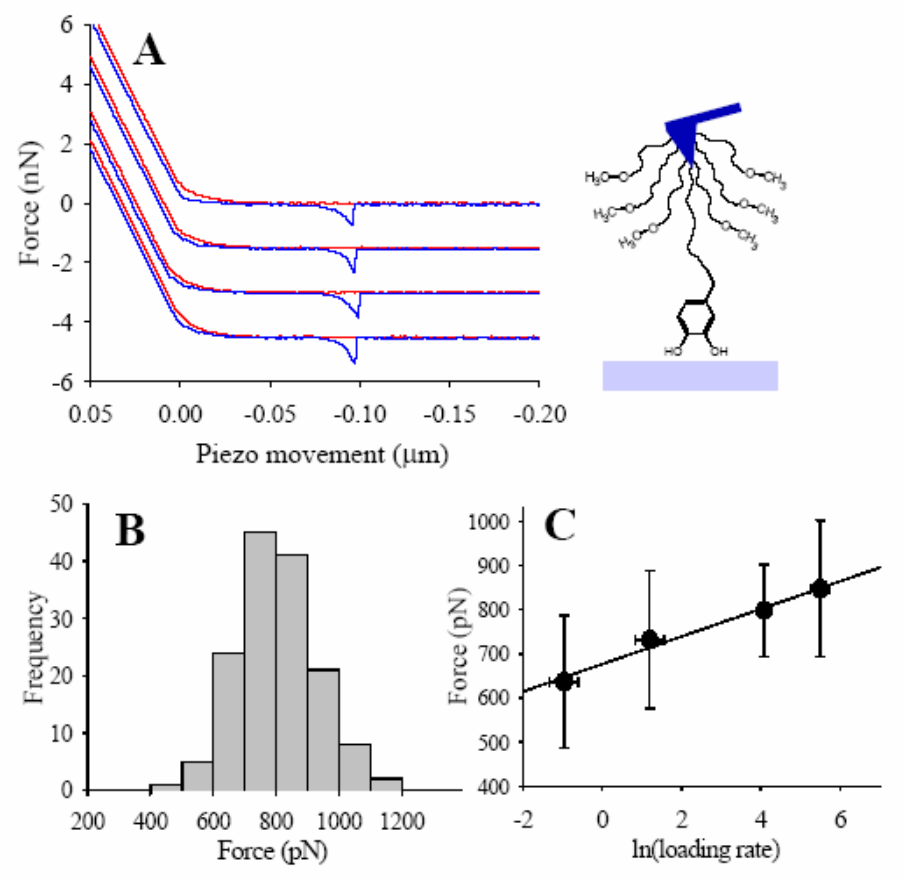

Figure 3-6. DOPA adheres strongly and reversibly to Ti surfaces.
A. Schematic of DOPA functionalized AFM tip and typical single molecule force-distance curves of DOPA interacting with a Ti surface. The red and blue traces indicate approach and retraction signals, respectively, in which DOPA-Ti adhesive (interaction) force was observed during retraction. The four different force curves were produced from the same DOPA functionalized tip and displaced vertically for clarity. B. Histogram (n = 147) of pull-off force values for DOPA-Ti obtained with a single AFM tip at a loading rate of 180.7 nN/s. The mean force value was calculated to be 805 ± 131 pN. C. A linear-log plot of force vs. loading rate for DOPA-Ti. The roading rates were 0.41 ± 0.15, 3.53 ± 1.48, 59.99 ± 9.01, and 250.21 ± 62.46 nN/sec which were determined by the slope from a force vs. time plot (see methods) (add Leckband reference here). Mean forces and standard deviations obtained from a minimum of 30 adhesion events were 847 ± 157 pN (1500 nN/s), 805 ± 131 pN (180.7 nN/s), 744 ± 207 pN (28.4 nN/s), and 636 ± 151 (2 nN/s).

appearance typical of elastic extension of a tethered PEG chain (*62*), culminating in detachment of DOPA from the surface. Several features of the observed F-D curves are remarkable and provide convincing evidence for a high strength reversible single- molecule interaction. First, the essential features of the F-D curves were observed repeatedly during multiple pull-off experiments performed with the same tip, indicating that the interaction between DOPA and the

surface was both strong (~800 pN) and reversible (i.e. could be repeatedly rebound and re-pulled). Second, the stretched contour length of PEG extrapolated from the F-D curves (36 nm) was consistent with the expected 37 nm contour length for the PEG molecular weight (3.4 kDa) used in this study. Third, inspection of data from multiple F-D curves revealed virtual overlap of the F-D traces and similar pull-off distances (Figure 3-6A), suggesting that the same exact DOPA-PEG chain was interacting with the Ti surface during successive tip contacts. Due to the high curvature of the cantilever tip (radius ≈ 25 nm) as well as the polydispersity of PEG, it would be unlikely to observe the same pull-off distances for DOPA residues tethered to different PEG chains. On very rare occasions this did occur, which was apparent from F-D profiles that exhibited multiple pull-off signals (Figure 3-4). Finally, the low probability of observed tip-surface binding event (ca. 10% of contacts yielded F-D curves as shown in Figure 3-6) provided additional evidence for single DOPA-Ti surface interactions.

The reversible nature of the interaction between a single DOPA and the Ti surface allowed us to construct a histogram of bond dissociation forces extracted from many F-D curves (Figure 3-6B), yielding a surprisingly large dissociation force of 805 ± 131 pN (147 events, 3 cantilevers) for the mean and standard deviation. To put this value in perspective, other investigators have determined that a few nN of applied force was required to rupture a single

covalent bond (*38*). Obviously, once covalent bonds have ruptured, one cannot study reversible binding dynamics of single molecules but must average over the behavior of many single molecules. On the other hand hydrogen bonds, while reversible, ruptured at tens of picoNewton forces(*65*). To our knowledge the DOPA-Ti interaction is the *strongest reversible binding interaction involving a small biological molecule ever reported*, underscoring the unique nature of the observed DOPA-Ti interaction.

In the absence of DOPA, PEG functionalized AFM tips showed essentially no hysteresis between approach and pull-off curves in experiments conducted under identical conditions (Figure 3-3, bottom curve), indicating that the PEG itself interacts very weakly with the Ti substrate. Furthermore, when *N*-Boc protected tyrosine (*N*-Boc-Tyr) was substituted for DOPA only small amplitude interaction forces (97 ± 28 pN), (Figure 3-5) were measured to Ti. This clearly demonstrates the significance of Tyr to DOPA post-translational modification in adhesion of mussel adhesive proteins.

To gain further insight into the energetics of this interaction we determined the average DOPA-Ti bond rupture force at several loading rates. The plot of force vs. loading rate is shown in Figure 3-6C, revealing the expected trend of increased force to break the bond at higher loading rates (*66*). The linear fit to the data provides the bond dissociation energy and the distance (x_b) beyond which the bond is completely dissociated along the applied force direction (*66*). The analysis revealed a dissociation energy of 28.1 kcal/mol and an x_b value of 1.8 Å for the DOPA-Ti bond. The determined bond dissociation energy is within the 25-30 kcal/mol range estimated by density functional theory for the coordination bond formed between dopamine and TiO_2 (*67*). Although the existence of metal-oxygen coordination is well established in biology,

this represents the first direct force measurement of a metal-oxygen coordination bond, and perhaps the only known example in biology where the primary function of the coordination bond is to achieve mechanical adhesion. Although the interaction is reversible in our single- molecule experiments, this may not be the case for whole mussel adhesive proteins, as cooperativity of multiple DOPA-surface interactions could allow for enormous force transmission across the interface. As few as 3-4 DOPA residues interacting with an oxide surface would eclipse the strength of a covalent bond, leading to irreversible cohesive failure (i.e., covalent bond breakage) within the bulk adhesive pad. This may help to explain previous observations that Mefp-3 and Mefp-5 proteins remain attached to surfaces after removal of the adhesive pad(*68*).

3.3.2 Effect of DOPA Oxidation on Adhesion

Oxidation of the catechol side chain of DOPA occurs in the alkaline marine environment, giving rise to quinones that further react to crosslink adhesive proteins via aryl-aryl coupling (di-DOPA formation) or possibly via Michael type addition reactions with amine-containing protein residues (*11, 25, 57, 58*). The prevailing view is that these reactions play key roles in bulk solidification of mussel glues, however very little is known about the impact of these oxidation reactions on adhesion to substrates (*60*). Measurement of adhesive interactions between oxidized DOPA and surfaces is complicated by the highly reactive nature of semi-quinones and quinones. This technical concern was alleviated through the use of a large excess of unreactive methoxy-PEG during tip functionalization, yielding a single DOPA molecule on the AFM tip. This suppressed possible intermolecular reactions between oxidized DOPA species and allowed us to investigate adhesive interactions between oxidized DOPA and various surfaces in great detail.

An AFM tip containing a single DOPA residue was first identified by obtaining F-D curves on Ti at neutral pH as described above. The pH of the aqueous solution was then increased to oxidize

the DOPA, after which additional F-D curves were obtained over a period of one hour. Interestingly, a bimodal distribution of force signals is observed, consisting of either large or small forces registered at similar pull-off distances (Figure 3-7A). Statistical analysis yields two non-overlapping histograms with force values of 180 ± 60 pN and 740 ± 110 pN (Figure 3-7B). By comparison to the data shown in Figure 3-6, we assign the high force signal to the interaction of DOPA with Ti. We deduce that the low force signal represents the interaction of DOPA-quinone and its resonance structures with Ti, as these signals only appeared under oxidizing conditions. These observations are very consistent with the notion of single-molecule fluctuations between two states in chemical equilibrium; i.e. between DOPA and DOPA-quinone (Figure 3-7C). The equilibrium between DOPA and DOPA-quinone is shifted toward DOPA-quinone at high pH (pKa = 9.2) (*69*). Considering the data in Figure 3-7 as well as the neutral pH data shown in Figure 3-6, we assign the high-force signal to the interaction of DOPA with Ti and deduce that the low-force signal represents the interaction of DOPA-quinone and its resonance structures with Ti, because these signals appeared only under oxidizing conditions. Assuming a value for the bond length, x_b, similar to that observed for DOPA-Ti (1.8 Å), the calculated bond dissociation energy of DOPAquinone to Ti was only 4.3 kcal/mol (~7 kT) (Appendix 3-1), confirming that oxidation of DOPA substantially reduces adhesion to Ti. It is, therefore, unlikely that mussel adhesion to wet Ti or similar oxide surfaces is mediated by DOPA-quinone and its resonance structures.

3.3.3 Adhesion Mechanism of DOPA on Organic Surfaces

Finally, we used similar methodology to elucidate the mechanism behind mussel adhesion to organic surfaces. In contrast to inorganic surfaces, we anticipated that oxidation of DOPA under elevated pH may result in covalent coupling to organic surfaces. Reactions between

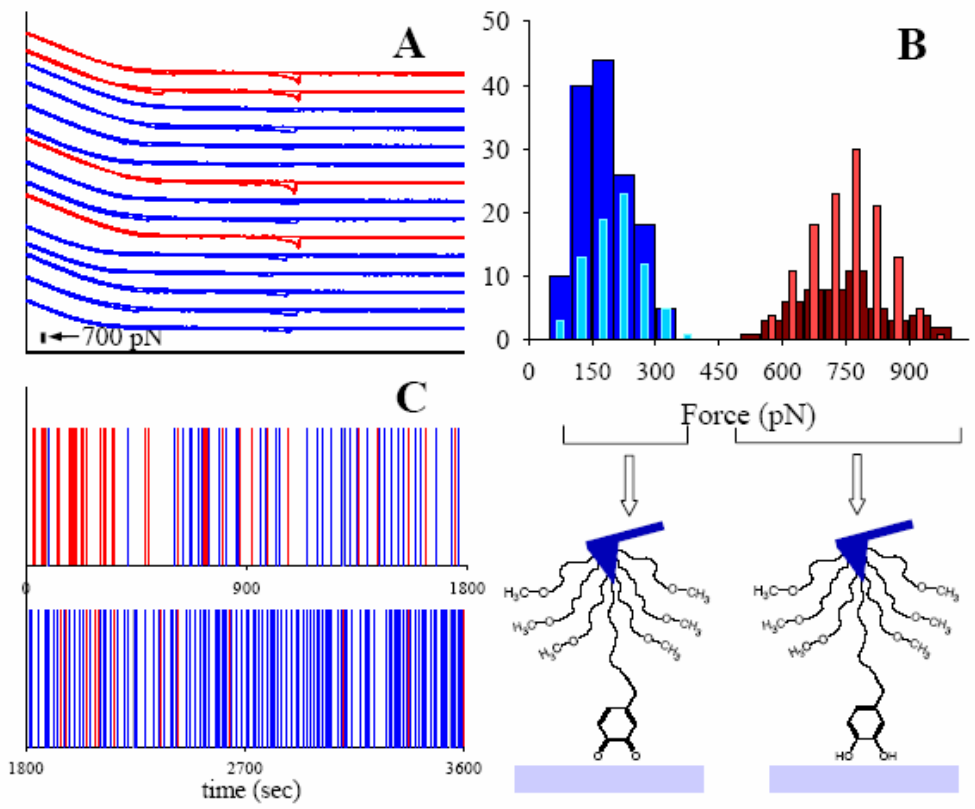

Figure 3-7. Oxidation of DOPA reduces adhesion to Ti surfaces.
A. Bimodal force signals from DOPA contacting Ti under alkaline pH conditions. Selected AFM force-distance scans obtained during a 1 hr experiment under alkaline conditions (20 mM Tris-Cl, pH 9.7) are shown with increasing time from top to bottom (top, t = 0; bottom, t = 1hr; 1800 repetitions total). Detectable force signals were found in ~10% of the force-distance curves obtained. Force-distance curves exhibiting strong DOPA-Ti interactions are shown in red, whereas force-distance curves shown in black exhibited much weaker interactions. The weak force signals only appeared under alkaline conditions and were not observed at neutral pH. B. Structure-based assignments of the adhesive molecules of DOPA and DOPA-quinone by analyzing the 1800 force-distance curves from each two pH conditions i.e. total 3600 F-D curves (pH 9.7 and 8.3). Bimodal force distributions were measured with averages of 180 ± 60 pN (145 events, pH 9.7) and 206 ± 66 pN (76 events, pH 8.3) in a low force regime whereas the distributions at high force were 740 ± 110 pN (51 events, pH 9.7) and 759 ± 88 pN (126 events, pH 8.3). Considering the pKa (= 9.2) of the DOPA hydroxyl group, the DOPA structure favors over DOPA-quinone at a low pH resulting in a more frequent detection at a high force region and vise versa. This result is agreed with the one shown in Figure 3-2, which was obtained under a neutral pH condition where no DOPAquinone adhesion was shown. Those pH dependent experiments confirmed structure based force assignments in which unoxidized DOPA-Ti interaction contributes strong adhesions whereas the weak binding is due to the DOPAquinone-Ti interactions. C. Time trajectory display of the force signals of DOPA (red) and DOPAquinone (black) at pH 9.7 (Time trajectory at pH 8.3 is available at Figure 3-8).

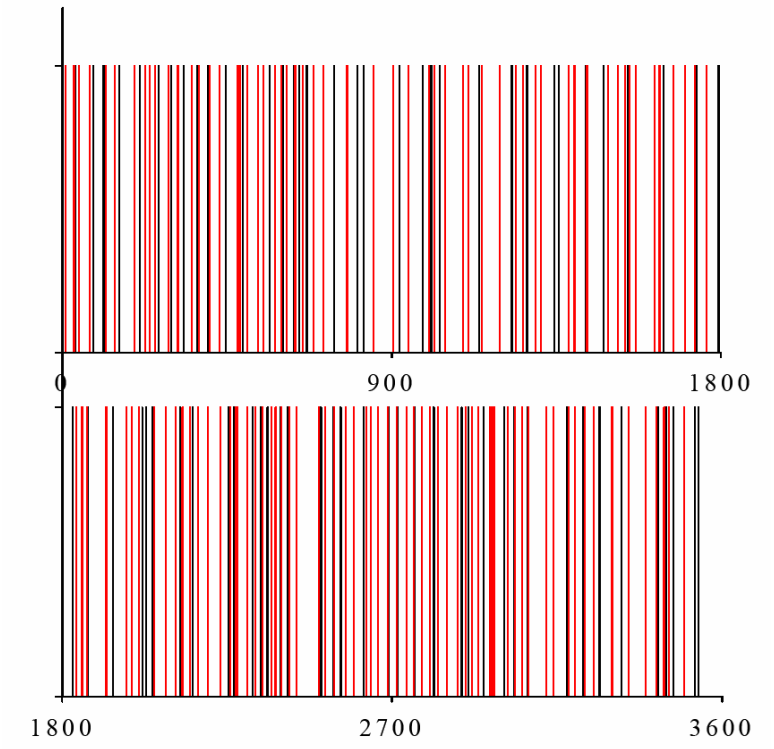

Figure 3-8. Time trajectory display of the AFM force signals of DOPA (red) and DOPA-quinone (black) on Ti observed over a 1 h period at pH 8.3. The strong DOPA adhesive force was observed 62.4% of the time whereas the DOPA-quinone frequency was 37.6 %.

DOPAquinone and either primary amines (*25*) or thiols (*68*), for example, have been speculated to give rise to bulk cohesive cross-linking of marine adhesive proteins. However, clear evidence for such reactions occurring at interfaces has been lacking.

Interfacial reactions between oxidized DOPA and organic surfaces were probed in three steps. First, the characteristic single-molecule DOPA-Ti interaction was identified through F-D curves obtained at neutral pH as described above. The Ti surface was then replaced with an amine modified Si surface (*70*) (Figure 3-9) and force experiments with the same tip were performed at pH 9.7. Initial F-D curves showed no significant hysteresis, however within a short period of time (156 seconds; 78^{th} contact/pull-off cycle) a dramatic increase in pull-off force to 2.2 nN is observed, after which an additional 800 contact/pull-off cycles revealed no measured interaction force (Figure 3-9, bottom curve). The extremely large force value together with the lack of subsequent adhesion events is consistent with covalent bond rupture, leading us to conclude that DOPA-nitrogen adducts form under the conditions of our experiment. We do not know where covalent bond breakage occurs, however the magnitude of the rupture force is consistent with rupture of a silicon-carbon bond (2.0 ± 0.3 nN)(*38*), suggesting that the broken covalent bond may be at the organic-inorganic interface. Although the pH used in our experiments is somewhat higher than that of seawater, we believe the results will be essentially similar at lower pH values, albeit with slower kinetics due to the shift in chemical equilibria of DOPAquinone/DOPA and NH_2/NH_3^+ towards DOPA and NH_3^+ species, respectively.

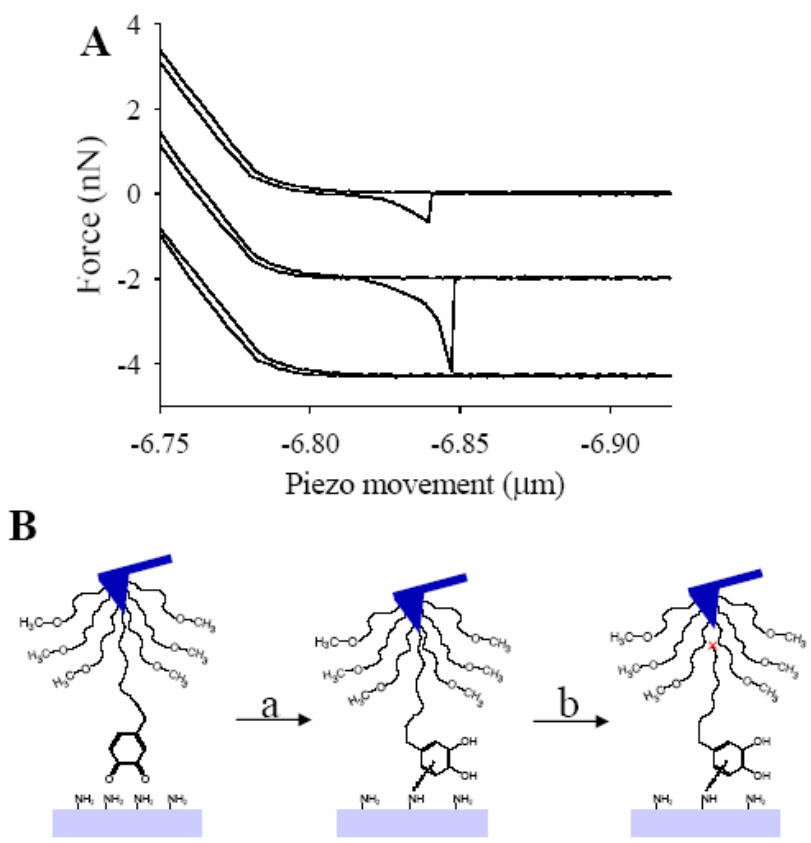

Figure 3-9. Oxidation of DOPA increases adhesion to organic surfaces.
A. Selected force-distance curves for interaction of a DOPA modified AFM tip with an organic surface. First, the presence of DOPA was confirmed by obtaining a force-distance curve at neutral pH on Ti (top curve), showing the expected pull-off force of ca. 800pN. Next, the same tip was allowed to interact with an amine presenting organic surface (see 3.2 Materials and Methods) at pH=9.7, upon which a pull-off force of 2.2 nN was observed (middle). The magnitude of the pull-off force is consistent with covalent bond rupture, and subsequent force-distance curves (N=800) failed to show a detectable interaction force (bottom). B. Schematic illustration of covalent bond formation between DOPA and amines at the organic surface. The high magnitude pull-off force, along with lack of subsequent observations of tip-molecule-surface interaction events, suggests that DOPAquinone formed a covalent bond to surface bound amine, possibly via a Michael addition type of reactions. The location of the ruptured covalent bond is not known, although under the conditions of this experiment it is not expected to re-form, explaining the lack of force observation in subsequent force-distance curves.

*3.3.4 Adhesion on Mucin Surfaces**

The strength of interaction between DOPA and adsorbed mucin was probed by measuring the force necessary to dissociate a DOPA modified AFM tip from a mucin coated TiO_2 substrate. The tips were prepared according to the method described by the previous section 3.2.1. As schematically illustrated in Figure 3-6A, the method results in a large excess of methoxy-terminated PEG on the tip, such that the probability of observing more than one DOPA residue per tip is low.

In previous sections, it has been demonstrated that a single DOPA residue exhibited a reversible binding force of ~800 pN on TiO_2 substrates. To employ this approach for determining DOPA-mucin interaction force, the presence of DOPA on the AFM tip was confirmed by measuring pull-off force on a pristine TiO_2 surface at neutral pH. The DOPA-TiO_2 force-distance (F-D) curves are shown in Figure 3-10A (black F-D curves, 748 and 812 pN respectively) and confirm the presence of a single DOPA residue on the AFM cantilever. The substrate was subsequently replaced with a mucin-coated TiO_2 substrate and additional F-D curves obtained at pH values of 4.5, 6.0, 7.4, and 8.5. Due to the single-molecule presence of DOPA on the AFM tip, the probability of detecting a DOPA-mucin interaction force when the tip was brought into contact with the mucin surface was observed to be less than 15%. Thus, most F-D curves exhibited no observable pull-off force, a common feature of single molecule experiments of this type (*71*).

For the tip-surface contacts where a clear DOPA-mucin interaction was observed during pull-off (Figure 3-10A, red curves), the F-D curves qualitatively exhibited features suggestive of a tethered polymer chain undergoing chain extension with increasing distance from the surface, followed by a rapid decrease to zero force. The pull-off events were directly attributable to the

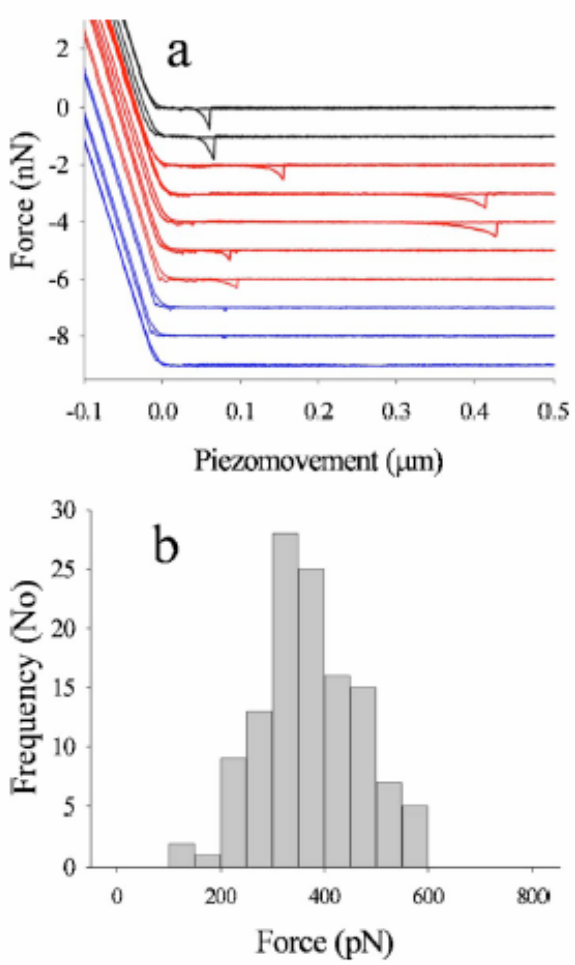

Figure 3-10. Single-molecule AFM results for interaction of DOPA with mucin.
A. Force-distance curves of DOPA-mucin interaction at pH 7.4. The AFM cantilever was first confirmed to contain PEG tethered N-Boc-DOPA by obtaining F-D curves on TiO_2 (black), revealing the expected ~800 pN pull-off force. After changing the substrate to mucin-coated TiO_2, DOPA-mucin interactions were revealed by force signals observable at pull-off distances of up to 400nm or more (red). DOPA free control AFM cantilevers prepared with methoxy terminated PEG showed only weak interactions with mucin (blue). B. Force histogram of DOPA-mucin interaction force. Statistical analysis revealed an average force value of 371 ± 98 pN (n = 121, pooled data for all pH value tested)

presence of DOPA, as control AFM tips prepared with methoxy terminated PEG (2kDa) exhibited very weak interactions (59 ± 18 pN) upon approach and retraction of the AFM tip (Figure 3-10A, blue F-D curves). The interaction between DOPA and mucin was apparently reversible, as similar F-D curves were observed upon repeated contacts between the tip and the mucin surface. This reversible property facilitated collection of a large number of F-D curves, from which a force histogram was prepared as shown in Figure 3-10B. The mean DOPA-mucin pull-off force at pH 7.4 was determined to be 356 ± 108 pN (n = 60/400). Consistent with the OWLS results for mucoadsorption of PEG-$(DOPA)_4$(*72*), the pull-off force was found to be independent of pH as summarized in Table 3-1.

An interesting feature of the F-D curves is the variable distance at which the DOPA-mucin pull-off event was observed (Figure 3-10A red, and Figure 3-11), which ranged from 59 nm to 428 nm from 'hard' tip-surface contact. The large observed pull-off distances are indicative of a very high mass molecule connecting the AFM tip to the TiO_2 surface. Given that the average end-to-end distance of a fully extended PEG chain of mass 3.4 kDa is less than 40 nm, and the magnitude of the pull-off force was inconsistent with that observed for DOPA-TiO_2, we eliminated the possibility that the pull-off event represented DOPA interacting with the underlying TiO_2 surfaces. We, therefore, interpret the extraordinarily large observed pull-off distances as arising from extension of the mucin protein, mediated through the interaction between DOPA and mucin.

3.4 Conclusions

The overall picture of mussel adhesion that emerges from our findings is one of unique chemical versatility that permits strong adhesion to both organic and inorganic surfaces. The conversion of

tyrosine to DOPA is a crucial event in MAP processing that leads to multiple adhesive roles for DOPA at interfaces. On inorganic surfaces the unoxidized DOPA forms high strength yet reversible coordination bonds, whereas on organic surfaces oxidized DOPA is capable of adhering via covalent bond formation. It may be that the remarkable ability of mussels to adhere to both organic and inorganic surfaces is related in part to the equilibrium that exists between DOPA and DOPA-quinone, allowing both species to interact with surfaces. It is also notable that interactions between DOPA and surfaces were unaffected by the presence of water, presumably a key feature in securing mussel adhesion in the marine environment. As our understanding of mussel adhesion expands, so do the prospects for exploiting this information for practical use. Indeed, the use of DOPA and related catecholic molecules has recently emerged as a promising method for anchoring synthetic and biological macromolecules onto oxide surfaces for medical applications (*73-75*).

Single-molecule measurements of the interaction force between DOPA and mucin revealed a surprisingly strong interaction between DOPA and mucin, although determining the origin of this interaction will require further study. As to the chemical basis of the DOPA-mucin interaction, we can immediately rule out covalent bond formation, as the magnitude of the pull-off force is several times lower than necessary to break a covalent bond, and the reversibility observed in the DOPA-mucin interaction also argues against covalent bond formation. On the other hand, it is noted that the measured interaction force between DOPA and mucin is quite large and over two times greater than that measured for interaction between a mucin peptide fragment and its antibody(*76, 77*). At this time we can only speculate that hydrogen bonding, hydrophobic interaction between DOPA and mucin. Further work will be necessary to fully elaborate the details.

Table 3-1. Mean pull-off force for DOPA-mucin interaction as a function of pH.

pH	**Force (pN)**	**N_{obs}**	**N_{total}**
4.5	366 ± 94	25	250
6.0	392 ± 83	27	340
7.4	356 ± 108	60	400
8.5	418 ± 76	9	68
pooled*	371 ± 98	121	1058
control**	59 ± 18	13	280

N_{obs} = number of F-D curves exhibiting pull-off event
N_{total} = total number of F-D curves performed
* pooled = pooled results for all pH values
** control = no DOPA, pooled results for all pH values

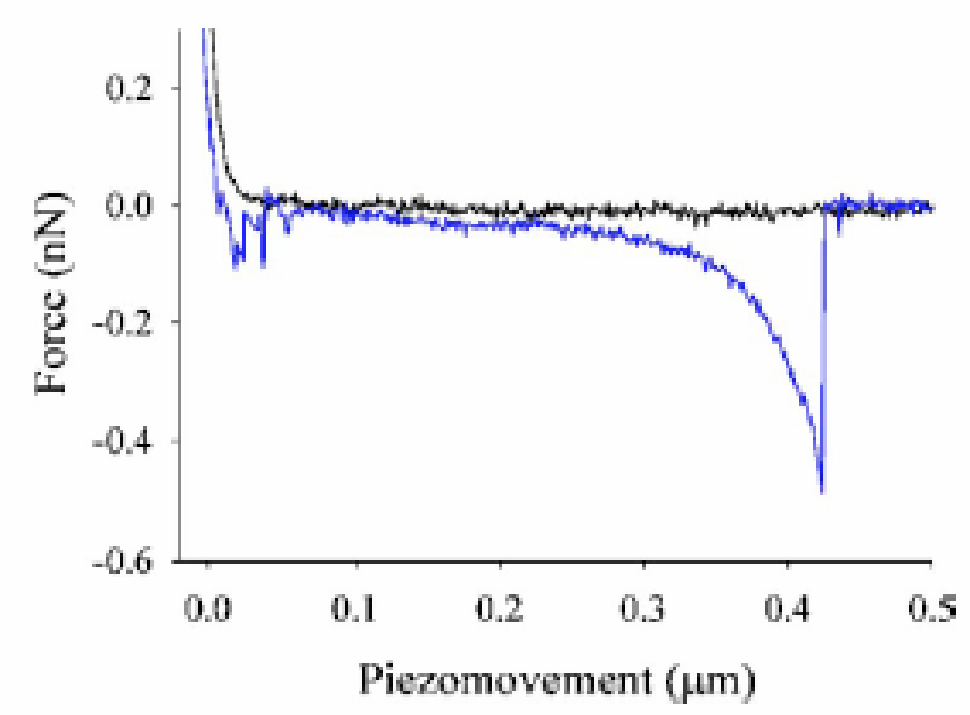

Figure 3-11. Detailed example of F-D curve showing approach (black) and retraction (blue) for interaction of DOPA with mucin at pH of 7.4.
The retraction curve deviated from the approach curve beginning at short distances and culminated in separation of DOPA from mucin at an extension of greater than 400 nm after which the force returned to zero.

3.5 Binding Energy of DOPA on TiO_2

3.5.1 Determination of Bond Dissociation Energy

The bond dissociation energy was calculated from the pulling rate dependence of the pull-off force as described by Evans and coworkers(*66*). The relationship between force (*F*) and pulling rate (*r*) is given by,

$$F = \left(\frac{kT}{x_b}\right) \cdot \ln\left(\frac{r}{k_0 \cdot kT / x_b}\right) = \left(\frac{kT}{x_b}\right) \cdot \ln r + \left(\frac{kT}{x_b}\right) \cdot \ln\left(\frac{k_0 kT}{x_b}\right) \qquad \text{Eq. (3-1)}$$

where x_b is the bond length, kT is the thermal energy. k_0 is given by

$$k_0 = v \cdot \exp\left(\frac{-E_b}{kT}\right) \qquad \text{Eq. (3-2)}$$

Where v is the molecular vibration frequency ($\sim 10^{10} s^{-1}$) and E_b is the bond dissociation energy.

3.5.2 Estimation of Bond Dissociation Energy for DOPAquinone on Ti

Since the Eq. 1 is linear, a plot of F vs. *ln*(r) would have a slope of $(\frac{kT}{x_b})$. Using x_b = 1.8×10^{-10} m from Fig. 2C gives $(\frac{kT}{x_b}) = 2.25 \times 10^{-11}$ (J/m).

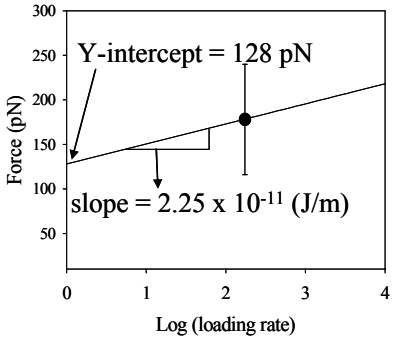

Based on the calculated slope and experimentally measured DOPAquinone-Ti force (180 pN at *ln*(r) = 2.24 from Figure 3-3B), the Y-intercept is estimated to be 128 pN (see plot above). k_0 is then determined from,

$$128\,pN = \left(\frac{kT}{x_b}\right)\cdot \ln\left(\frac{k_0 kT}{x_b}\right)$$

yielding a k_0 value of 1.32 x 10^{13} (s^{-1}). Finally, using Eq. 3-2, the bond dissociation energy for DOPAquinone-Ti was estimated to be 4.35 kcal/mol using Eq. 3-2.

Chapter 4: Polydopamine Coating: Mussel-inspired Surface Chemistry for Multifunctional Coatings

4.1 Objectives

We report a method to form multifunctional polymer coatings through simple dip-coating of objects in a dopamine aqueous solution. Inspired by the composition of mussel adhesive proteins, dopamine self-polymerizes to form thin, surface-adherent polydopamine films onto a wide range of inorganic and organic materials including noble metals, oxides, polymers, semiconductors, and ceramics. Secondary reactions can be used to create a variety of ad-layers, including self-assembled monolayers through deposition of long-chain molecular building blocks, metal films by electroless metallization, and bioinert and bioactive surfaces via grafting of macromolecules.

Methods for chemical modification of bulk material surfaces play central roles in modern chemical, biological and material sciences, and in applied science, engineering and technology (*78-81*). The existing toolbox for functional modification of material surfaces

includes methods such as self-assembled monolayer (SAM) formation, functionalized silanes, Langmuir-Blodgett deposition, layer-by-layer assembly, and genetically engineered surface-binding peptides (*82-86*). Although widely implemented in research, many available methods have limitations for widespread practical use; specific examples include the requirement for chemical specificity between interfacial modifiers and surfaces (e.g., alkanethiols on noble metals and silanes on oxides), the use of complex instrumentation and limitations of substrate size/shape (Langmuir-Blodgett deposition), or the need for multi-step procedures for implementation (layer-by-layer assembly and surface-binding genetically engineered peptides).

Development of simple and versatile strategies for surface modification of multiple classes of materials has proven challenging, and few generalized methods for accomplishing this have been previously reported (*87*). Our approach is inspired by the adhesive proteins secreted by mussels for attachment to wet surfaces (*54*). Mussels are promiscuous fouling organisms and have been shown to attach to virtually all types of inorganic and organic surfaces (*59*), including classically adhesion-resistant materials such as poly(tetrafluoroethylene) (PTFE) (Figure 4-1A). Clues to mussels' adhesive versatility may lie in the amino acid composition of proteins found near the plaque-substrate interface (Figure 4-1B-D), which are rich in 3,4-dihydroxy-L-phenylalanine (DOPA) and lysine amino acids (*15*). In addition to participating in reactions leading to bulk solidification of the adhesive(*11, 25, 88*), DOPA forms strong covalent and noncovalent interactions with substrates(*89*).

DOPA and other catechol compounds perform well as binding agents for coating inorganic surfaces (*60, 73-75, 90, 91*), however coating of organic surfaces has proven much more elusive. Hypothesizing that the coexistence of catechol (DOPA) and amine (lysine) groups

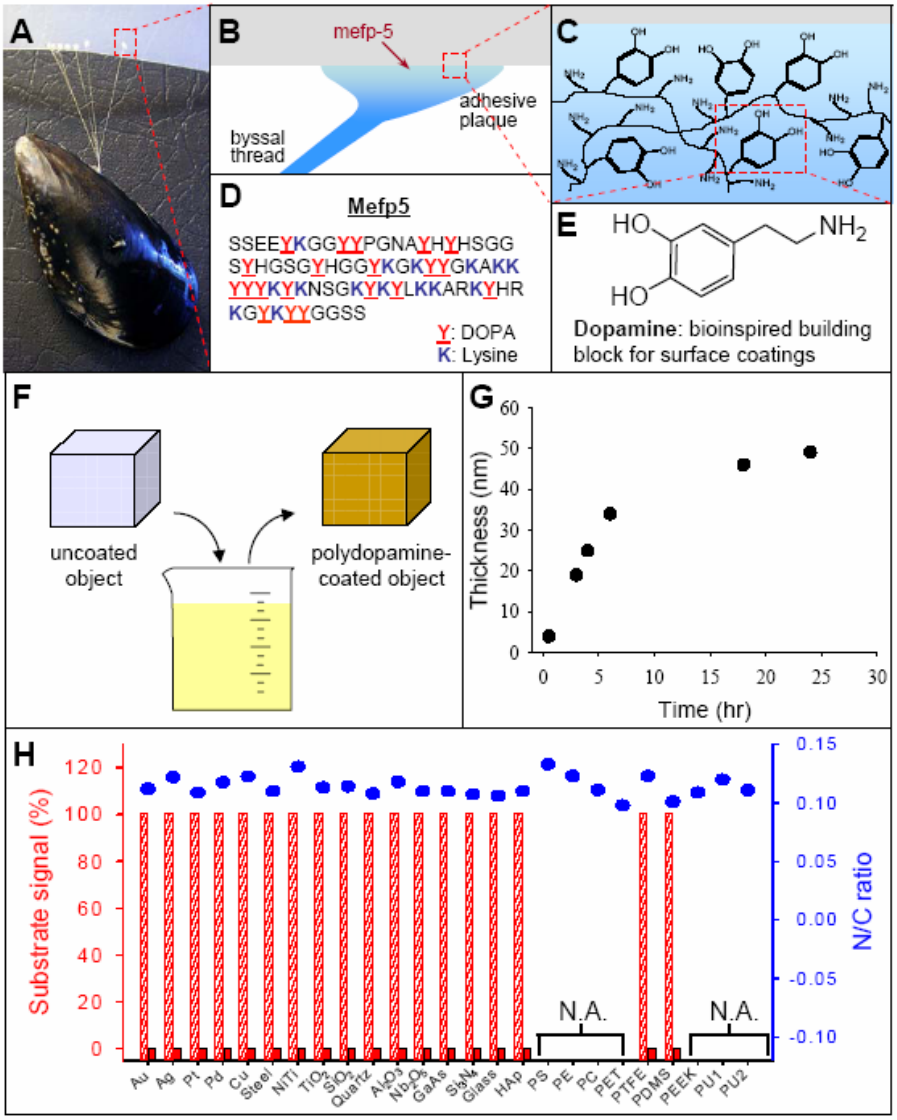

Figure 4-1. Mussel-inspired material-independent polydopamine coating.
A. Photograph of a mussel attached to commercial poly(tetrafluoroethylene) (PTFE). B and C. Schematic illustrations of the interfacial location of Mefp-5 and a simplified molecular representation of characteristic amine and catechol groups. D. The amino acid sequence of Mefp-5. E. Dopamine contains both amine and catechol functional groups found in Mefp-5 and was used as a molecular building block for polymer coatings. F. A schematic illustration of thin film deposition of polydopamine by dip-coating an object in an alkaline dopamine solution. G. Thickness evolution of polydopamine coating on Si as measured by AFM of patterned surfaces. H. XPS characterization of 25 different polydopamine-coated surfaces. The bar graph represents the intensity of characteristic substrate signal before (hatched) and after (filled) coating by polydopamine. The intensity of the unmodified substrate signal is in each case normalized to 100%. Substrates with characteristic XPS signals indistinguishable from polydopamine are marked by N.A. The blue circles represent the nitrogen-to-carbon ratio (N/C) after polydopamine coating (details of XPS data analysis are available in Figure 4-2 and Table 4-2).

may be crucial for achieving adhesion to a wide spectrum of materials, we identified dopamine as a small molecule compound that contains both functionalities (Figure 4-1E). It was previously shown that dopamine can be electropolymerized onto conducting surfaces(*92*). Here we show that this simple structural mimic of Mefp-5 is a powerful building block for spontaneous deposition of thin polymer films on virtually any bulk material surface, and that the deposited films are easily adapted for a remarkable variety of functional uses.

4.2 Materials and Methods

4.2.1 Materials

Platinum, silver, copper, and palladium (Alfa Aesar, Ward Hill, MA), sapphire (Al_2O_3, Rubicon Tech Inc. IL), quartz (MTI crystal, MA), stainless steel, NiTi, Si (MEMC electronics, Italy), Carbothane®, Tecoflex®, polycarbonate and polyethylene terephthalate (PET) (McMaster Carr Inc, Chicago, IL), poly(styrene) (Sigma), glass (Fischer scientific), polydimethysiloxane (PDMS, Sylgard 184, Dow corning), GaAs (University Wafer, Boston, MA), and silicon nitride (generous donation by Dr. Keun-Ho Kim and Prof. H. Espinosa, Northwestern University) were cleaned ultrasonically in 2-propanol for ten minutes before use. Titanium (20-50 nm) and gold (20 nm deposited onto 5 nm Ti) surfaces were prepared by electron beam deposition (Edwards FL400, Boc Edwards, Sussex, UK) on Si-wafers. PDMS (Dow Corning) was prepared by mixing 10 parts of backbone and 1 part of curing agent and cured at 100 ^{o}C for 2 hrs.

4.2.2 Polydopamine coating

Dopamine (2 mg/mL) was dissolved in 10 mM Tris-HCl (pH 8.5), and substrates were dipped into the solution. pH-induced oxidation changes the solution color to dark brown. Stirring and/or vertical sample orientations were necessary to prevent non-specific microparticle

deposition on surfaces. The coated surfaces were rinsed with ultrapure water and dried by N_2 gas before storage or treated as described below for ad-layer formation. Surfaces coated in this manner remain stable on inorganic substrates unless scratched, treated by ultrasound, or dipped in a strong acid solution (< pH 1). Coatings on some organic substrates such as commercial plastics, latex beads and Sephadex resins remain stable even in the presence of 1 N HCl combined with ultrasound.

Incubation of dopamine solution at room temperature for several days (>3days) prior to immersion of substrates did not produce surface discoloration (to dark-brown) typical of polydopamine coatings, indicating that the coating did not occur or was too thin to observe visually. Furthermore, the coating reaction appears to be prevented under anaerobic conditions, as purging of dopamine solution with argon resulted in dramatically reduced solution color change and coating formation on immersed substrates.

4.2.3 Polydopamine-assisted electroless metallization

Polydopamine coated substrates were metallized through immersion in copper(II) or silver salt solutions. For electroless copper plating, a solution of 50 mM ethylenediaminetetraacetic acid (EDTA), 50 mM copper(II) chloride ($CuCl_2$), and 0.1 M Boric Acid (H_3BO_3) was prepared in ultrapure water, and the pH was adjusted to 7.0 using 1 N of NaOH. This solution can be stored in a refrigerator for future use. Immediately before use, 0.1 M dimethylamine-borane (DMAB) was added to the copper plating solution, after which polydopamine-coated substrates were placed in the solution for 2-3 hrs at 30°C. Surfaces were then washed with ultrapure water and dried with N_2 gas.

For electroless silver deposition, use of an exogenous reducing agent was not necessary, implying oxidation of the underlying polydopamine layer during metal ion reduction. Polydopamine-coated surfaces were dipped into a 50 mM aqueous silver nitrate solution for 18 hrs (room temperature). Surfaces were then washed with ultrapure water and dried with N_2 gas.

4.2.4 Photolithography

Photoresist (Microposit S-1818, Shipley, Marlborough, MA) was spin-cast at 4000 rpm for 50 sec and then baked for 1 min at 95 ^{o}C. Utilizing a contact mask aligner (Q2000, Quintel Corp. San Jose, CA), the photoresist was exposed to UV (345 nm) light for 6 s and was subsequently developed for 40 sec (MF-CD-26, Shipley, MA). Polydopamine coating was applied to the patterned surfaces for 3 - 6 hrs as described above. Finally, photoresist was removed by immersion in N-methyl-pyrollidinone (NMP) for 5-10 sec. The patterned surfaces were used to measure the coating thickness and electroless silver metallization.

4.2.5 Polydopamine-assisted self-assembled monolayer formation and PEG grafting.

For alkanethiol ad-layer formation, 5 mM of dodecanethiol (Sigma-Aldrich, Milwaukee, WI), 1-mercapto-11-undecyl tri(ethylene glycol) (OEG3-C11-SH), or OEG6-C11-SH (Asemblon Inc, Redmond, WA) was dissolved in dichloromethane (DCM) which was pre-equilibrated by bubbling with He or N_2. Polydopmaine-coated substrates were subsequently added followed by triethylamine (final concentration 10 mM). After 5hrs or more (typically overnight reaction for 18 hrs), the substrates were rinsed by either DCM or ethanol and dried with N_2.

For PEG grafting, 5 mg/mL of methoxy-poly(ethylene glycol)-thiol (mPEG-SH, 5 kDa, SunBio, Ahn-Yang, South Korea) or methoxy-poly(ethylene glycol)-amine (mPEG-NH_2, 5 kDa, Nektar, San Carlos, CA) was dissolved in 10 mM Tris pH 8.0 or sodium phosphate buffer pH 8.0. The buffer used for mPEG-SH was vacuum degassed for >1 hr to prevent oxidation (-S-S-)

between thiol groups.

4.2.6 Short-term (4hr) fibroblast adhesion

3T3-Swiss albino fibroblasts (ATCC, Manassas, VA) were maintained at 37 ^{o}C with 5% CO_2 in Dulbecco's Modified Eagle's medium (DMEM, Cellgro, Herndon, VA) containing 10% fetal bovine serum (FBS) and 100 μg/ml of penicillin and 100 U/ml of streptomycin. Trypsinized cells were resuspended in DMEM with 10% FBS and then counted for sub-cultures and/or seeded onto the test substrates at a cell density of 5.0 x 10^3 cells/cm^2. After 4 hrs, cells were stained with 2.5 μM calcein-AM (Molecular Probes) in complete PBS for 1 hr at 37 ^{o}C culture. Cell attachment was quantified by acquiring nine images from random locations of each substrate using a fluorescence microscope (Olympus BX-40, λ_{ex}=549 nm, λ_{em}=565 nm) equipped with a CCD camera (Roper Scientific, Trenton, NJ). Finally, the resulting images were processed using Metamorph software (Universial Imaging, Downington, PA).

4.2.7 Surface characterization

XPS spectra were obtained using an Omicron ESCALAB (Omicron, Taunusstein, Germany) with a monochromatic Al Kα (1486.8 eV) 300-W X-ray source, a flood gun to counter charging effects, and ultrahigh vacuum (~10^{-9} torr). The takeoff angle was fixed at 45^{o} except as otherwise mentioned. High-resolution scans were acquired to calculate the chemical compositions of the surfaces. Time-of-flight secondary ion mass spectroscopy (Physical Electronics, Eden Prairie, MN) was used to characterize the atomic composition of polydopamine coatings and metal ad-layers (copper and silver). The mass spectrometer was equipped with Ga ion gun operated at 15 keV with a raster size of typically 100-200 μm. Multi-

mode atomic force microscopy (Veeco Inc., Santa Barbara, CA) was used for imaging (tapping-mode using Si-cantilever, Veecoprobes, resonance frequency = 210-240 kHz)).

4.2.8 Total internal reflection fluorescence (TIRF) microscopy.

Detailed experimental procedures have been described elsewhere(*93*). Briefly, an Olympus IX71 inverted fluorescence microscope (Melville, NY) and a 60x objective (Olympus, N.A.=1.45 oil immersion) were used for single-molecule adsorption images. A 532-nm laser (New Focus 3951-20, 20 mW power, San Jose, CA) was used as a light source. An O.D. = 1 neutral density filter was used for most experiments. The incident laser power was roughly 0.5 mW, illuminating a circular region of 40 μm in diameter. After excitation, the emitted photons were collected by a filter cube (Chroma Q560LPBS, HQ585/40M, Rockingham, VT), magnified by a 3.3x eyepiece and detected by a TE-cooled and frame-transfer charge-coupled CCD detector (Andor, DV435-BV, South Windsor, CT). The protein used in this experiment was Cy3 conjugated Enigma homolog (Enh). The protein was dissolved in 50 mM phosphate buffer pH 7.0 (1 μM) and experiments performed at room temperature (exposure time = 33 msec).

4.2.9 Polydopamine-assisted grafting of hyaluronic acid (HA) adlayer

17 kDa HA (Lifecore, Chaska, MN) was thiolated using a previously published protocol(*94*). The modified HA had approximately 50% substitution (by NMR) with thiol groups. Thiolated HA (0.001 – 2 mg/mL in de-oxygenated 10 mM Tris buffer, pH 8.0) was reacted with polydopamine-coated substrates for typically overnight to yield HA-functionalized surfaces. HA-tethered, polydopamine-coated glass or indium-tin oxide (ITO) surfaces were attached to a bottomless 16-well chamber slide (Nunc, Rochester, NY) via the injection of a self-curing silicone rubber (Silastic® Dow Corning) gasket. For TCPS, standard 96-well plates were used,

and the polydopamine coating and HA ad-layer formation steps were performed directly in each well.

4.2.10 M07e cell culture

M07e cells (DMSZ, Germany) were adapted to grow in IMDM (Sigma) supplemented with 2.5% FBS (Hyclone), 10 ng/mL GM-CSF (Berlex Laboratories), and 1 mg/mL gentamicin sulfate (Sigma). Cells were maintained in exponential growth phase between 5 x 10^5 and 1 x 10^6 cells/mL. Normal-force cell adhesion assays were performed as previously described(*95*). Briefly, M07e cells were stained with 5 μg/mL Calcein AM (Molecular Probes) in PBS and incubated in normal growth media on surfaces for 2h prior to removal of non-adherent cells by inverted centrifugation at 30 rcf. Image analysis of pre- and post-spin images was used to calculate the percent cell adhesion. Substrates for extended cell culture were sterilized with short-wave UV light for 30 minutes prior to seeding cells in normal growth medium at a density of 3.75 x 10^5 cells/mL. Adhesion was measured on days 2 and 4 using the normal-force cell adhesion assay. However, in this case the cells were stained directly in the wells via addition of 40 uL of Calcein AM (diluted to 5 μg/mL PBS) 30 minutes prior to pre-centrifugation imaging. For HA competition, soluble 17 kDa HA was incubated with M07e cells for 30 minutes at 37 ^oC prior to loading onto HA-tethered, polydopamine-coated wells. For M07e expansion assay, cell density was measured by total nuclei counts in a solution of hexadecyltrimethylammoniumbromide (Sigma; 30g/L), sodium chloride (8.33 g/L) and EDTA (366.25 mg/L) with a Coulter Multisizer.

4.2.11 Flow cytometry analysis of CD44 levels on M07e cells

Flow cytometry was used to determine the expression levels of the HA receptor CD44 on M07e cells. Briefly, cells were washed with PBS containing 1 g/L sodium azide and 0.5%

bovine serum albumin. Allophycocyanin (APC)-conjugated mouse anti-human-CD44 antibody or APC-conjugated isotype control mouse-$IgG_{2b,\kappa}$ antibody (Becton Dickinson) were incubated with the cells for 30 minutes at room temperature. After washing, cells were analyzed on a Becton Dickinson LSRII flow cytometer using FACSDiva software (Becton Dickinson).

4.3 Results and Discussions

4.3.1 Polydopamine coating on a variety of material surfaces

Simple immersion of substrates in a dilute aqueous solution of dopamine buffered to a pH typical of marine environments (2 mg/mL dopamine, 10 mM Tris, pH 8.5), resulted in spontaneous deposition of a thin adherent polymer film (Figure 4-1F,G,H). Analysis using atomic force microscopy (AFM) indicated that the polymer film thickness was a function of the immersion time and reached a value of up to 50 nm after 24 hours (Figure 4-1G). X-ray photoelectron spectroscopy (XPS) analysis of 25 diverse materials coated for 3 hours or more revealed the absence of signals unique to the substrate (red bars, Figure 4-1H, and Figure 4-2), indicating the formation of a polymer coating of 10 nm or more in thickness. Little variation in the atomic composition of the coating was found (blue dots, Figure 4-1H), suggesting that the composition of the polymer coating was independent of substrate. The nitrogen-to-carbon signal ratio (N/C) of 0.1 - 0.13 is similar to the theoretical value for dopamine (N/C = 0.125), implying that the coating is derived from dopamine polymerization. Evidence for dopamine polymerization was found through analysis of the modification solution by gel permeation chromatography (Figure 4-3) and of coated substrates by time-of-flight secondary-ion mass spectrometry (ToF-SIMS) (Figure 4-4). Polymer was found both in solution and on the substrate,

with ToF-SIMS clearly revealing signals corresponding to dihydroxyphenyl-containing polymer fragments. Although the exact polymerization mechanism is unknown at this time, it is likely to involve oxidation of the catechol to a quinone followed by polymerization in a manner reminiscent of melanin formation, which occurs through polymerization of structurally similar compounds (*96*) (Figure 4-4).

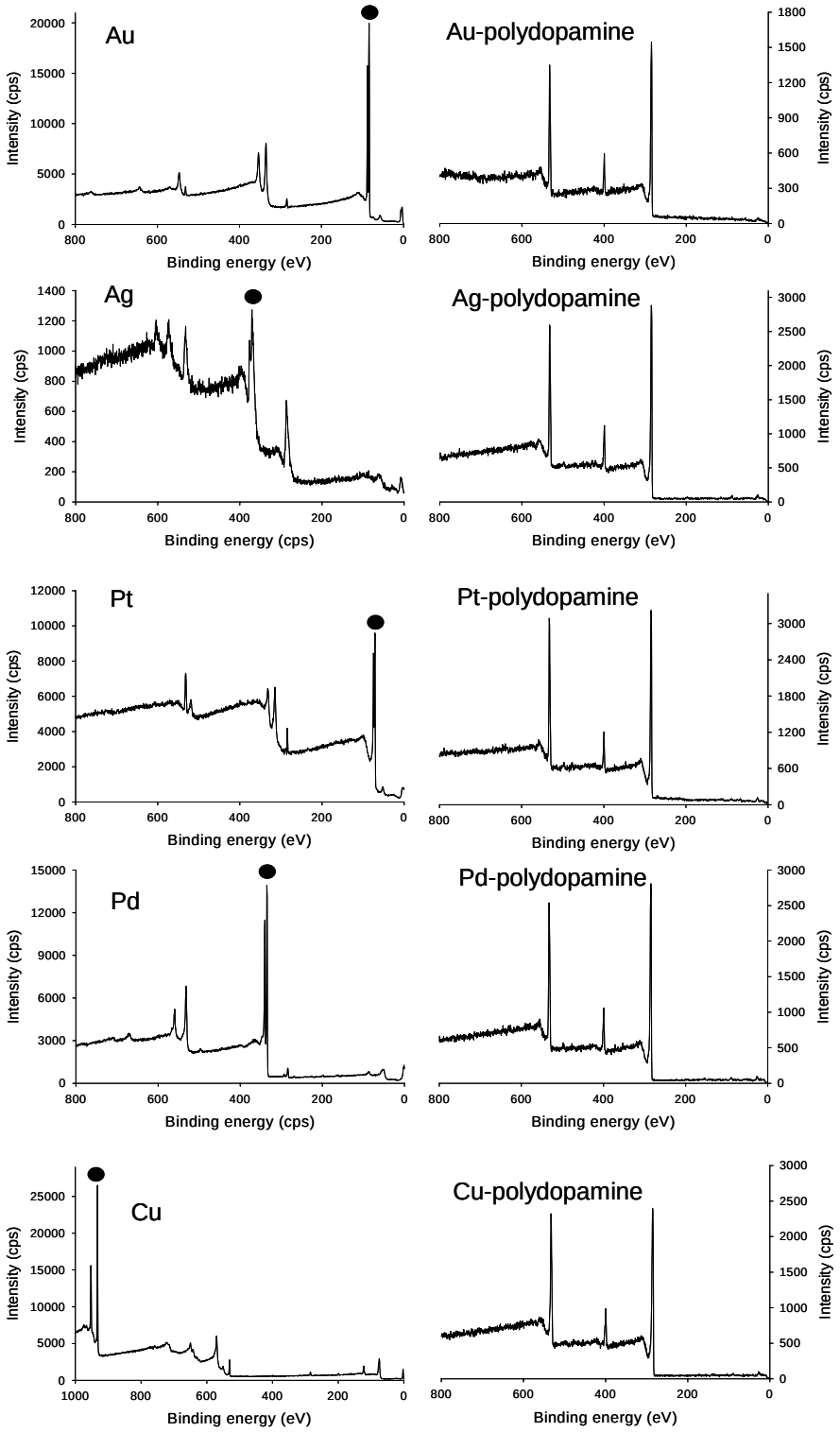
Au
Au-polydopamine
Ag
Ag-polydopamine
Pt
Pt-polydopamine
Pd
Pd-polydopamine
Cu
Cu-polydopamine
Intensity (cps)
Binding energy (eV)
Binding energy (cps)

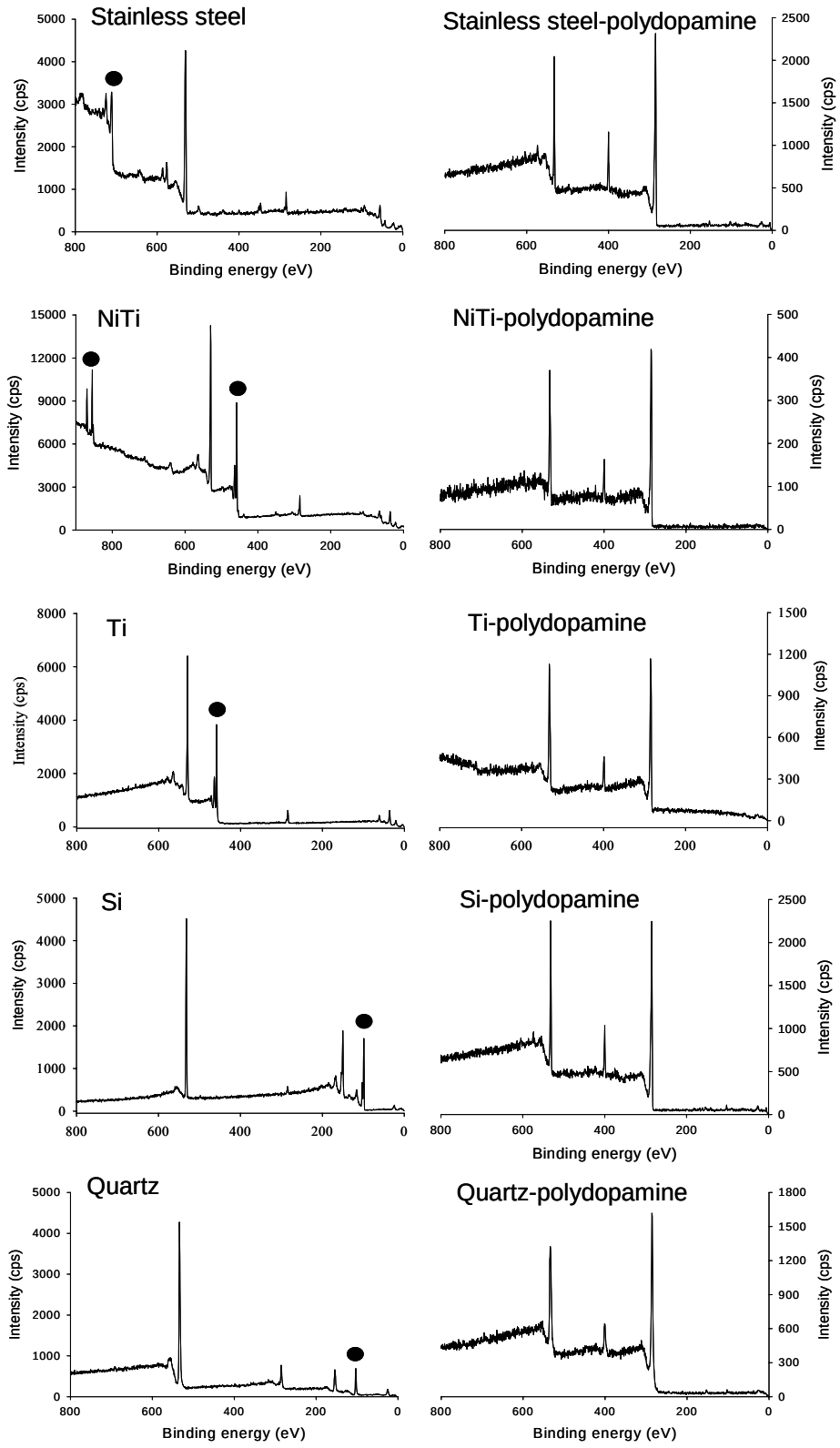
Stainless steel
Stainless steel-polydopamine
NiTi
NiTi-polydopamine
Ti
Ti-polydopamine
Si
Si-polydopamine
Quartz
Quartz-polydopamine
Intensity (cps)
Binding energy (eV)

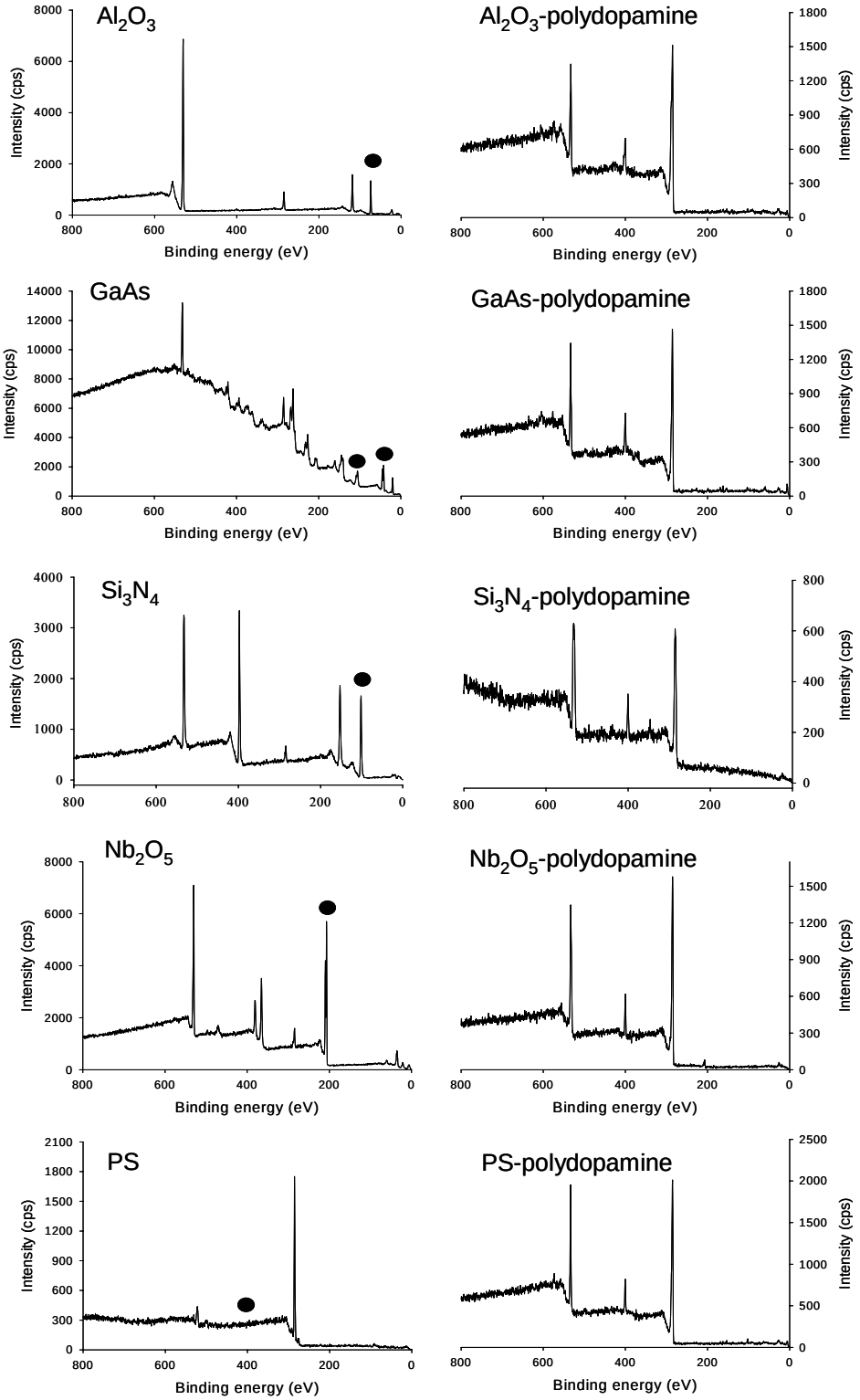
Al2O3
Al2O3-polydopamine
GaAs
GaAs-polydopamine
Si3N4
Si3N4-polydopamine
Nb2O5
Nb2O5-polydopamine
PS
PS-polydopamine
Intensity (cps)
Binding energy (eV)

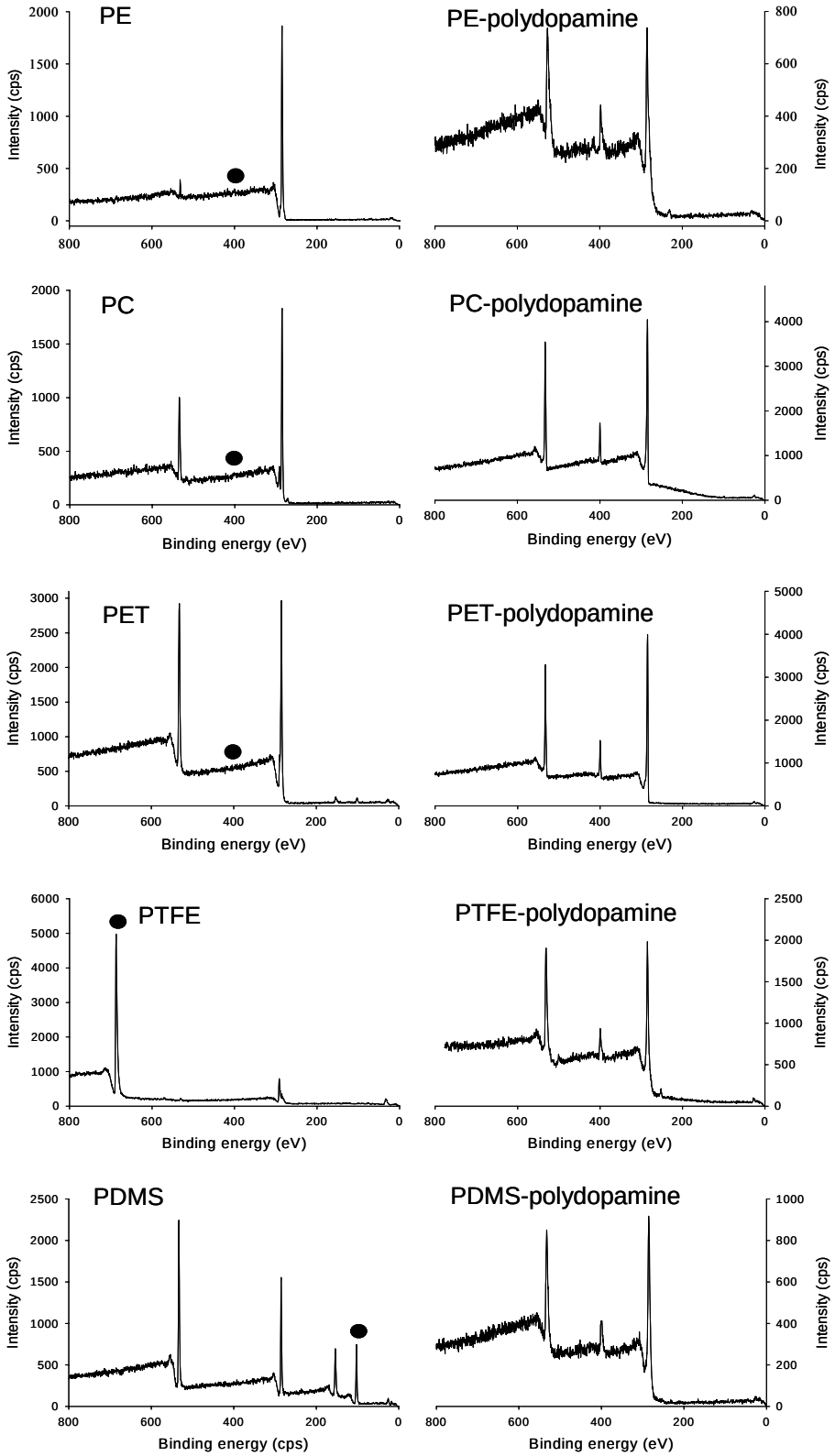
PE
PE-polydopamine
PC
PC-polydopamine
PET
PET-polydopamine
PTFE
PTFE-polydopamine
PDMS
PDMS-polydopamine
Intensity (cps)
Binding energy (eV)
Binding energy (cps)

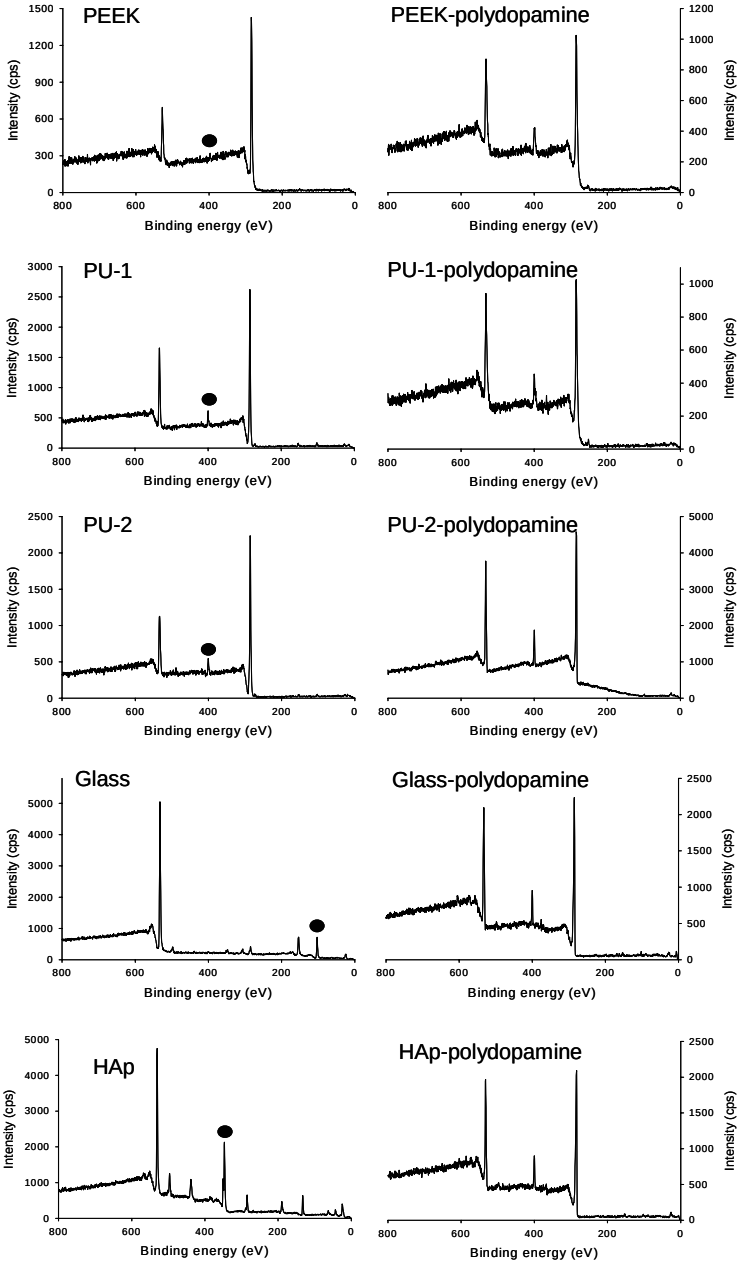

Figure 4-2. XPS characterization of polydopamine-coated surfaces
XPS spectral changes of 25 test materials before and after polydopamine coating. The characteristic XPS substrate signals for unmodified substrates (left) were marked by filled circles, which were completely suppressed after polydopamine coating (right). Instead, carbon (~285 eV), nitrogen (~399.5 eV), and oxygen (~532.5 eV) photoelectron peaks (in order from low to high binding energy) were observed. The area ratio of nitrogen-to-carbon was determined for 25 different substrates, and those values are shown in Figure 1H (blue scatter plot). Substrate XPS peaks used in the experiments were summarized in Table 4-1.

Table 4-1. Substrates and corresponding atoms (binding energy and orbital) used as characteristic substrate peaks for XPS characterization shown in Figure 4-1H (Asterisk * indicates synthetic, polymeric substrates without unique XPS signals except for carbon, nitrogen and oxygen. Polydopamine coating on those substrates was confirmed by the appearance of N1s signal after coating as shown in Figure 4-2 (399.5 eV for PS, 399.1 eV for PE, 399.7 eV for PC, 399.6 eV for PET, and 399.8 eV for PEEK). Polydopamine coating on PU-1,2 was confirmed by the nitrogen-to-carbon ratio after coating due to the presence of substrate nitrogen)

Substrate	**Binding energy (eV) (photoelectron orbital)**
Au	84.1/84.9 ($Au4f_{7/2,5/2}$)
Ag	369.9/373.9 ($Ag3d_{5/2,3/2}$)
Pt	71.1/74.7 ($Pt4f_{7/2,5/2}$)
Cu	952.5/932.5 ($Cu2p_{1/2,3/2}$)
Pd	335.1/340.5 ($Pd3d_{5/2,3/2}$)
Stainless steel	740.0/723.0 ($Fe2p_{3/2,1/2}$)
TiO_2	456.5/462.4 ($Ti2p_{3/2,1/2}$)
NiTi	854.1/870.9 ($Ni2p_{3/2,1/2}$)
Quartz, Glass	103(quartz), 102(glass) (Si2p)
SiO_2, Si_3N_4	99.2/99.8 ($Si2p_{3/2,1/2}$)
Al_2O_3	118.6 (Al_{2s})
GaAs	41.7, 106.5 ($As3d_{3/2}$, $Ga3p_{1/2}$)
PDMS	102.2 (Si2p)
Nb_2O_5	207/209.5 ($Nb3d_{5/2,3/2}$)
PTFE	686.1 (F1s)
PS*	284.7 (C1s)
PE*	284.8 (C1s)
PC*	284.7 (C1s)
PET*	284.7 (C1s)
PEEK*	284.8 (C1s)
HAp	346.5/350.2 ($Ca2p_{3/2,1/2}$)

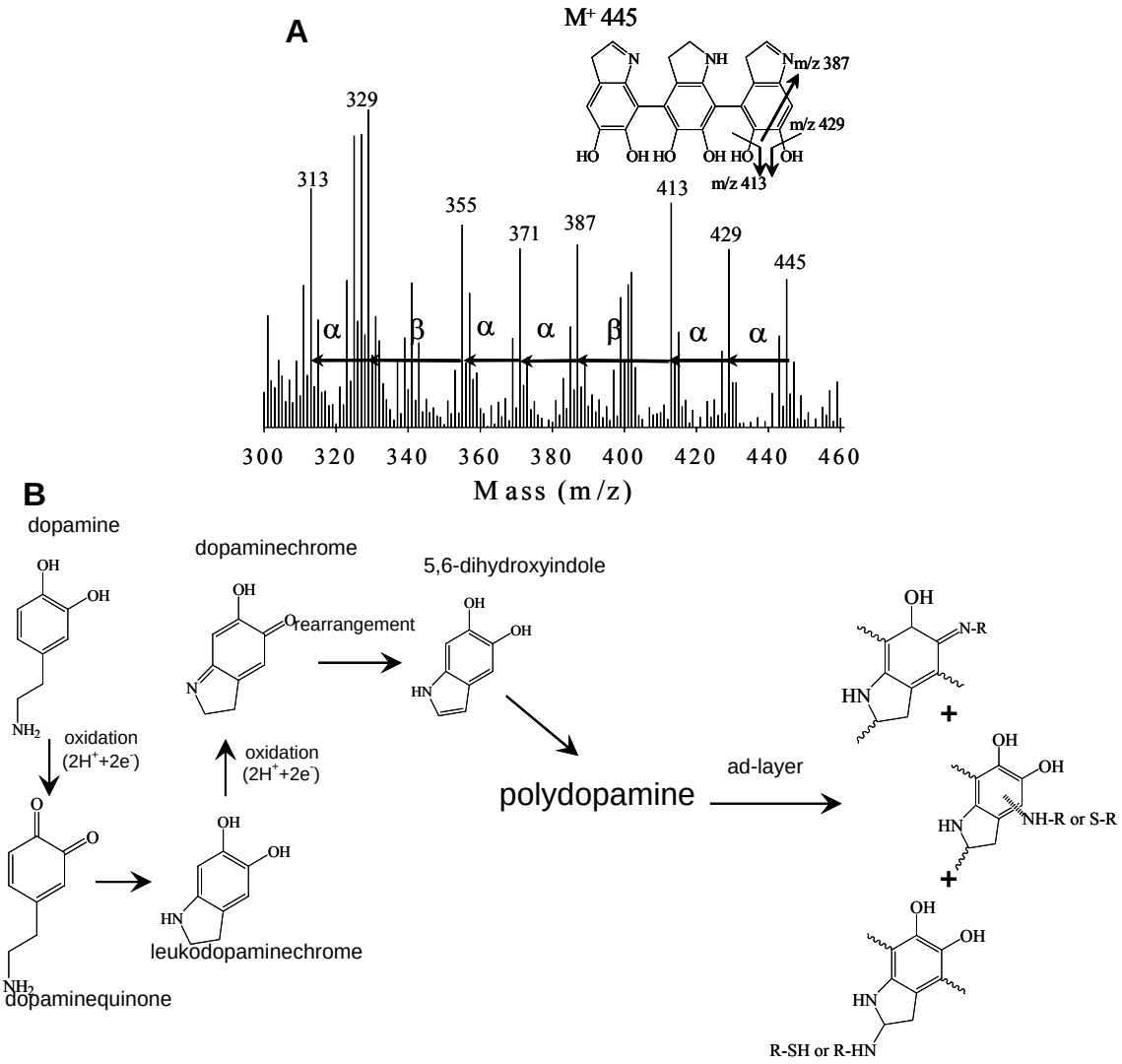

Figure 4-3. ToF-SIMS analysis of polydopamine coating, suggested reaction, and organic ad-layer formation mechanisms

A. ToF-SIMS spectra of polydopamine-coated glass. The mass spectrum showed a trimer of 5,6-dihydroxyindole, possibly fragmented from a long-chain polymer of similar composition. The characteristic pattern of fragmentation (α → α → β) suggests liberation of two hydroxyl groups and a portion of the phenyl group, identifying each subunit as derived from dopamine polymerization. B. Possible structural evolution and polymerization mechanisms of dopamine as well as suggested reaction mechanisms for organic ad-layer formation on polydopamine-coated substrates. Under an oxidative condition, e.g. alkaline pH, dihydroxyl group protons in dopamine are deprotonated, becoming dopamine-quinone, which subsequently rearranges via intramolecular cyclization to leukodopaminechrome. Further oxidation and rearrangement leads to 5,6 dihydroxyindole, whose further oxidation causes inter-molcular cross-linking to yield a polymer that is structurally similar to the bio-pigment melanin. The polydopamine-coated surface subsequently reacts with a variety of molecules via Shiff-base (top) and Michael addition chemistries.

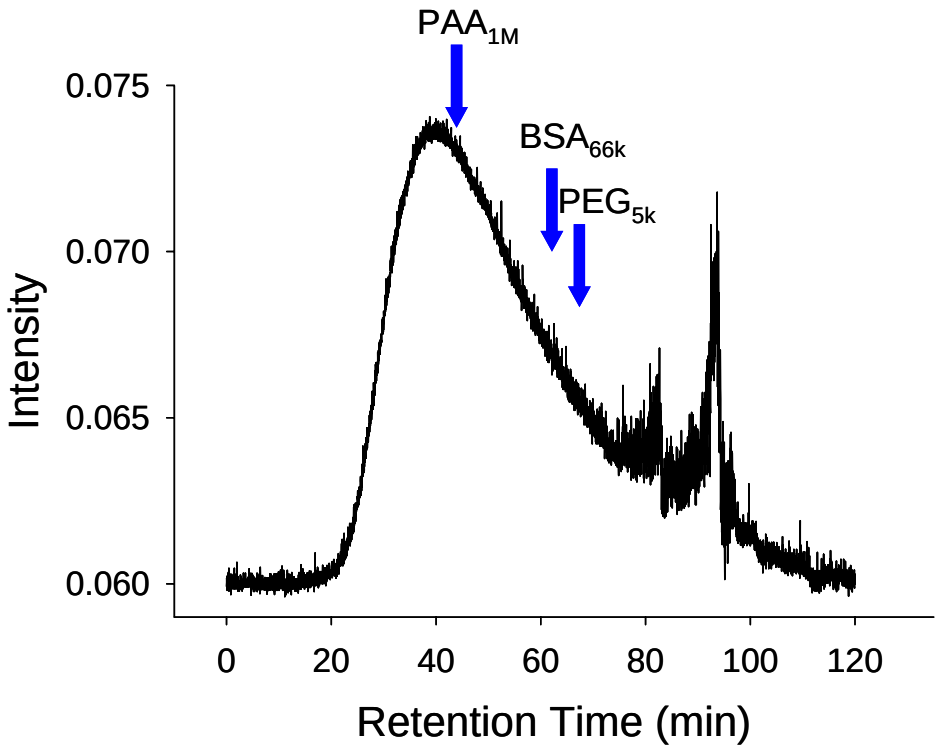

Figure 4-4. Gel permeation chromatography analysis of polydopamine solution. Mobile phase buffer: 50 mM sodium phosphate, 100 mM NaCl, pH 6.5 with a flow rate of 0.3 mL/mim. The sample was filtered before injection (pore size ~ 0.8 μm) and the retention times of molecular weight standards are indicated by the blue arrows. The broad peak at a retention time ~40min correlates to polydopamine at an approximate molecular weight of about several million Dalton based on molecular weight standards (PEG 5kDa, Bovine Serum Albumin (BSA) 66kDa, and polyacrylic acid (PAA)~ 1 MDa). A second peak at an elution time of 80 min indicates oligomer formation, and a third peak found at the retention time of 95 min is due to a contaminant in the GPC system.

The polydopamine coating is able to form on virtually all types of material surfaces (Figure 4-1H): noble metals (Au, Ag, Pt and Pd), metals with native oxide surfaces (Cu, stainless steel, NiTi shape memory alloy), oxides (TiO_2, SiO_2, quartz, Al_2O_3, and Nb_2O_5), semiconductors (GaAs and Si_3N_4), ceramics (glass and hydroxyapatite (HAp), and synthetic polymers (polystyrene (PS), polyethylene (PE), polycarbonate (PC), polyethylene terephthalate (PET), polytetrafluoroethylene (PTFE), polydimethylsiloxane (PDMS), polyetheretherketone (PEEK), and polyurethanes (carbothane® (PU1) and tecoflex® (PU2))).

4.3.2 Polydopamine-assisted secondary functionalization: electroless metallization

The polydopamine coating was found to be an amazingly versatile platform for secondary reactions, leading to tailoring of the coatings for diverse functional uses. For example, the metal binding ability of catechols (*97*) present in the polydopamine coating was exploited to deposit adherent and uniform metal coatings onto substrates by electroless metallization. This was demonstrated through deposition of silver and copper metal films via dip-coating of polydopamine-coated objects into silver nitrate and copper(II) chloride solutions, respectively (Figure 4-5). Metal film deposition was confirmed by XPS and ToF-SIMS analysis, which demonstrated successful metal film deposition on a number of ceramic, polymer and metal substrates: nitrocellulose, coinage metals, commercial plastics, silicon nitride, glass, gold, titanium, Si, polycarbonate, polystyrene, PEEK, gold, niobium oxide, aluminum oxide, and nickel-titanium (Figures 4-6 and 4-7). Metal coatings were successfully applied in this manner to flexible polymer substrates and bulk objects with complex shapes (Figure 4-5A-C), as well as to flat surfaces in which the polydopamine coating had been patterned using standard photolithography techniques (Figure 4-5D-F). Unlike many other approaches to electroless metallization (*98*), the use of (immobilized) colloidal metal seed particles was unnecessary for

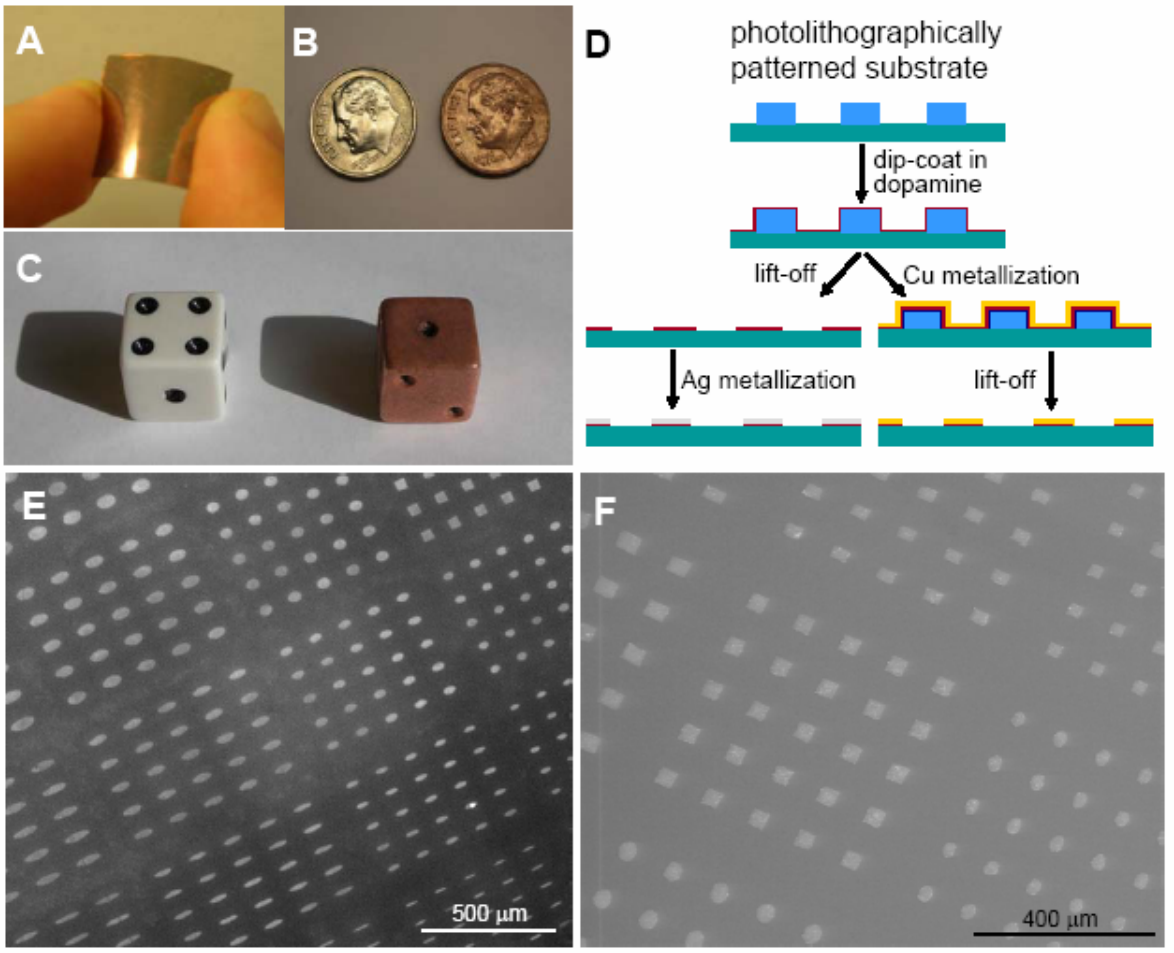

Figure 4-5 Polydopamine-assisted electroless metallization of substrates.
A-C. Electroless copper deposition on polydopamine-coated (A) nitrocellulose film, (B) coin, and (C) three-dimensional plastic object. D. Schematic representation of electroless metallization of photoresist-patterned surfaces coated with polydopamine. Photoresist (blue) was removed before silver metallization (left) or after copper metallization (right). E and F. Scanning electron microscopy (SEM) images showing micropatterns of silver on Si (E) and copper on a glass substrate (F).

spontaneous formation of adherent metal films. In the case of silver film deposition the apparent reductive capacity of the polydopamine sub-layer was sufficient to eliminate the need for addition of exogenous reducing agent in the metal salt solution, implying oxidation of the underlying polydopamine layer.

4.3.3 Polydopamine-assisted surface reactions

Polydopamine coatings also support a variety of reactions with organic species for the creation of functional organic ad-layers. For example, under oxidizing conditions, it is known that catechols react with thiols and amines via Michael addition or Schiff base reactions(*25, 99*) (Figure 4-4B). Thus, immersion of polydopamine-coated surfaces into a thiol- or amine-containing solution provided a convenient route to organic ad-layer deposition through thiol- and amine-catechol adduct formation (Figure 4-8A). We demonstrated this approach for deposition of organic ad-layers in the form of alkanethiol monolayer, synthetic polymer, and biopolymer coatings.

A monolayer of alkanethiol was spontaneously formed through simple immersion of polydopamine-coated substrates (Figure 4-8B). Monolayer formation on the polydopamine sub-layer is believed to involve reaction between terminal thiol groups and the catechol/quinone groups of the polydopamine coating, in a manner analogous to the reaction between thiols and

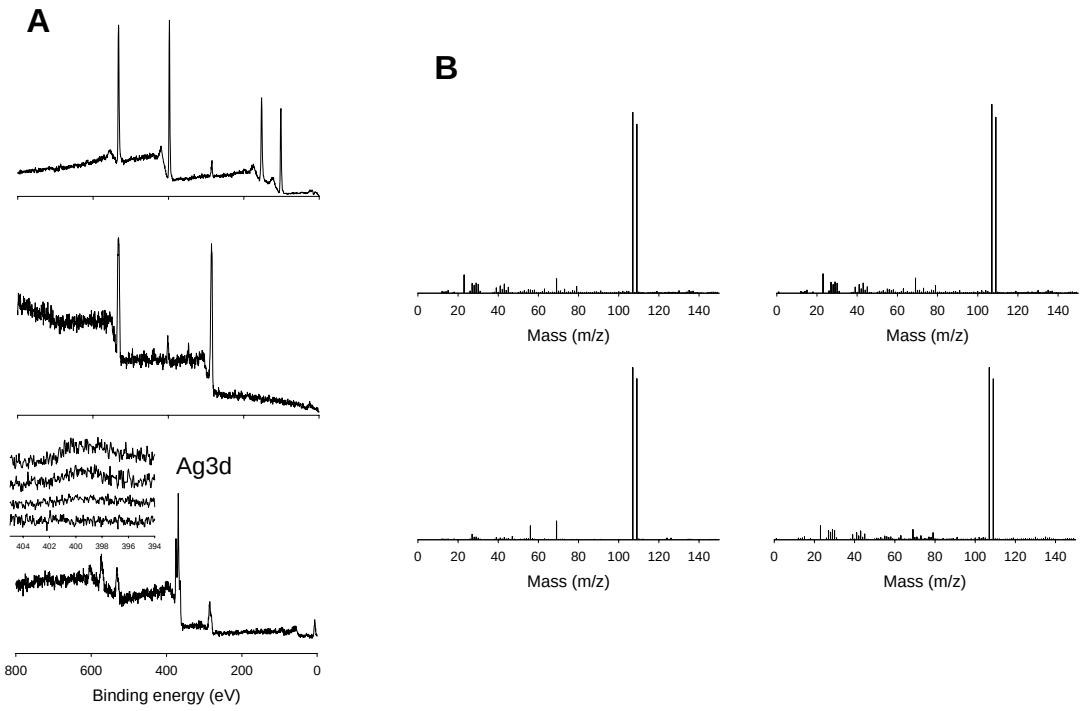

Figure 4-6. XPS and ToF SIMS characterization of silver ad-layer deposited on polydopamine-coated surfaces by electroless metallization.
A. XPS spectra taken at each step of surface modification. (Top) Clean unmodified silicon nitride exhibited Si (2p=101.5 eV), N (1s=397.5 eV), and O (1s=532.5 eV) peaks. (Middle) Polydopamine-coated silicon nitride exhibited C, N, and O signals (similar to Figure S1A) characteristic of polydopamine. (Bottom) The silver metal layer formed on polydopamine coated silicon nitride, showing strong metallic Ag ($3d_{5/2}$ = 368.6 eV; $3d_{3/2}$ = 374.7 eV) and minor hydrocarbon contamination. Inset: Angle-dependent (60, 45, 30, and 20 degrees from top to bottom) XPS showed no nitrogen 1s at take-off angles of 30 deg or less, confirming metallic silver ad-layer formation on top of polydopamine.
B. Electroless silver deposition on various substrates. Silver on glass (top left), gold (top right), Ti (bottom left), and PEEK (bottom right) showed nearly identical ToF-SIMS spectra in which two strong silver isotope peaks at 106.8 (theoretical 106.9) and 108.8 (theoretical 108.9) m/z were observed.

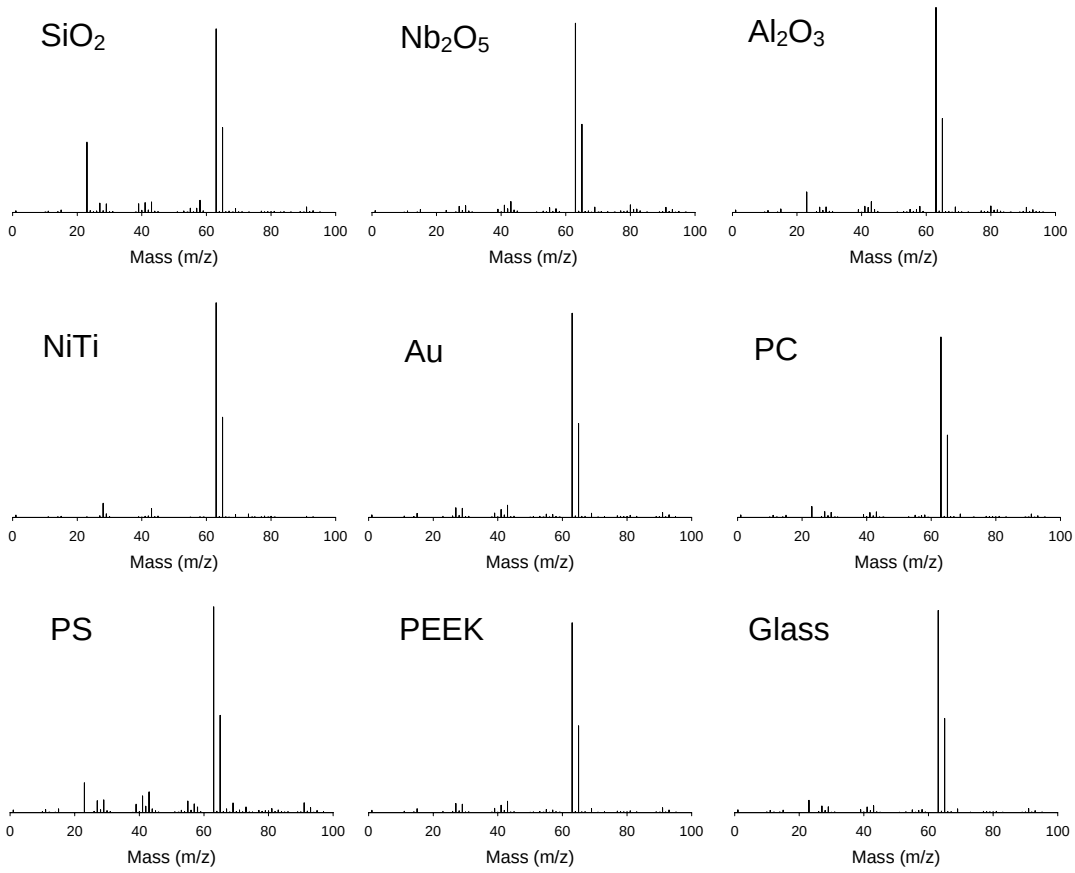

Figure 4-7. ToF-SIMS characterization of copper ad-layer deposited by electroless metallization onto diverse polydopamine-coated substrates.
All ToF SIMS mass spectra were similar regardless of underlying substrates (62.9 and 64.9 m/z with an isotopic ratio of roughly 100% (62.9 m/z) to 40% (64.9 m/z)), indicating successful metallic copper deposition in a substrate-independent manner. The peak at 23 m/z was Na^+ contamination.

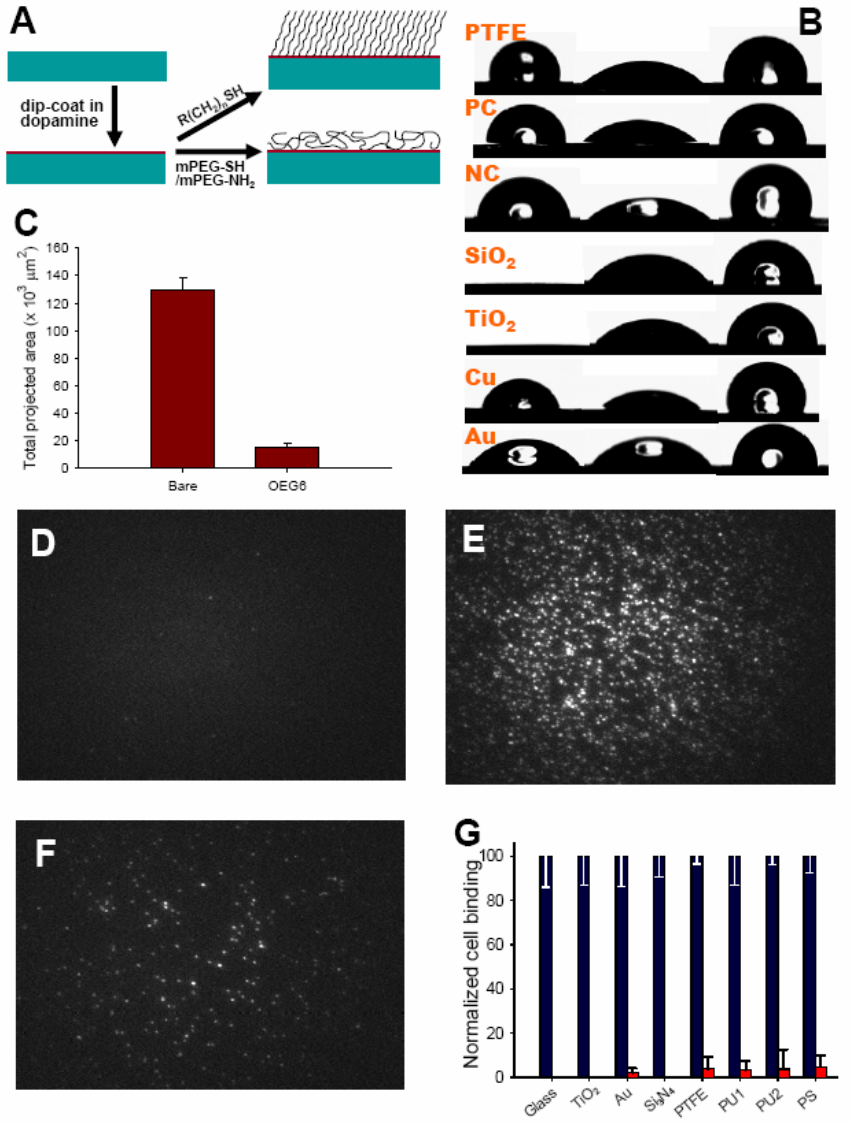

Figure 4-8. Polydopamine-assisted grafting of various organic molecules.
A. Schematic illustration of alkanethiol monolayer (top right) and PEG polymer (bottom right) grafting on polydopamine-coated surfaces. B. Pictures of water droplets on several unmodified (left), polydopamine-coated (middle), and alkanethiol-grafted substrates (right). Substrates investigated include organic polymers (PTFE, PC, and nitrocellulose (NC)), metal oxides (SiO_2 and TiO_2), and noble metals (Cu and Au). Contact angle values are shown in Table S1. C. NIH 3T3 fibroblast cell adhesion to unmodified glass and OEG6-terminated alkanethiol monolayer formed on polydopamine-coated glass. D-F. Total internal reflection fluorescence (TIRF) microscopy of Cy3 conjugated Enigma homolog protein adsorption to mPEG-NH_2-grafted polydopamine-coated glass (48 hr exposure to protein solution) (D), bare glass (30 min exposure) (E), and mPEG-silane immobilized on bare glass (48 hr exposure) (F). G. NIH 3T3 fibroblast cell adhesion to polydopamine-coated surfaces after grafting with mPEG-SH (Pre-normalized data are available in Table 4-3).

noble metal films in the formation of conventional SAMs. Alkanethiol monolayers formed by this approach are likely to contain defects, but nevertheless appear to be functionally similar to conventionally formed SAMs. We therefore refer to these monolayers of alkanethiols as 'pseudo-SAMs' (pSAMs). For example, spontaneous formation of pSAMs using methyl-terminated alkanethiol (C12-SH) was suggested by water contact angles of greater than 100° (Figure 4-8B, Table 4-2) (*100*) and XPS spectra revealing the presence of sulfur in the modified surfaces (Figure 4-9). pSAMs were formed in this way on at least 7 different materials including several ceramics and polymers.

Through proper choice of secondary reactants, polydopamine coatings can be transformed into surfaces that have specific chemical properties, such as the suppression of non-specific biological interactions, or the promotion of specific ones. We first demonstrated this by formation of pSAMs from heterobifunctional molecular precursors on polydopamine-coated surfaces as described above. pSAMs terminated by oligo(ethylene glycol) (OEG6) were found to be largely resistant toward fibroblast cell attachment (Figure 4-8C), behaving in a qualitatively similar fashion to nonfouling SAMs formed on gold (*101*).

Grafting of polymer ad-layers onto polydopamine coatings was accomplished through the use of thiol- or amine-functionalized polymers in the secondary reaction step, giving rise to bioresistant and/or biointeractive surfaces. For example, fouling-resistant surfaces were made by covalently grafting amine- or thiol- terminated methoxy-poly(ethylene glycol) (mPEG-NH_2 or mPEG-SH in 10 mM Tris, pH 8.5, 50^{o}C) to the polydopamine-coated surface (Figure 4-10).

mPEG-NH_2 modified polydopamine-coated glass exhibited substantial reduction in nonspecific protein adsorption compared to uncoated glass, and also outperformed glass surfaces

Table 4-2. Evolution of contact angles of SAMs formed on various polydopamine- coated substrates.

θ_{adv} and θ_{stat} are advancing and static contact angles, respectively. The average contact angles of polydopamine-coated and SAM-formed substrates are shown in the last row.

	Bare	Polydopamine	SAM
	θ_{adv} (θ_{stat})	θ_{adv} (θ_{stat})	θ_{adv} (θ_{stat})
PTFE	115 (106)	60 (49)	111 (102)
PC	103 (96)	54 (42)	104 (96)
NC	95 (84)	53 (41)	118 (106)
SiO_2	21 (<10)	66 (54)	101 (92)
TiO_2	22 (<10)	63 (51)	103 (94)
Cu	88 (78)	55 (43)	119 (109)
Au	68 (54)	57 (46)	101 (90)
Average	- -	58 (47)	108 (98)

Table 4-3. Pre-normalized cell adhesion data (n = 4) described in Figure 4-8G.

Substrates	# of cell (bare)	# of cell (PEGylated)
Glass	68.7 ± 14	0 ± 0
TiO_2	72.1 ± 13	0 ± 0
Au	62.9 ± 14	1.3 ± 1
Si_3N_4	57.1 ± 9	0 ± 0
PTFE	7.8 ± 4	0.2 ± 0.4
PU1	16.9 ± 13	0.6 ± 0.7
PU2	15.1 ± 4	0.6 ± 1.3
PS	23.6 ± 8	1.1 ± 1.6

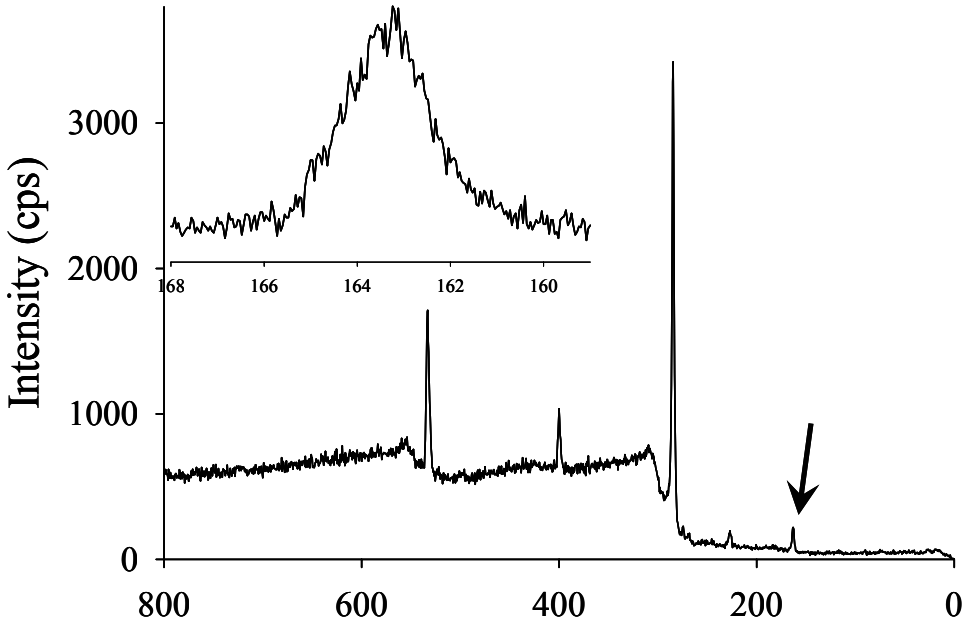

Figure 4-9. XPS analysis of self-assembled monolayer formed on polydopamine-coated polycarbonate. XPS survey spectrum after reaction between dodecanethiol and polydopamine-coated polycarbonate. Arrow represents the sulfur 2p (163 eV) signal derived from the surface immobilized dedecanethiol molecules. Inset shows the high-resolution spectrum of the sulfur 2p region marked by the arrow.

modified by a silane-terminated PEG in terms of fouling resistance after two days of continuous exposure to protein solution (Figure 4-8D-F). Similarly, mPEG-SH grafting onto a variety of polydopamine-coated substrates led to dramatic reduction of fibroblast cell attachment compared to the unmodified substrates (Figure 4-8G, Table 4-3). The polydopamine coating itself was supportive of fibroblast cell adhesion at a level similar to bare substrates (for example, the total area of attached cells on polydopamine modified SiO_2 ($46 \pm 1.4 \times 10^3$ μm^2) was similar to unmodified SiO_2 ($55 \pm 8.6 \times 10^3$ μm^2)), leading us to conclude that the observed decrease in cell adhesion was due to the grafted mPEG-SH.

Finally, we engineered polydopamine surfaces for specific biomolecular interactions by forming an ad-layer of the glycosaminoglycan hyaluronic acid (HA). HA/receptor interactions are important for physiological and pathophysiological processes including angiogenesis, hematopoietic stem cell commitment and homing, and tumor metastasis (*102, 103*). Partially thiolated HA(*94*) was grafted onto a variety of polydopamine-coated substrates (Figure 4-11) and HA ad-layer bioactivity was measured via adhesion of the human megakaryocytic M07e cell line. Unlike fibroblasts, M07e cells did not adhere to polydopamine but did adhere to HA-grafted polydopamine surfaces in a dose dependent manner (Figure 4-11B). Together with decreased binding in the presence of soluble HA (Figure 4-11C), these findings are consistent with expression of the HA receptor CD44 by M07e cells (Figure 4-12). Polydopamine and HA-grafted polydopamine surfaces were biocompatible as evidenced by similar levels of M07e cell expansion compared to tissue culture polystyrene, although only the HA-grafted polydopamine surfaces supported cell adhesion (Figure 4-11D-F; Figure 4-13).

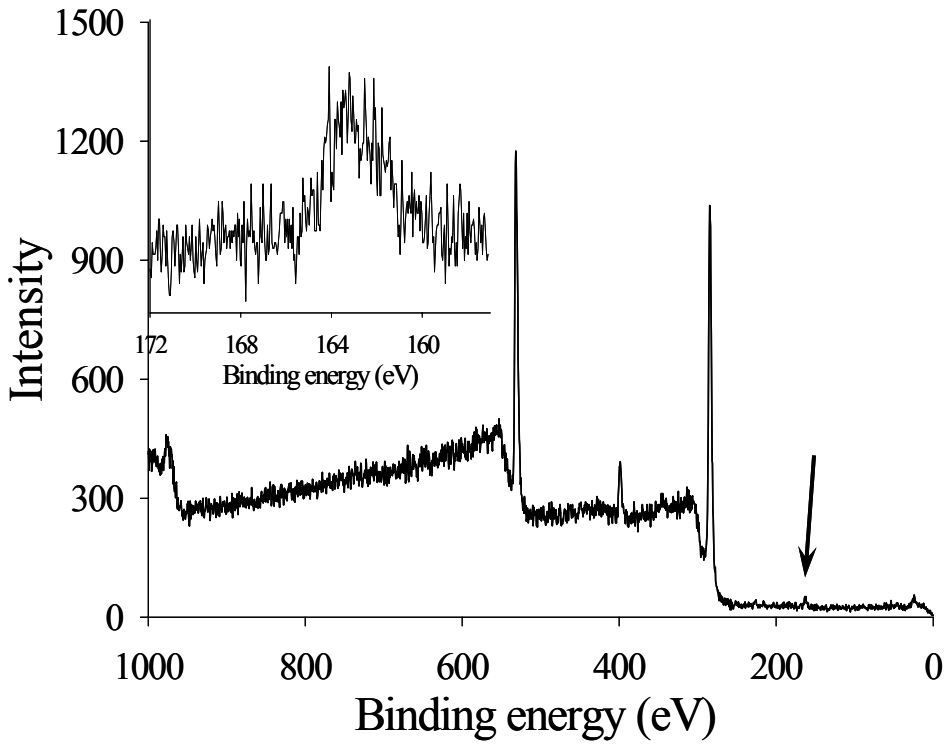

Figure 4-10. XPS analysis of PEG grafted onto polydopamine-coated glass.
XPS survey spectrum after reaction between mPEG-SH and polydopamine-coated glass. Arrow represents the sulfur 2p (163 eV) signal derived from the surface-immobilized mPEG-SH molecules. Inset shows the high-resolution spectrum of the sulfur 2p region marked by the arrow.

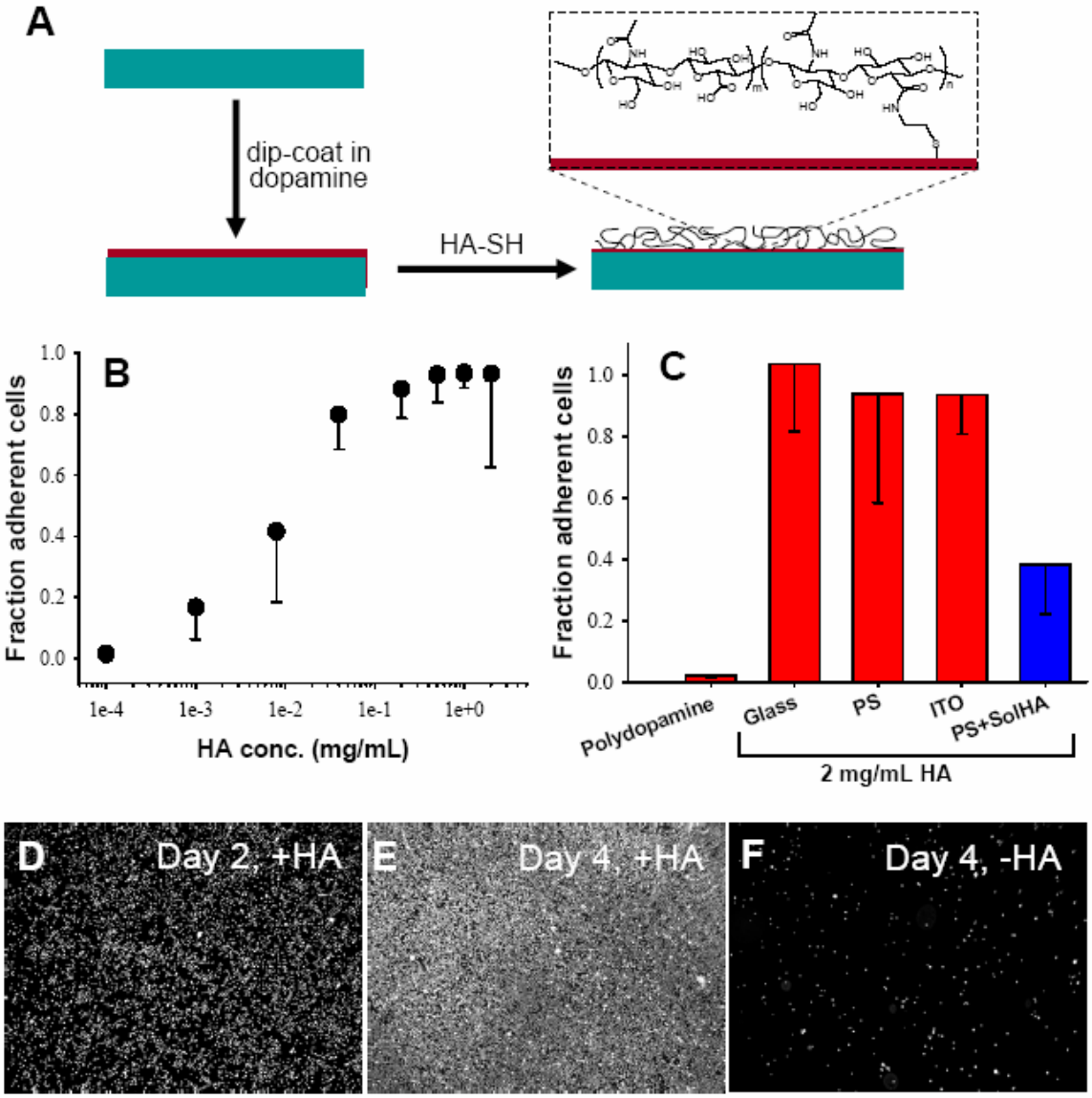

Figure 4-11. Polydopamine-assisted grafting of a biomacromolecule for biospecific cell interaction.

A. Representative scheme for hyaluronic acid (HA) conjugation to polydopamine-coated surfaces. B. Adhesion of M07e cells on polydopamine-coated polystyrene (PS) increases with the HA solution concentration used during grafting. C. Bioactive HA ad-layers were formed on polydopamine-coated glass, tissue-culture PS, and indium tin oxide (ITO), as demonstrated by attachment of M07e cells (red bars). Competition with soluble HA (blue bar) confirmed that cell adhesion was due to grafted HA. D-F. Polydopamine-modified PS grafted with HA (0.5 mg/mL) retains bioactivity during long-term culture with M07e cells. Images taken after normal-force centrifugation show almost 100% attachment of expanding M07e cells at days 2 (D; 2760 ± 390 cells/cm^2) and 4 (E; 5940 ± 660 cells/cm^2). In the absence of HA, the polydopamine-coated surface supported similar levels of M07e cell expansion at day 4, but did not support cell adhesion (610 ± 630 cells/cm^2) (F).

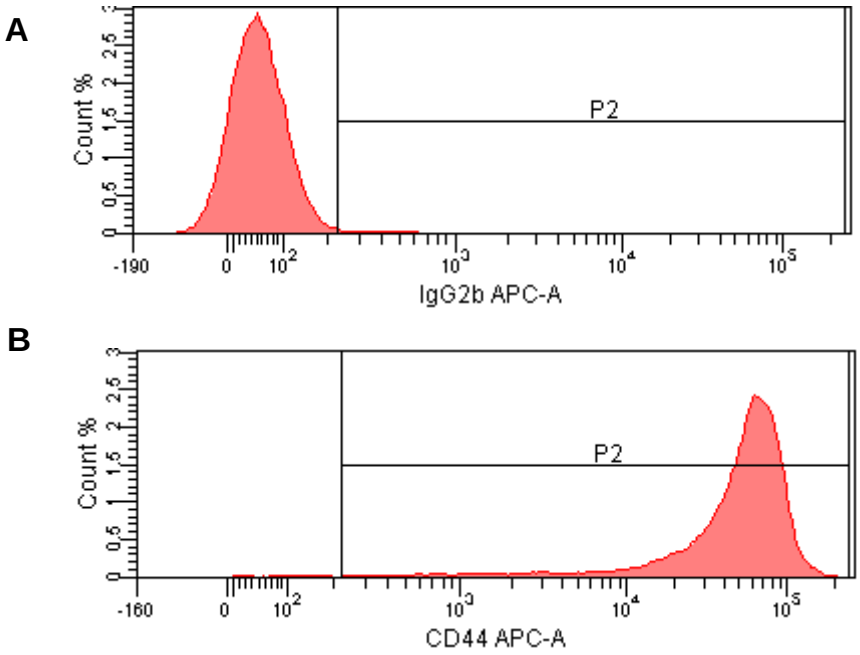

Figure 4-12. Flow cytometry analysis of CD44 levels on M07e cells.
M07e cells were stained with either isotype control (A) or anti-CD44-APC (B) antibodies to determine the surface expression of CD44 receptors. The fraction of cells expressing CD44 was determined by quantifying the number of cells within the sample having fluorescence intensity greater than isotype-control-stained cells (P2 = 99.4% for CD44-APC stained cells). Data are representative of two independent experiments.

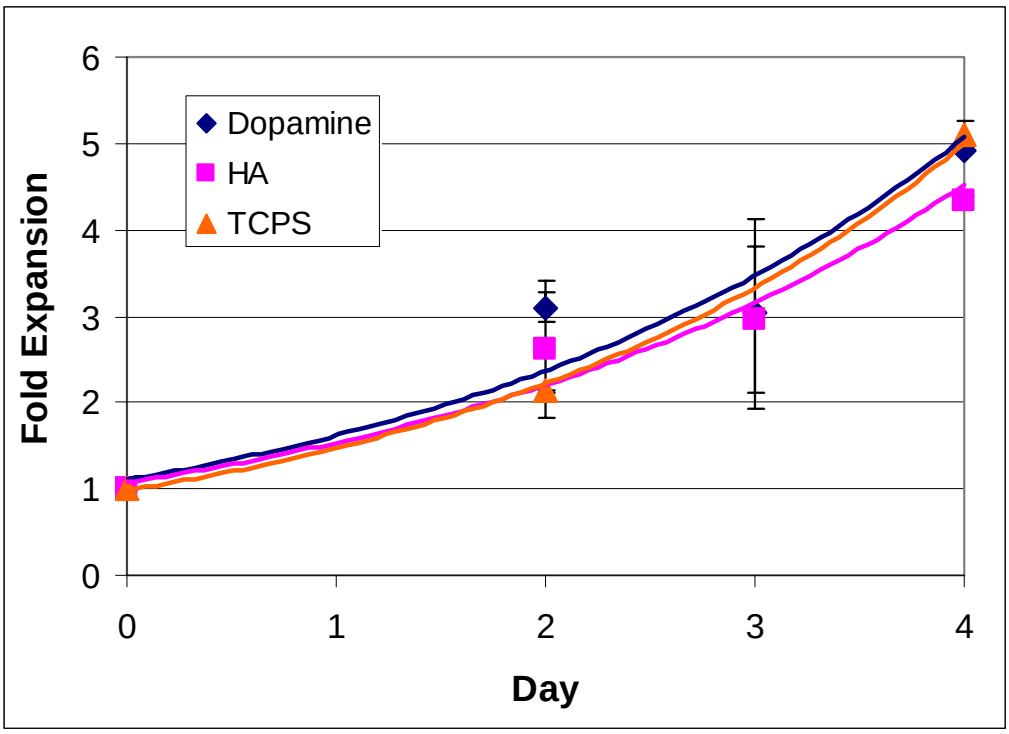

Figure 4-13. M07e cell expansion on TCPS, polydopamine, and polydopamine-HA surfaces. Similar cell expansion is observed on all three surfaces. Curves are best-fit exponential (MS Excel) and error bars show standard deviation. Represents average of 1-3 experiments/timepoint.

4.4 Conclusions

In conclusion, we introduced a facile approach to surface modification in which self-polymerization of dopamine produced an adherent polydopamine coating on a wide variety of materials. Polydopamine coatings can, in turn, serve as a versatile platform for secondary surface-mediated reactions leading ultimately to metal, self-assembled monolayer, and grafted polymer coatings. This two-step method of surface modification is unique in its ease of application, use of simple ingredients and mild reaction conditions, applicability to many types of materials of complex shape, and capacity for multiple end-uses.

Chapter 5: Surface-independent Layer-by-Layer Assembly

5.1 Objectives

Layer-by-layer (LbL) assembly has attracted much attention because of its ability to create multifunctional films on surfaces while maintaining bulk properties(*104*). The method relies on sequential adsorption of polymers onto bulk surfaces from solution, giving rise to complex multilayered films. LbL assembly is simple to implement and offers extensive control over film properties and composition during stepwise adsorption of components. Although the vast majority of LbL films are built from polyelectrolytes via electrostatic interaction between layers, more recently LbL films have been made with hydrogen bonding of polymers(*105*), and other building blocks such as inorganic nanoparticles have been used, giving access to even greater control of chemical and physical properties of LbL films.

In principle, LbL assembly can be performed on a wide variety of substrates, including noble metals (Au, Pt, etc.), oxides (quartz, Si, TiO_2, mica etc.), and synthetic polymers (polyethylene terephthalate (PET), poly(methyl methacrylate) (PMMA), polyetherimide, etc.)(*106, 107*). In practice, however, formation of well-ordered LbL layers on many polymeric surfaces has proven challenging(*108-110*), and LbL assembly on hydrophobic polymers such as poly(tetrafluoroethylene) (PTFE), and polyethylene (PE) often requires aggressive 'priming' methods such as plasma treatments (*108, 110*), oxidative chemical reactions (piranha/persulfonation)(*111, 112*), or polymeric adsorption(*109, 113, 114*). Our goal is to develop a simple, non-destructive and versatile method that enables LbL assembly to be performed on virtually any substrate (noble metals, semiconductors, metal oxides, synthetic polymers, ceramics, and composites) as a useful addition to the LbL toolbox.

5.2 Materials and Methods

5.2.1 The synthesis of PEI-C and HA-C

3 g of PEI (Mw = 25 kDa, Sigma-Aldrich) was dissolved in 300 ml of PBS solution adjusted to pH 5.5 using 1 N HCl solution. 1.52 g (17.4 mmol) of 3-(3,4-dihydroxyphenyl)propionic acid and 2.71 g (34.9 mmol) of EDC were added, and the hpH of the reaction solution was maintained at 5.5 for 2 hrs with 1.0 N NaOH. Unreacted chemicals and urea byproducts were removed by extensive dialysis. Degree of substitution was determined by ninhydrin test.

1 g of HA (Mw = 130 kDa, Lifecore) was dissolved in 100 ml of PBS solution adjusted to pH 5.5 using 1 N HCl solution. 388.1 mg (2.5 mmol) of EDC and 474.1 mg (2.5 mmol) of dopamine hydrochloride were added, and the pH of the reaction solution was maintained at 5.5

for 2 hrs with 1.0 N NaOH. This reaction resulted in modification of 35.6% of primary amine groups.

5.2.2 Layer-by-layer assembly

PTFE, PE, PC, PET, PMMA, Si, and Au surfaces were ultrasonically cleaned in deionized water for 5 min and transferred to the PEI-C and HA-C solutions (5 mg/mL in water, pH 6.5) for LbL assembly. The following cycle was generally used: (1) PEI-C for 3 min, (2) wash in water for 1 min, (3) HA-C for 3 min, and (4) wash in water for 1 min. For PTFE, the first PEI-C/HA-C adsorption was carried out for 2 hrs, and subsequent steps were same as described. A control experiment involving LbL on PTFE using as-supplied PEI (no catechol) in each assembly step was performed with overnight adsorptions (18-24 hrs). The same method was used for heterogeneous assembly of PEI-C/PAA (M_w = 90 kDa, Polysciences) followed by alternating PLL/PAA adsorption. Concentrations of PAA and PLL (Ave M_w = 28,000 Da, Sigma-Aldrich) were 3 mg/mL in 10 mM Tris, pH 7.0

5.2.3 Surface characterization

Spectroscopic ellipsometry (Woollam Co., Inc. Lincoln, NE) was used to determine the film thickness. AFM surface topography was measured in air using an MFP-3D atomic force microscopy (Asylum Research, San Diego, CA) operated in AC and contact modes. X-ray photoelectron spectroscopy (Omicron ESCALAB) (Omicron, Taunusstein, Germany) was performed to measure surface atomic composition. XPS is configured with a monochromated Al Ka (1486.8 eV) 300-W X-ray source with an ultrahigh vacuum (< 10^{-8} Torr). The takeoff angle was fixed at 45^{o}, and all spectra were calibrated using the hydrocarbon C(1s) peak (284.5 eV).

5.2.4 Bactericidal effect of silver nanoparticles

E. coli (ATCC 35218) was grown in MHB (Mueller-Hinton Broth, cation adjusted) at 37°C for 24h from previously frozen inoculums. Substrates were sterilized by UV treatment and incubated at 37°C with 1 mL of phosphate buffered saline (PBS) containing ~10^5 CFU/mL *E. coli* for 4 hrs with mild agitation. Substrates were rinsed with PBS and stained with Syto 9 and propidium iodide in PBS (2 uL/mL) for 10 min and then mountained on glass slides. Attached bacteria were imaged using a Leica epifluorescence microscope (40x mag).

5.3 Results and Discussions

5.3.1 Synthesis of catechol-containing polymers for layer-by-layer assembly on poly(tetrafluoroethylene)

Poly(ethylenimine) (PEI), a cationic polymer with a history of use in LbL assembly(*113, 115*), was conjugated with 3-(3,4-dihydroxyphenyl)propionic acid to make catechol functionalized PEI (PEI-C) (Figure 5-1). The degree of catechol modification in PEI-C was 63% as determined by the ninhydrin test, thereby preserving the cationic character of the polymer for use in LbL while at the same time mimicking the high catechol content of mussel adhesive proteins(*116*). For an anionic polymer we chose hyaluronic acid (HA), a linear polysaccharide found in extracellular matrix (ECM) of connective tissues which has also been used in LbL assembly(*117, 118*). A catechol modified HA was synthesized by reacting dopamine with HA in the presence of EDC, yielding HA-catechol (HA-C) with 35.6 % of carboxyl groups modified by dopamine (Figure 5-1, bottom).

We first demonstrated LbL assembly on PTFE, chosen as an example of a particularly challenging substrate for LbL due to its anti-adhesive property(*119*). The progress of LbL assembly was monitored by X-ray photoelectron spectroscopy (XPS) as shown in Figure 5-1.

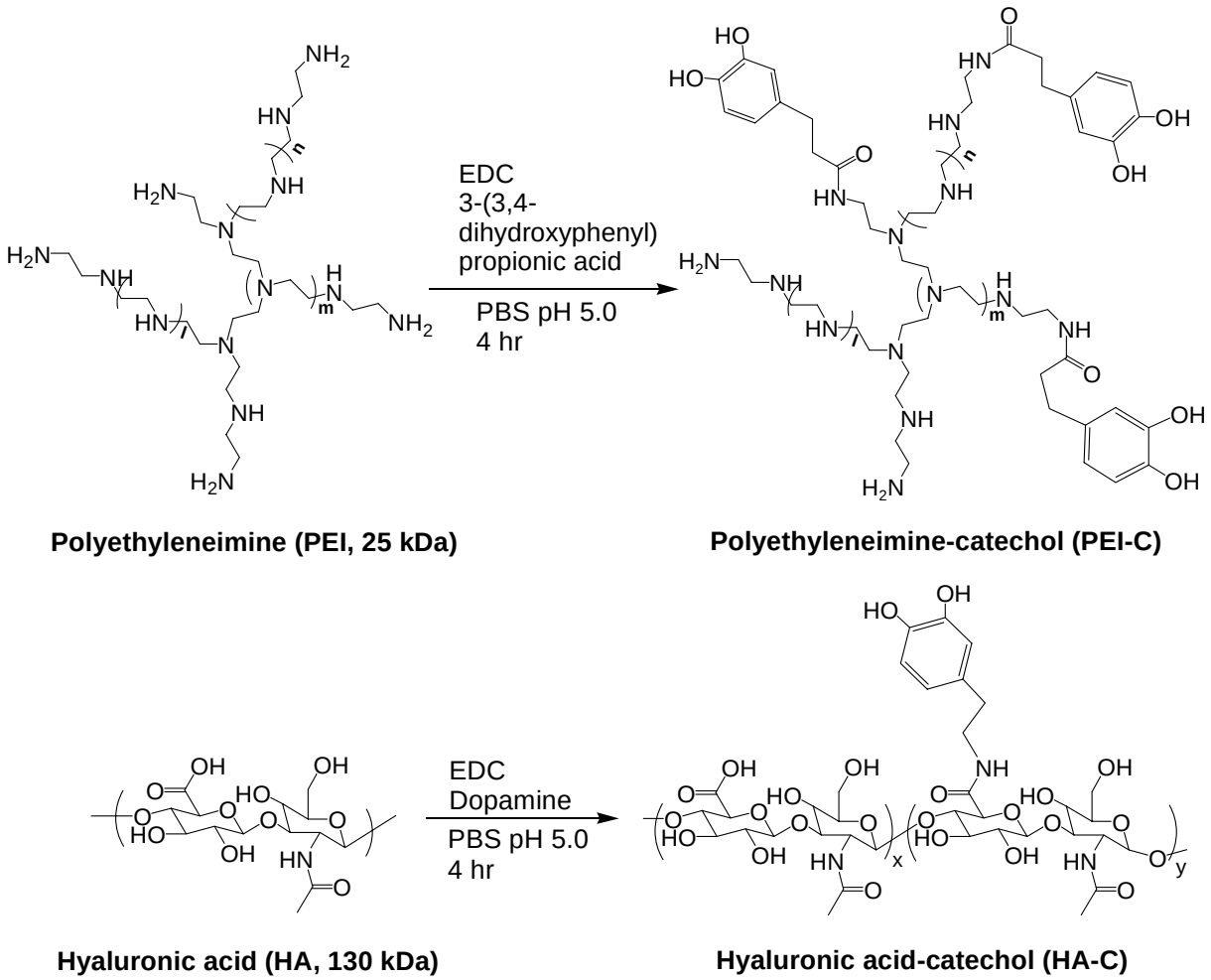

Figure 5-1. Synthesis of catechol-containing polymers for surface independent layer-by-layer assembly.

The intensity of fluorine 1s (F1s) (690 eV) and carbon 1s (C1s) (292 eV, C-F) peaks from bare PTFE (Figure 5-2A, top) decreased after the first cycle of PEI-C/HA-C assembly (Figure 5-2A, middle) and completely disappeared after only three cycles (Figure 5-2A, bottom). The fluorine composition at the PTFE surface decreased from 69 percent initially to only 1.6 percent after two-cycles of PEI-C/HA-C assembly (Figure 5-2B), demonstrating well-controlled LbL deposition on untreated PTFE. Contact angle measurements clearly showed the stark contrast in wetting characteristics of the PTFE surface before and after LbL assembly (Figure 5-2C,D); the advancing contact angle (θ_{adv}) decreased from 115° for unmodified PTFE to 27.8° after three-cycle assembly $(PEI\text{-}C/HA\text{-}C)_3$. The importance of the catechol functionality in effective LbL on PTFE was illustrated by poor wetting (θ_{adv} = 69.5°) when unmodified PEI and HA were used under the condition of significantly extended adsorption times (18~24 hrs per each assembly) (E).

5.3.2 Poly(ethylenimine)-mediated surface-independent priming and layer-by-layer assembly

To demonstrate the substrate versatility of LbL using catechol functionalized polymers, LbL assembly was also performed on several other polymeric surfaces (PE, PET, and polycarbonate (PC)) generally considered to be difficult to functionalize without prior surface modification. Comparative XPS studies of PEI vs. PEI-C adsorption on these substrates confirmed the importance of catechol residues in first layer adsorption. For example, the nitrogen signal (N1s), a useful indicator due to its presence in PEI-C chains but not in the substrate, showed that PE was anti-adsorptive to PEI but was readily modified by PEI-C. On PET and PC, trace amounts of nitrogen were detected following adsorption of PEI, although the nitrogen

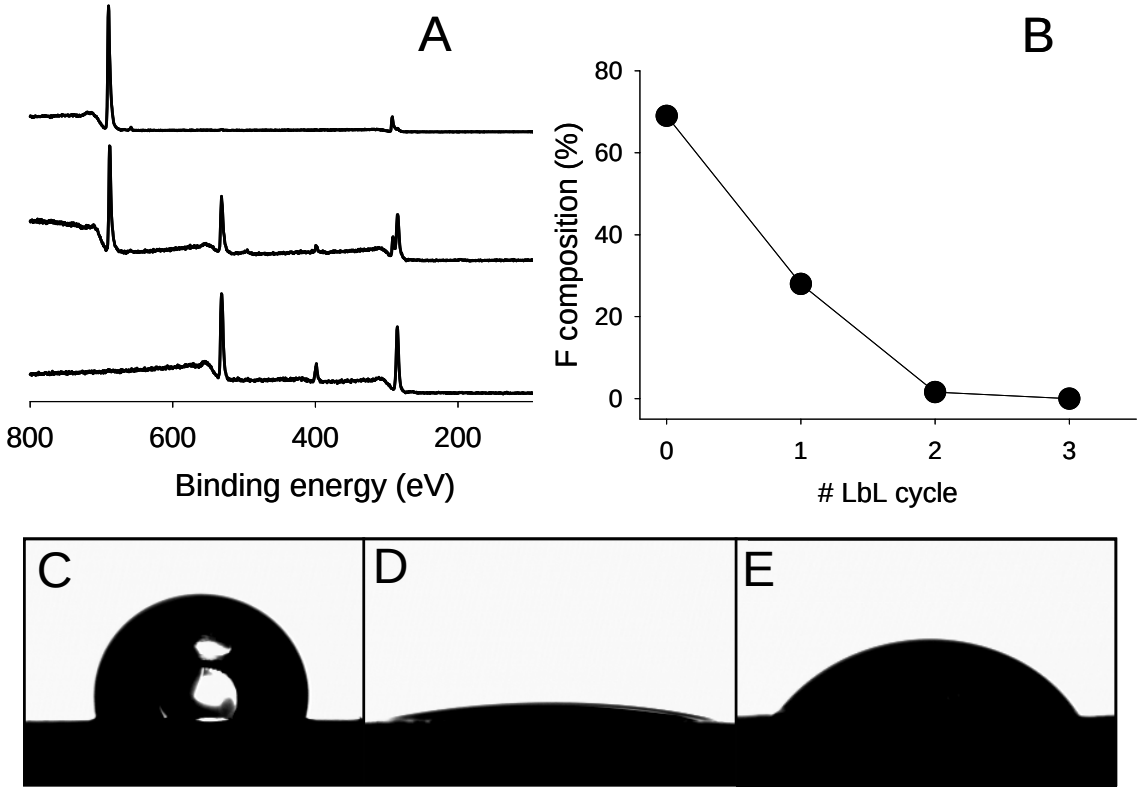

Figure 5-2. Layer-by-layer assembly on PTFE.
A. XPS spectra of bare PTFE (top), after the first cycle assembly of PEI-C/HA-C (middle), after three cycles (bottom). B. Surface composition of fluorine (F1s) as a function of the number of LbL deposition cycles of PEI-C/HA-C. C-E. Wetting of water on bare PTFE (C, θ_{stat}=106°), PTFE after three cycles of LbL assembly using PEI-C and HA-C (D, θ_{stat}=19.7°), and PTFE after three cycles assembly using PEI and HA (E, θ_{stat}=55.4°)

amount was higher when PEI-C was used. Quantitative XPS analysis of surfaces (Supporting Information) modified by PEI-C all contained similar nitrogen levels (5-7 percent) regardless of substrate, whereas PEI modification of the same surfaces yielded uniformly low nitrogen content (0-2 percent) (Figure 5-3A).

In this manner, LbL assembly on a variety of organic and inorganic surfaces was facilitated using alternating cycles of PEI-C/HA-C adsorption. We used Au, SiO_x, and PMMA as representatives of noble metal, oxide, and polymer substrates, respectively. Ellipsometric measurement of film thickness resulting from PEI-C/HA-C adsorption revealed a film deposition rate of 2.1 nm/cycle (n) regardless of substrate (Figure 5-3B). The results suggest that catecholamine polymers such as PEI-C facilitate LbL assembly on a wide variety of substrates, a strategy we refer to as substrate-independent layer-by-layer (siLbL) assembly.

PEI-C also functions as a universal primer to facilitate subsequent LbL with other polymers. We demonstrated this concept on a silicon wafer with poly(acrylic acid) (PAA) and poly-L-lysine (PLL), two polymers that have a history of use in LbL assembly (*120*). First, PEI-C was adsorbed as a primer layer on SiO_x, after which XPS analysis revealed peaks representative of both substrate (99.5 eV for Si2p, and 143 eV for Si2s) and polymer (285 eV for C1s and 400 eV for N1s) (Figure 5-4A). The strong oxygen 1s (O1s) peak at 535 eV contains contributions from the silicon oxide and hydroxyl groups of the catechol. Adsorption of PAA followed by ten subsequent cycles of PLL/PAA adsorption [$(PEI\text{-}C/PAA)_1$-$(PLL/PAA)_{10}$] and XPS analysis resulted in complete suppression of substrate signals (Si2p,2s), leaving only C1s, N1s and O1s peaks corresponding to PAA and PLL (Figure 5-4B). The thickness of the multilayer film was monitored by spectroscopic ellipsometry during LbL assembly, revealing a roughly linear increase in thickness with PLL/PAA deposition (Figure 5-4C). Atomic force

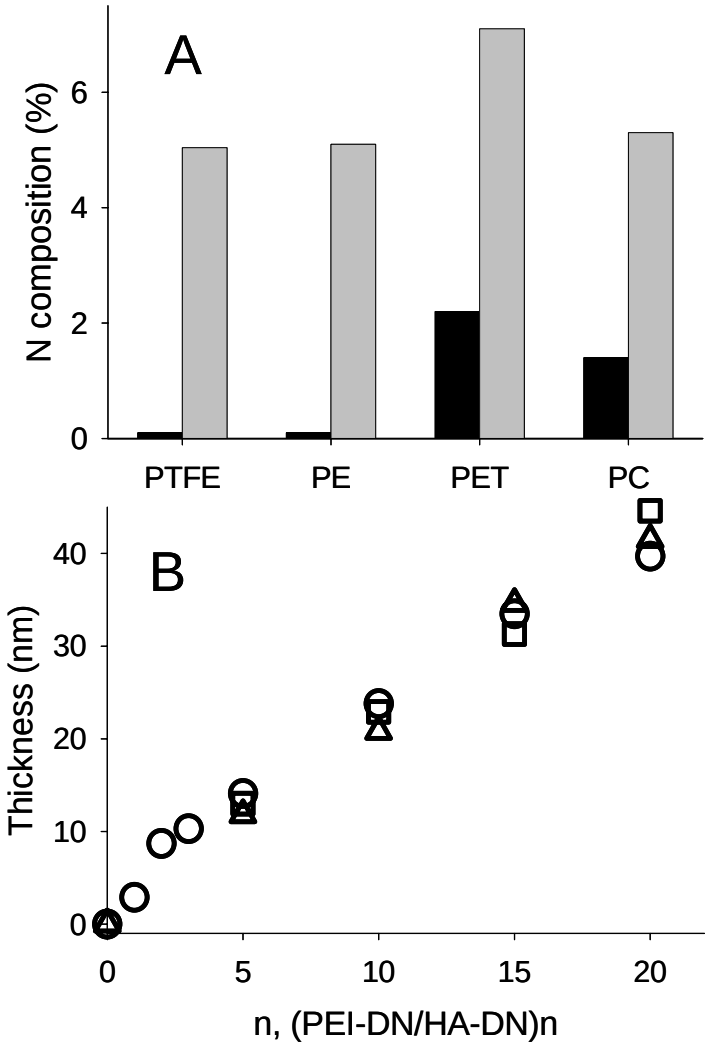

Figure 5-3. Characterization of layer-by-layer assembly on various surfaces. A. XPS spectra of bare PTFE (top), after the first cycle assembly of PEI-C/HA-C (middle), after three cycles (bottom). B. Surface composition of fluorine (F1s) as a function of the number of LbL deposition cycles of PEI-C/HA-C. C-E. Wetting of water on bare PTFE (C, θ_{stat}=106°), PTFE after three cycles of LbL assembly using PEI-C and HA-C (D, θ_{stat}=19.7°), and PTFE after three cycles assembly using PEI and HA (E, θ_{stat}=55.4°)

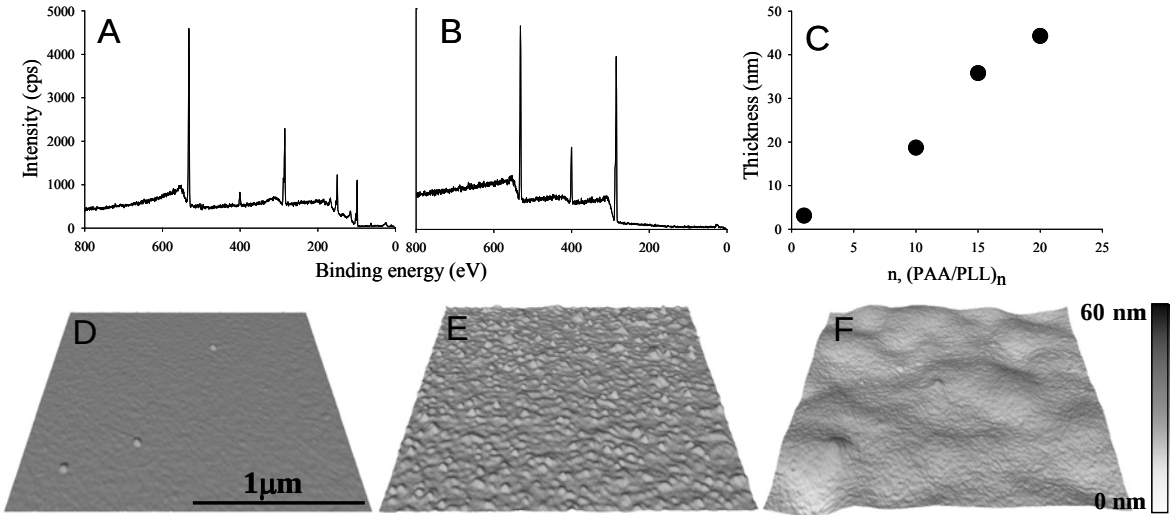

Figure 5-4. Layer-by-layer assembly of PAA and PLL on PEI-C primed SiO_x. A. XPS spectrum after single-step PEI-C adsorption on SiO_x B. XPS spectrum of $(PEI\text{-}C/PAA)_1$ -$(PLL/PAA)_{10}$ adsorption on SiO_x. C. Ellipsometry thickness of $(PEI\text{-}catechol/PAA)_1$ -$(PLL/PAA)_n$. AFM image of a bare SiOx substrate (D), after $(PEI\text{-}C/PAA)_1$ deposition (E), and after $(PEI\text{-}C/PAA)_1$-$(PLL/PAA)_{10}$ deposition (F). AFM images showed relatively smooth topography of the polymeric deposition.

microscopy (AFM) imaging revealed a morphological transition from rough at an early stage to uniform film formation after many layers (Figure 5-4 D-F). The change of surface morphology could influence contact angle measurements.

Certain functional properties of LbL films may be enhanced by incorporation of catechol residues into LbL films. For example, the strong interaction of catechols with surfaces(*89, 121*) suggests that LbL films deposited onto a primer layer of PEI-C should enhance adhesion and help prevent delamination of LbL films from substrate surfaces. Likewise, catechols could enhance mechanical properties within LbL composite films- a preliminary report of enhanced mechanical properties of catechol-containing LbL nanocomposite multilayer films has recently appeared(*122*). Here, we demonstrate a useful functional property of LbL multilayer films constructed from catechol containing polymers.

5.3.3 Spontaneous formation of silver nanoparticles embedded in catechol-containing polyeletrolyte layers

The catechol groups in the LbL film are redox active and therefore can function as a reducing agent to oxidize metal ions, as we previously demonstrated for spontaneous electroless Ag and Cu metallization of catecholamine polymer coated surfaces from aqueous metal salt solutions(*123*). In this case, we employed the latent reactivity of catechol functional groups in PEI-C/HA-C LbL films for in-situ reduction of Ag(III) to Ag(0) within the LbL multilayer (Figure 5-5A). First, LbL films of PEI-C/HA-C (n=20) were assembled on SiO_x. Subsequently, the LbL film and substrate were transferred to a silver nitrate solution (1 mM), upon which AFM imaging of the surface revealed topological changes corresponding to Ag nanoparticle formation (Figure 5-5 B-D). XPS analysis indicated a strong signal at 368.4 eV (Figure 5-5E), corresponding to the reported binding energy of metallic silver ($3d_{5/2}$)(*124*). Given the

antimicrobial activity of metallic silver(*125*), the bactericidal effect of the incorporated silver particles in the LbL film was tested in an *in-vitro* adhesion experiment with *Escherichia coli*. Surfaces were inoculated with 10^5 CFU of E. coli for four hours and then the number of dead bacteria attached to the surface counted. Ag nanoparticle-embedded LbL films showed enhanced anti-bacterial effects compared to the LbL film without Ag and the bare SiOx surface (Figure 5-5F).

5.4 Conclusions

In conclusion, we described a simple approach to substrate-independent LbL assembly by exploiting the strong interfacial binding property of catechol containing polymers. In particular, use of the catecholamine polymer PEI-C as a universal surface primer facilitated LbL assembly on metal, oxide and polymer substrates. The strategy avoids the need for aggressive chemical or physical pre-treatment regimens normally required for LbL on challenging substrates such as neutral and hydrophobic polymers. Finally, the latent redox activity of catechol groups incorporated throughout the LbL film was exploited for in-situ deposition of Ag nanoparticles, imparting an antibacterial property to the multilayer film. With further improvements and through full exploitation of the substrate versatility afforded by siLbL, silver incorporated LbL films may be employed in the future to minimize bacterial fouling on a variety of materials.

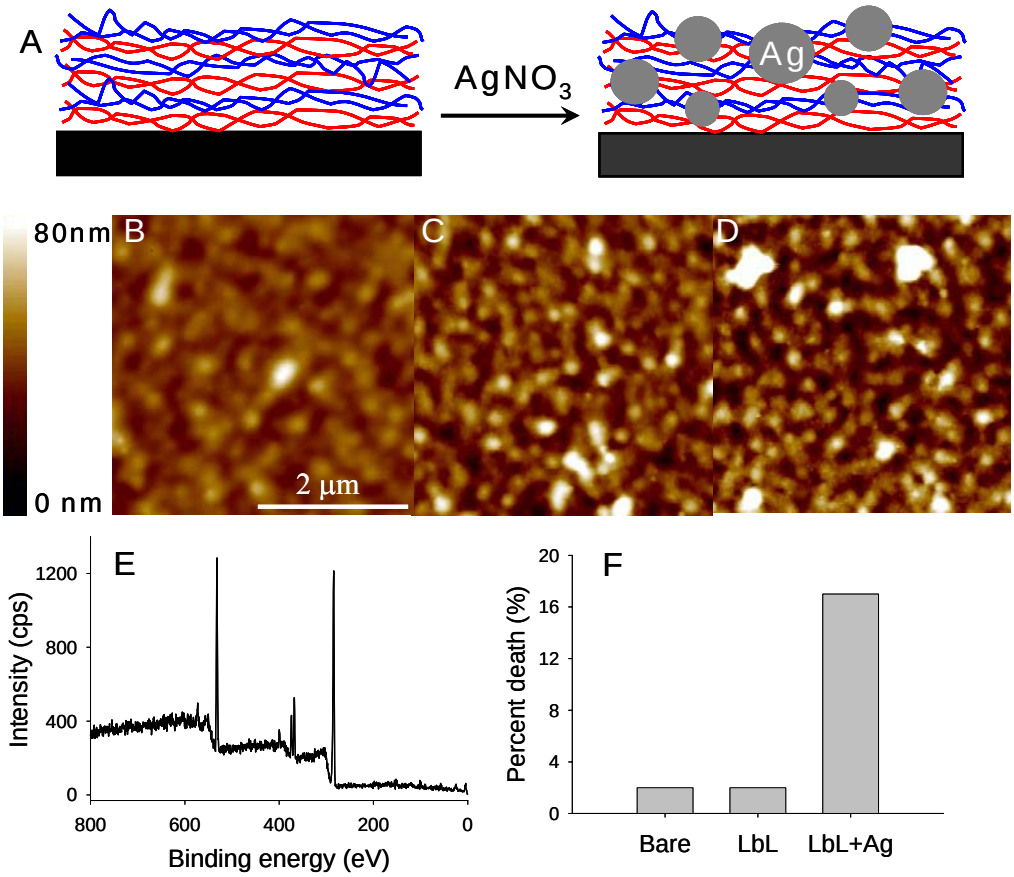

Figure 5-5. Catechol-mediated silver nanoparticle formation in LbL films of PEI-C/HA-C and antibacterial activity of the nanocomposite films. A. Schematic illustration of Ag nanoparticle formation in LbL film via catechol oxidation in the presence of Ag(III). B-D. Topographic AFM images of the LbL film after PEI-C/HA-C (n=20) deposition (B), and the same film incubated in 1 mM $AgNO_3$ solution for 30 min (C) and 18 hrs (D). E. XPS spectra of the silver incorporated LbL film shown in D (18 hrs). Metallic silver photoelectron ($3d_{5/2}$) was detected at the binding energy of 368.4 eV. F. Live-dead assay of adhered *E.coli* on bare Si, LbL (n=20), and LbL+Ag (n=20, 18 hrs) surfaces.

Chapter 6: A New Reversible Adhesive Inspired by Geckos and Mussels

6.1 Objectives

The adhesive strategy of the gecko relies on foot pads composed of specialized keratinous foot-hairs called setae, which are subdivided into terminal spatulae of dimensions approximately 200 nm(*39*). Contact between the gecko foot and an opposing surface generates adhesive forces that are sufficient to allow the gecko to cling onto vertical and even inverted surfaces. Although strong, the adhesion is temporary, permitting rapid detachment and reattachment of the gecko foot during locomotion. Researchers have attempted to capture the unique properties of gecko adhesive in synthetic mimics with nanoscale surface features reminiscent of setae,(*46-48, 126-128*). However, maintenance of adhesive performance over many cycles has been elusive,(*46, 129*) and gecko adhesion is dramatically diminished upon full immersion in water(*42, 43*).

The adhesive forces of the gecko have been observed to be on the order of 40 μN or more per seta (*41, 44*) and 10 nN per spatula(*130*). Gecko adhesion has been explained as arising from weak secondary bond forces such as van der Waals(*44*). However, adhesion of a single spatulae varies as a function of humidity and is dramatically reduced under water (*42, 43*) suggesting some contribution from capillary forces. Contact mechanics arguments have been invoked to explain the subdivision of the setal contact surface into multiple independent nanosized spatulae, giving rise to enhancement of the mechanical behavior (*131*). Although the scaling depends on contact geometry, for the idealized case of a hemispherical contact, the theory suggests that the adhesion strength scales as $n^{1/2}$, where n is the number of independent contacts into which the area is subdivided. The contact splitting theory qualitatively explains the scaling of dry adhesive systems employed by some amphibians and insects, and provides guidance for development and optimization of synthetic gecko mimics (*47, 132, 133*). Synthetic gecko adhesives that exhibit dry adhesion have been fabricated from polymers (*46, 126, 127*) as well as multiwalled carbon nanotubes(*128*). However, maintenance of adhesion during repetitive contacts has only been demonstrated for a few contact cycles (*46, 129*), and none have been shown to function under water.

A celebrated biological model for wet adhesion is the mussel, which is well known for its ability to cling to wet surfaces (*53, 134*). Mussels secrete specialized adhesive proteins containing high content of the catecholic amino acid 3,4-dihydroxy-L-phenylalanine (DOPA) (*13, 15, 135*). Both natural and synthetic adhesives containing DOPA and its derivatives have demonstrated strong interfacial adhesion strength (*21, 60, 61, 136*). Using single- molecule measurements in aqueous media, we recently demonstrated that DOPA formed extraordinarily

strong yet reversible bonds with surfaces(*89*). In fact, the force necessary to dissociate DOPA from an oxide surface (~800 pN) was the highest ever observed for a reversible interaction between a small molecule and a surface(*89*). We speculated that the incorporation of mussel adhesive protein (MAP) mimetic polymers into a gecko mimetic nanoadhesive would yield strong yet reversible wet/dry adhesion- a property that existing materials do not exhibit.

6.2 Materials and Methods

6.2.1 Synthesis of dopamine methacrylamide (DMA)

20g of sodium borate and 8g of $NaHCO_3$ were dissolved in 200mL of deionized water and bubbled with Ar for 20 min. 10g of dopamine-HCl (52.8 mmol) was then added followed by the dropwise addition of 9.4 mL of methacrylate anhydride (58.1 mmol) in 50 mL of THF, during which the pH of solution was kept above 8 with addition of 1N NaOH as necessary. The reaction mixture was stirred overnight at room temperature with Ar bubbling. The aqueous mixture was washed twice with 100 mL of ethyl acetate 2 times and then pH of the aqueous solution was reduced to less than 2 and extracted with 100 mL of ethyl acetate 3 times. The final three washes were combined and dried over $MgSO_4$ to reduce the volume to around 50mL. 450 mL of Hexane was added with vigorous stirring and the suspension was held at 4^{o}C overnight. The product was recrystalized from hexane and dried to yield 9.1 g of grey solid. ^{1}H NMR (400 MHz, DMSO-*d*/TMS): δ 6.64-6.57 (m, 2H, $C_6H\mathit{H}_2(OH)_2$-), 6.42 (d, 1H, $C_6H_2\mathit{H}(OH)_2$-), 5.61 (s, 1H, -C(=O)-C(-CH_3)=C*H*H), 5.30 (s, 1H, -C(=O)-C(-CH_3)=C*H*H), 3.21 (m, 2H, $C_6H_3(OH)_2$-CH_2-CH_2(NH)-C(=O)-), 2.55 (t, 2H, $C_6H_3(OH)_2$-CH_2-CH_2(NH)-C(=O)-), 1.84 (s, 3H, -C(=O)-C(-CH_3)=CH_2). ^{13}C NMR (400 MHz, DMSO-*d*/TMS): δ 167.3 (s, 1C, -NH-*C*(=O)-

$C(CH_3)=CH_2$), 145.0 (s, 1C, -NH-C(=O)-*C*$(CH_3)=CH_2$), 143.5-115.5 (6C, *C*$_6H_3$(O-C(=O)-$CH_3)_2$), 130.3 (s, 1C, -NH-C(=O)-C(CH_3)=*C*H_2), 41.0 (s, 1C, $C_6H_3(OH)_2$-CH_2-*C*H_2(NH)-C(=O)-), 34.6 (s, 1C, $C_6H_3(OH)_2$-*C*H_2-CH_2(NH)-C(=O)-), 18.7 (s, 1C, -C(=O)-C(-*C*H_3)=CH_2).

6.2.2 Synthesis of p(DMA-co-MEA)

12.5mL of MEA was passed through a column packed with 30g of Al_2O_3 to remove inhibitor. 7.5g of purified MEA (57.9 mmol), 1.7g of DMA (7.4 mmol), and 106 mg of AIBN (0.64 mmol) were added to 20 mL of DMF in an AirFree® flask. The solution mixture was degassed through pump-freeze-thaw cycles 3 times. While sealed under vacuum, the solution was heated to 60^{o}C and stirred overnight. The reaction mixture was diluted with 50mL of methanol and added to 400mL of Et_2O to precipitate the polymer. After precipitating in DCM/ethyl ether two more times and dried in the vacuum desicator, 5.7 g of white, sticky solid was obtained. ^{1}H NMR (400 MHz, $CDCl_3$/TMS): δ 6.81-6.70 (d, br, 2H, C_6H*H*$_2(OH)_2$-), 6.58 (s, br, 1H, C_6H_2*H*$(OH)_2$-), 4.20 (s, br, 2H, CH_3-O-CH_2-C*H*$_2$-O-C(=O)-), 3.57 (s, br, 2H, CH_3-O-C*H*$_2$-CH_2-O-C(=O)-), 3.36 (s, br, 3H, C*H*$_3$-O-CH_2-CH_2-O-C(=O)-), 2.69 (s, br, 2H, $C_6H_3(OH)_2$-CH_2-C*H*$_2$(NH)-C(=O)-), 2.39 (s, br, 1H, -O-C(=O)-C*H*$(CH_2$-)-CH_2-), 2.14 (s, br, 2H, $C_6H_3(OH)_2$-C*H*$_2$-CH_2(NH)-C(=O)-), 1.93 (s, 3H, -NH-C(=O)-C(C*H*$_3)(CH_2$-)-CH_2-), 1.68 (m, br, -O-C(=O)-CH(CH_2-)-C*H*$_2$-), 0.98 (m, br, -NH-C(=O)-C(CH_3)(CH_2-)-C*H*$_2$-). Analysis indicated a 1:6 ratio of DMA to MEA in the copolymer. GPC-MALLS (Wyatt Technology, Santa Barbara, CA with mobile phase of 20mM LiBr in DMF and Shodex-OH Pak columns): M_n (average) = 252 kDa, PD = 1.73. For control experiments, a catechol-free p(MEA) homopolymer (M_w (average) = 100 kDa, Scientific Polymer Products, Ontario, NY) was used.

6.2.3 Electron-Beam Lithography

Electron-beam resist (950PMMA A3, MicroChem) was spin-coated (4000 rpm, 40 sec) on silicon wafer several times until the resist thickness, as measured by ellipsometry (Woolam Co. Lincoln, NE), reached 600~700 nm. The resist was patterned at 30 kV with an area dose between 650-800 $\mu C/cm^2$ using Quanta 600F (FEI Co. Hillsboro, OR). Resist development was performed for 1 min with a solution of methyl isobutyl ketone/isopropanol (1/3, v/v), followed by rinsing with water. The patterned substrates were treated with oxygen plasma (Harrick, Pleasantville, NY) for 30 sec and repeated 2-3 times to completely remove residual resist from the exposed Si regions. The patterned substrates were then exposed to a triethoxyoctylsilane vapor for 30 min. PDMS was prepared as follows: 4 μL of Pt-catalyst (platinum-divinyl tetramethyl-disiloxane in xylene) and 4 μL of modulator (2,4,6,8-tetramethyl-2,4,6,8-tetravinylcyclotetrasioxane) were added to a 7-8% vinylmethylsiloxane solution (3.5 g). The solution was subsequently mixed with a 25-30% methylhydrosiloxane (1g) solution. Finally the solution was cured (80 ^oC) after spin-coating (1000 rpm for 1 min) onto the PMMA/Si master. The spin-coated substrate was covered either by thin cover glass for force measurements or sylgard-184 PDMS for other experiments such as optical imaging or x-ray photoelectron spectroscopy (XPS). Gecko adhesive was obtained by PDMS pattern lift-off and brief exposure to oxygen plasma (100 W, 30 sec) and used within 2-3 hrs after plasma treatment. Geckel adhesive was prepared by dip-coating gecko adhesive in a 1 mg/mL solution of p(DMA-co-MEA) in ethanol at 70°C. Unstructured controls were fabricated in the same manner using flat PDMS.

6.2.4 X-ray Photoelectron Spectroscopy

The presence of p(DMA-co-MEA) and p(MEA) on PDMS surfaces was confirmed by x-ray photoelectron spectroscopy (XPS) (Omicron, Taunusstein Germany) equipped with a

monochromatic Al Kα (1486.8 eV) 300 W x-ray source and an electron gun to eliminate charge build-up.

6.2.5 Atomic Force and Optical Microscopy

All force data were collected on an Asylum Mfp-1D AFM instrument (Asylum Research, Santa Barbara, CA) installed on a Nikon TE2000 microscope. Spring constants of individual cantilevers (Veecoprobes, NP-20 tipless Si_3N_4 tips, Santa Barbara, CA) were calibrated by applying the equipartition theorem to the thermal noise spectrum(*64*). Due to the large forces exhibited by the adhesive, only tips exhibiting high spring constants (280 – 370 pN/nm) were used. Metal and metal oxide coated cantilevers were formed by sputter coating ~10 nm of Au or Ti (a native oxide formed at the Ti surface, TiO_x) using a Denton Vacuum Desk III (Moorestown, NJ). The surface composition of each cantilever was confirmed by time-of-flight secondary ion mass spectrometry (ToF-SIMS), using a PHI-TRIFT III (Ga^+, 15keV, Physical Electronics, Eden Prairie, MN). Cantilevers were treated by oxygen plasma (100 W, 150 mTorr) for 3 min before use. Force measurements were conducted either in millipore water or ambient (air) conditions at a cantilever pulling speed of 2 μm/sec. In wet experiments, optical microscopic examination of the contact region indicated the absence of air bubbles trapped between nanopillars and on the nanopillar surface (not shown). Tapping mode AFM images were obtained using a multimode Veeco Digital Instrument (San Diego, CA) with a Si cantilever (resonance frequency of 230-280 kHz). Contact area was imaged by an inverted optical microscope using a 40x objective illuminated by a fiber-optic white light source perpendicular to the objective.

6.3 Results and Discussions

6.3.1 Fabrication of Geckel Hybrid Adhesive

Our strategy employed arrays of gecko foot-mimetic nanoscale pillars coated with a thin MAP-mimetic polymer film (Figure 6-1). Designs of both pillar array and coating polymer were undertaken in view of current knowledge of the respective biological systems. For the pillar array, primary design criteria include dimensions of the pillars and their spacing, as well as the stiffness of the material(*132, 133*). For flexibility in adapting to rough surfaces, both supporting substrate and pillar material were fabricated from poly(dimethylsiloxane) (PDMS) elastomer, which is a well-known organic material with a long history of use in microfabrication (*137*). We successfully fabricated arrays of PDMS pillars 200-, 400-, and 600nm in diameter, 1-3 μm center-to-center distance, and 600-700 nm in height using electron-beam lithography (eBL). The pillar arrays are supported on a continuous film of PDMS (2-3 mm in thickness), with each PDMS pillar representing a single spatula found at the surface of a gecko foot (Figure 6-2A, B). Pillar arrays of 400nm diameter and 600nm height were tested for adhesion.

Inspection of mussel adhesive protein composition gave insight into a rational design for a mussel-mimetic polymer. First, the synthetic polymer should have a high catechol content since DOPA accounts for as much as 27% of amino acids in the adhesive proteins found at the interface between mussel byssal pads and their substrate(*15*). Second, long-lasting waterproof adhesion requires polymers with low water solubility to prevent their loss into the aqueous medium(*116*). Thus, we synthesized poly(dopaminemethacrylamide-co-methoxyethylacrylate) (p(DMA-co-MEA); Figure 6-2C) through free-radical polymerization where the adhesive monomer, DMA, accounts for 17% of this copolymer by weight (^{1}H-nuclear magnetic resonance spectroscopy, NMR). p(DMA-co-MEA) possesses high molecular weight and is insoluble in water.

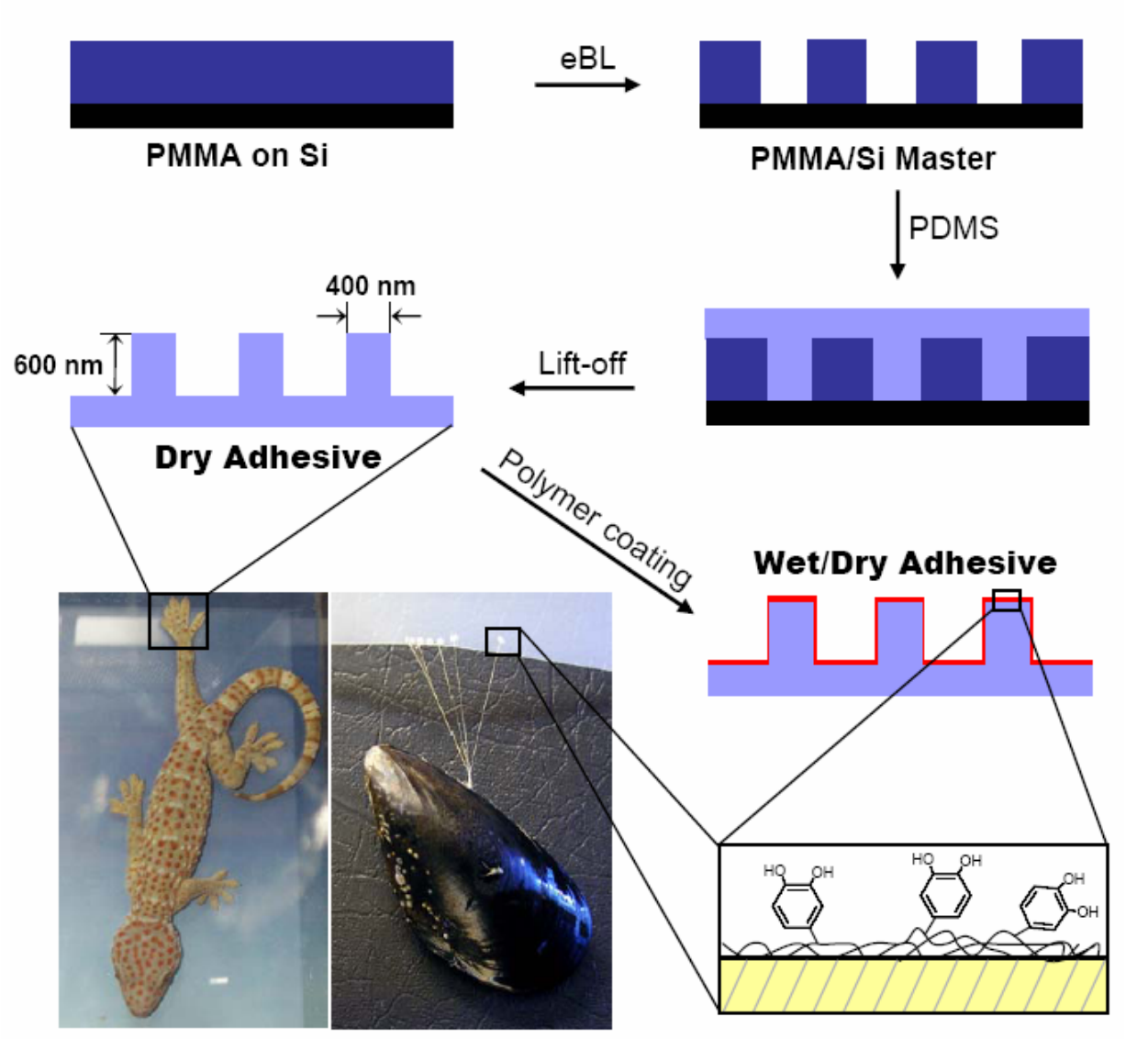

Figure 6-1. Rational design and fabrication of wet/dry hybrid nanoadhesive.
E-beam lithography was used to create an array of holes in a PMMA thin film supported on Si (PMMA/Si master). Casting of PDMS onto the master followed by curing and lift-off resulted in gecko mimetic nanopillar arrays. Finally, a mussel adhesive protein mimetic polymer is coated onto the fabricated nanopillars. The topmost organic layer contains catechols, a key component of wet adhesive proteins found in mussel holdfasts.

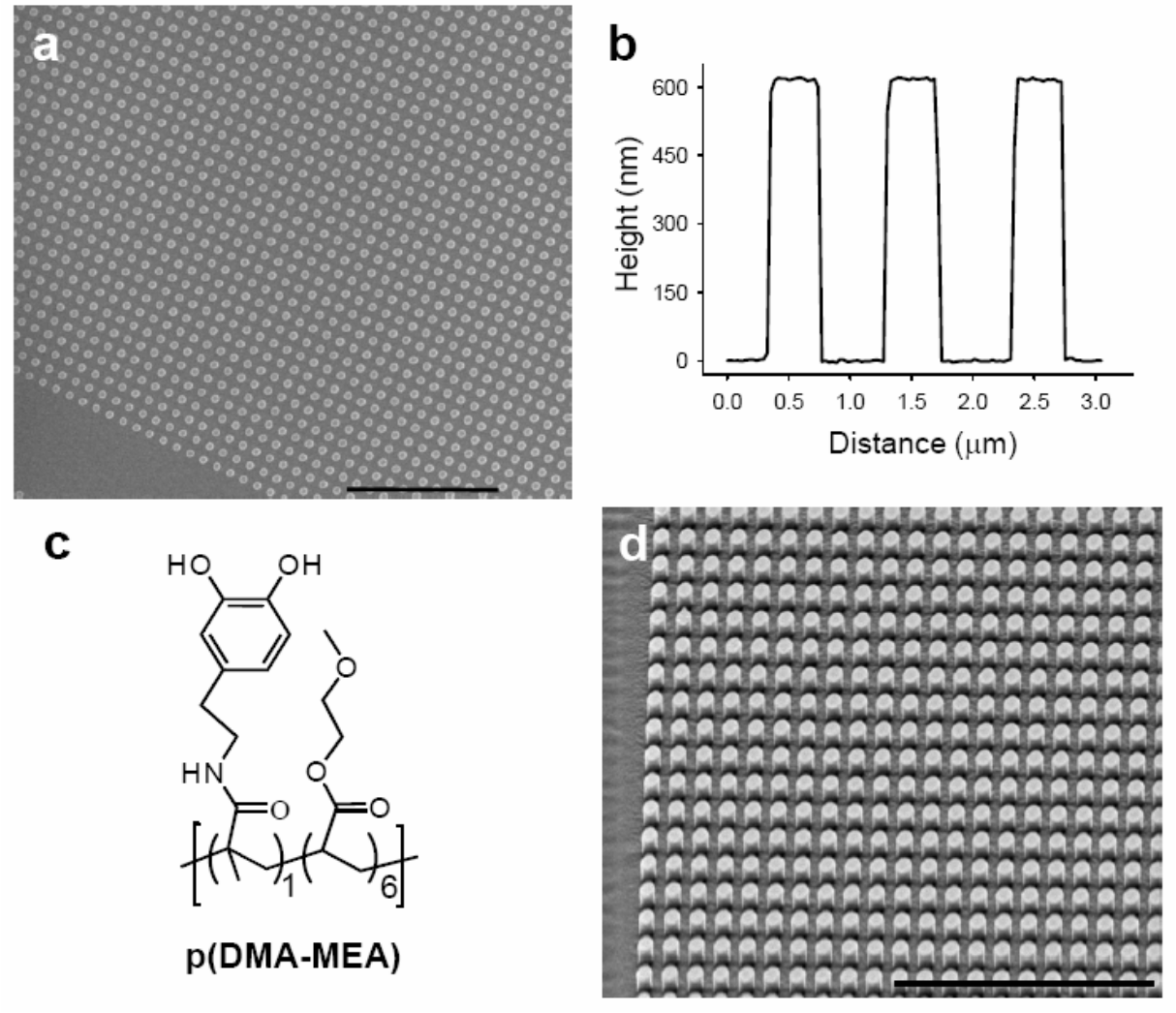

Figure 6-2. Fabricated gecko and geckel adhesives.
A. SEM image of eBL fabricated gecko nanopillar array (scale=10 μm). B. AFM line scan of the gecko nanopillars. The height and diameter of the pillars used in this study were 600nm and 400nm, respectively. The apparent widening of the pillars near the base is believed to be an artifact arising from the pyramidal shape of the AFM tip used for imaging. C. Chemical structure of the mussel adhesive protein mimetic polymer, p(DMA-co-MEA), which is applied to the surface of the gecko nanopillars. D. SEM image of geckel adhesive after coating nanopillar array with p(DMA-co-MEA). The coating has little effect on the pillar geometry (scale=10 μm).

p(DMA-co-MEA) was applied to the PDMS pillar array by dip coating in an ethanol solution of p(DMA-co-MEA). X-ray photoelectron spectroscopy (XPS) analysis of the coated substrate indicated a thin coating (<20 nm) as demonstrated by the presence of both silicon (103 eV, Si 2p) from PDMS and nitrogen (399 eV, N 1s) from p(DMA-co-MEA) (Figure 6-3). A thin coating was desired for minimizing the change in pillar dimensions during coating, which was confirmed by scanning electron microscopy after coating with p(DMA-co-MEA) (Figure 6-2D). We refer to the resulting flexible organic nanoadhesive as 'geckel', reflecting inspiration from both gecko and mussel.

6.3.2 Controlling Contact Area for Adhesive Force Measurement

The performance of geckel adhesive was evaluated using an atomic force microscopy (AFM) system fully integrated with optical microscopy, which permitted simultaneous measurement of the adhesive contact force along with clear visualization of nanoscale contact area down to the single pillar level. In a typical adhesion experiment (Figure 6-4), the AFM piezo was used to bring a tipless cantilever (Si_3N_4) into contact with the geckel pillar array, and upon retraction the force necessary to separate the cantilever from the pillar array was measured. Furthermore, independently changing the spacing (d) between pillars (d = 1, 2, and 3 μm) and the angle of orientation (θ) between the pillar array and the cantilever axis (Figure 6-4B) allowed us to control the number of pillars contacting the cantilever precisely from one to six. For example, a geckel adhesive with d = 3 μm and $\theta = 45^o$ resulted in a single pillar contact (Figure 6-4C), whereas d = 1 μm and $\theta = 0^o$ resulted in six pillars interacting with the cantilever simultaneously (Figure 6-4D).

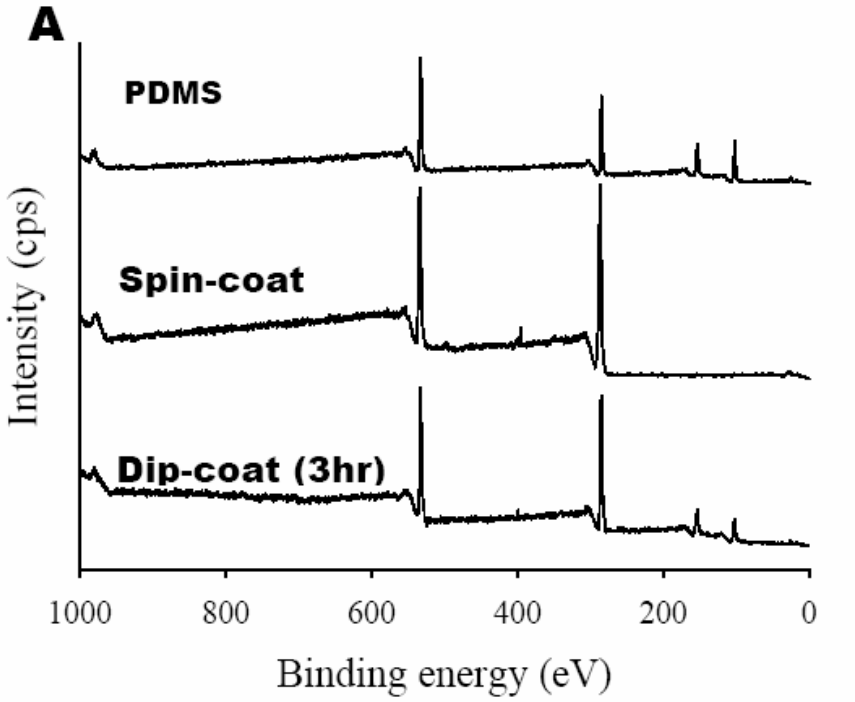

B

Surface atomic composition (%)

	Si	C	O	N
Bare	33.2	48.8	18.0	0
Dip-coat	23.6	52.0	23.9	~0.5

Figure 6-3. X-ray photoelectron spectroscopy (XPS) of gecko and geckel adhesives.
A. XPS was used to probe p(DMA-co-MEA) coating thickness in a semi-quantitative way. Spin-coated PDMS showed no silicon signals (2s, 153 eV and 2p 103 eV) indicating that the coating thickness is more than the x-ray penetration depth, typically around 20 nm. Dip-coating methods showed both silicon and nitrogen signals, thus indicating that the coated polymer thickness is <20 nm. B. Surface atomic compositions of unmodified and modified PDMS substrates from the XPS data shown in (A). Dip-coated sample showed both silicon and nitrogen compositions.

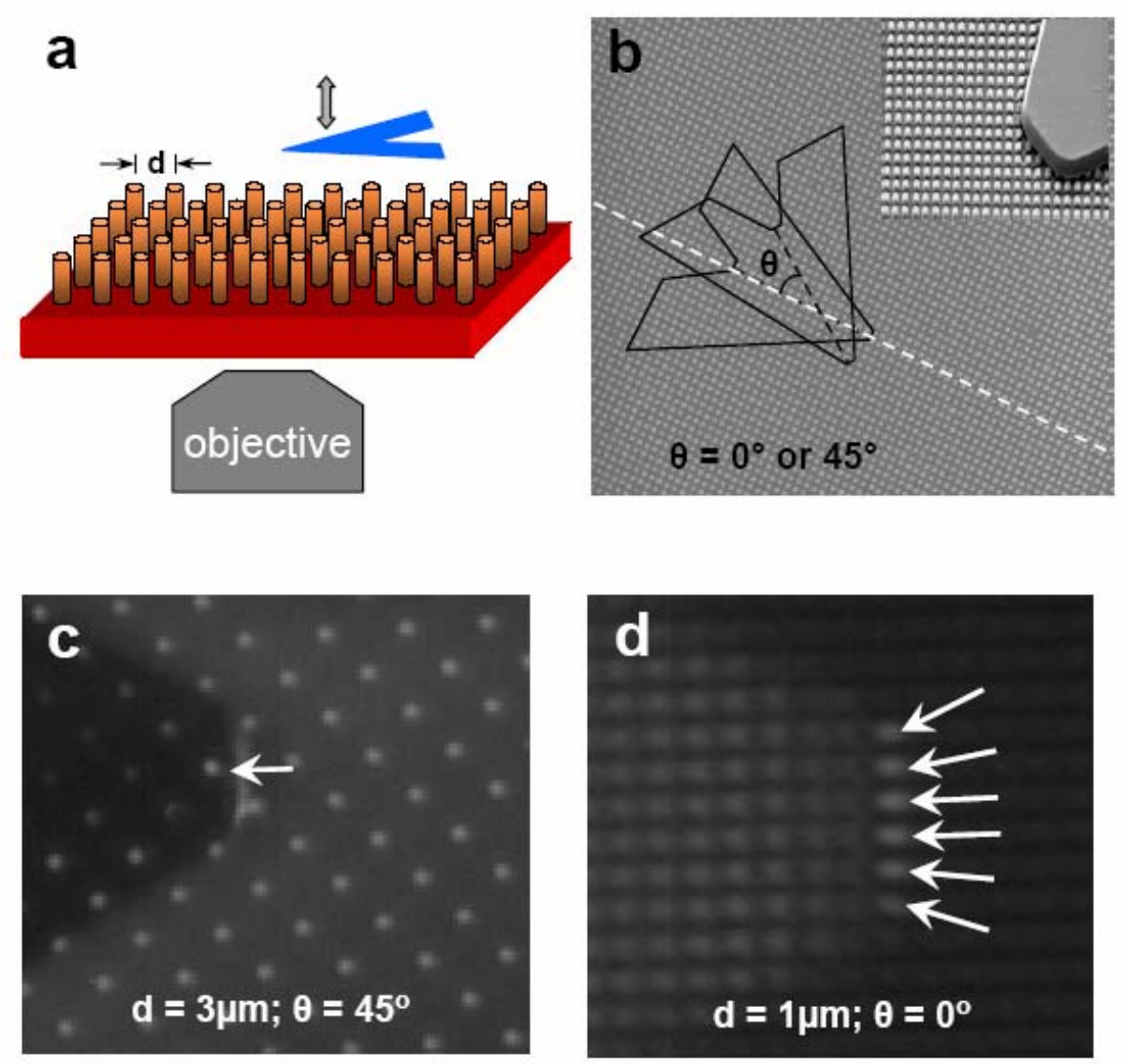

Figure 6-4. AFM method for adhesion measurement and imaging of contact area at the single pillar level.
A. Experimental set-up for measuring adhesion. A tipless AFM cantilever is brought into contact with the nanopillar array and then retracted while the contact area is imaged from an objective located the underneath adhesive film. B. The number of pillars contacting the cantilever was controlled through the distance, d, between pillars (d = 1, 2, and 3 μm) and the angle, θ, between the cantilever and the axis of the pillar array (θ = either 0^o or 45^o). The inset shows an SEM image of a cantilever contacting a geckel pillar array to yield a five pillar contact condition (d = 1 μm and θ = 45^o). C and D. Optical microscope images showing contact between AFM tip and pillar array. One pillar contact was achieved when d = 3 μm and θ = 45^o (C), and six pillars were in contact when d = 1 μm and θ = 0^o (D).

6.3.3 Adhesive Strength of Geckel

Adhesion experiments were performed both in air and under water for uncoated (hereafter 'gecko') and p(DMA-co-MEA) coated ('geckel') pillar arrays (Figure 6-5). Pillar-resolved (i.e. area-defined) force measurements showed strong adhesive forces when the cantilever is pulled away from the pillar surface. Figures 6-5A and B show typical force-distance (F-D) curves, with each curve representing a specific number (1-6) of 400nm diameter pillars interacting with the Si_3N_4 cantilever surface. The pull-off force was determined from each F-D curve and mean values from multiple experiments plotted in Figure 6-5D as a function of the number of contacting pillars. The observed linear increase in force with pillar number indicates constructive force accumulation, i.e. simultaneous detachment of individual pillars from the cantilever. The adhesive force per pillar (Figure 6-5E) was calculated from the individual slopes: 39.8 ± 2 (gecko in air), 5.9 ± 0.2 (gecko in water), 120 ± 6 (geckel in air), and 86.3 ± 5 (geckel in water).

Although the addition of p(DMA-co-MEA) coating on the pillars significantly increased dry adhesion, the enhancement of wet adhesion was particularly dramatic, as the wet adhesive force per pillar increased nearly 15 times (5.9 → 86.3 nN/pillar, Si_3N_4) when coated with p(DMA-co-MEA). The geckel wet-adhesion strength was also high when tested against other surfaces: titanium oxide (130.7 ± 14.3 nN/pillar) and gold (74.3 ± 4.1 nN/pillar) (Figure 6-6).

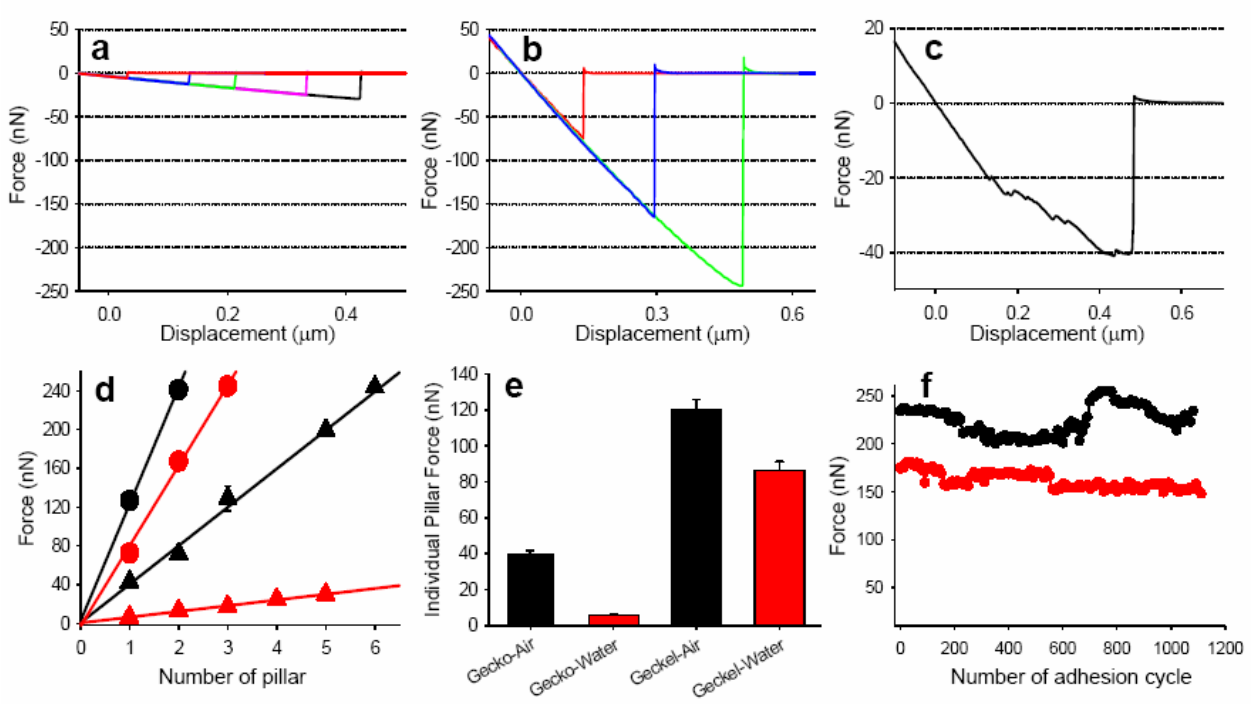

Figure 6-5. Force-distance curves and adhesion strength of geckel adhesive.
All data are for contact with a Si_3N_4 cantilever. A and B. Retraction F-D curves for uncoated gecko (A) and p(DMA-co-MEA) coated geckel (B) in water. The force required to separate the cantilever from the adhesive was closely correlated to the number of pillars in contact. The gecko adhesion F-D curves (A) were obtained for contact with one (red), two (blue), three (green), four (pink), and five (black) pillars. Similarly, geckel adhesive F-D curves (B) were obtained for one (red), two (blue), and three (green) pillar contacts. Significant wet adhesion was only observed in geckel adhesives. C. Retraction F-D curve for contact between cantilever and flat p(DMA-co-MEA) coated PDMS (contact area = 5.3 μm^2). The F-D curve showed complex peeling behavior indicated by deviation from linearity beginning at a force value of approximately -20nN. D. Mean separation force values vs. number of pillars for gecko (triangle) and geckel (circle) in water (red) and air (black) ($n > 60$, for each data point). The linear accumulation of adhesive force suggests no peeling during measurement. E. Adhesion force per pillar, obtained from the slopes of the regression lines shown in panel D. Wet adhesion was increased 15-fold in water. F. Long-term performance of geckel adhesive. Multiple cycles of attachment/detachment of geckel adhesive were performed in water (red) and air (black). Adhesion strength decreased by only 15% in water (red) and 2% in air (black) after 1100 successive cycles of contact/separation (two-pillar contact).

The versatility of geckel is not surprising given recent single molecule force experiments showing the ability of DOPA to interact strongly with both organic and inorganic surfaces(*89*). These interactions can take many forms, including metal coordination bonds, pi electron interactions, and covalent bonds. The lower adhesion strength of geckel on gold is in qualitative agreement with our earlier single molecule pull-off and polymer adsorption studies that indicated DOPA interacts less strongly to gold than to titanium oxide(*75, 89*).

Furthermore, as suggested by our previous study in which we observed the strong bond between DOPA and a metal oxide surface to rupture upon pulling and then re-form when brought back into contact with the surface(*89*), we speculated that geckel hybrid nanoadhesive may exhibit reversible adhesion to substrates. Repetitive AFM force measurements showed that geckel's wet- and dry-adhesion power was only slightly diminished during many cycles of adhesion, maintaining 85% in wet (red) and 98% in dry (black) conditions after 1100 contact cycles (Figure 6-5F). To our knowledge no other gecko mimetic adhesive has demonstrated efficacy for more than a few contact cycles(*46, 129*), and none have been shown to work under water. Control experiments involving pillar arrays coated with catechol-free polymer, p(MEA), showed lower adhesion strength (26 nN/pillar for the first contact cycle) as well as rapid decay in the adhesion performance under cyclic testing (Figure 6-7), emphasizing the importance of the mussel-mimetic catechol groups in enhancing wet adhesion as well as anchoring the p(DMA-co-MEA) polymer on the pillar array. At the same time, it appears that the nanostructured surface is essential to the observed geckel adhesive behavior. Force measurements on flat substrates coated with p(DMA-co-MEA) indicated a complex peeling behavior initiating at low adhesive strength (Figure 6-5C), which is in distinct contrast to the linear force accumulation behavior exhibited by the geckel adhesive (Figure 6-5D).

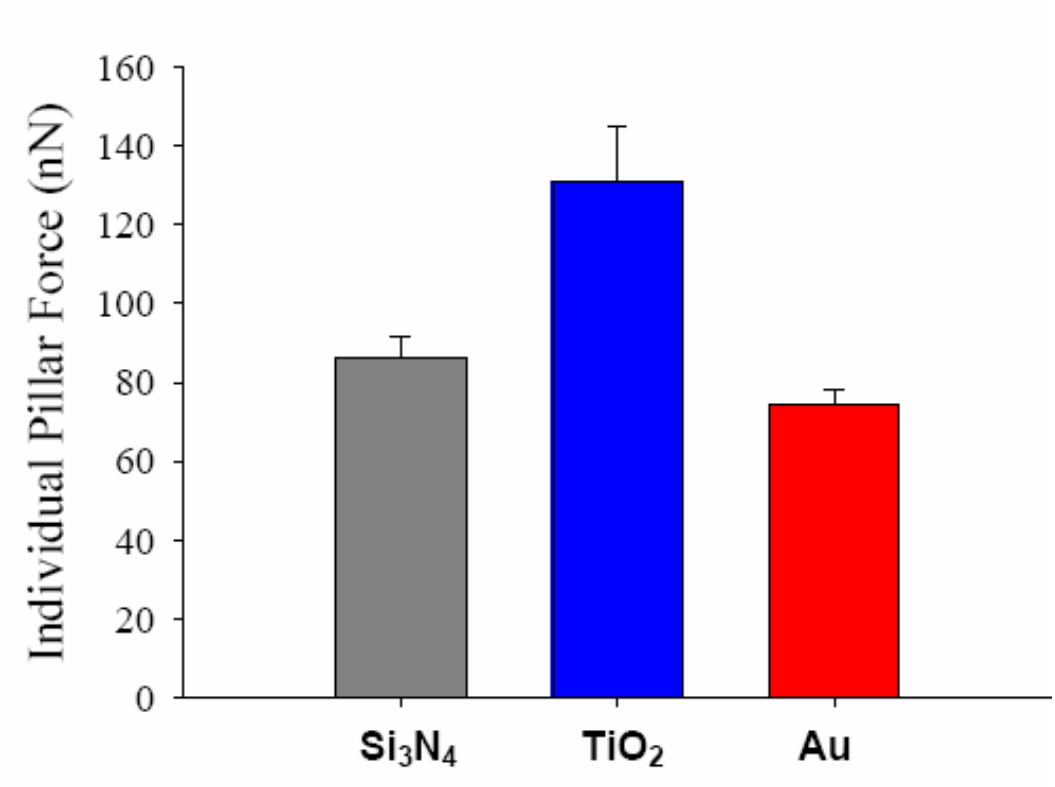

Figure 6-6. Substrate-dependent wet adhesion of geckel.
AFM force measurements revealed changes in wet adhesion of geckel on different substrates (Si_3N_4, TiO_x, and Au). 86.3 ± 5 nN for Si_3N_4 (the data from Figure 4D, Geckel-Water), 130.7 ± 14.3 nN for TiO_x (n = 50), and 74.3 ± 4.1 nN for Au (n = 65).

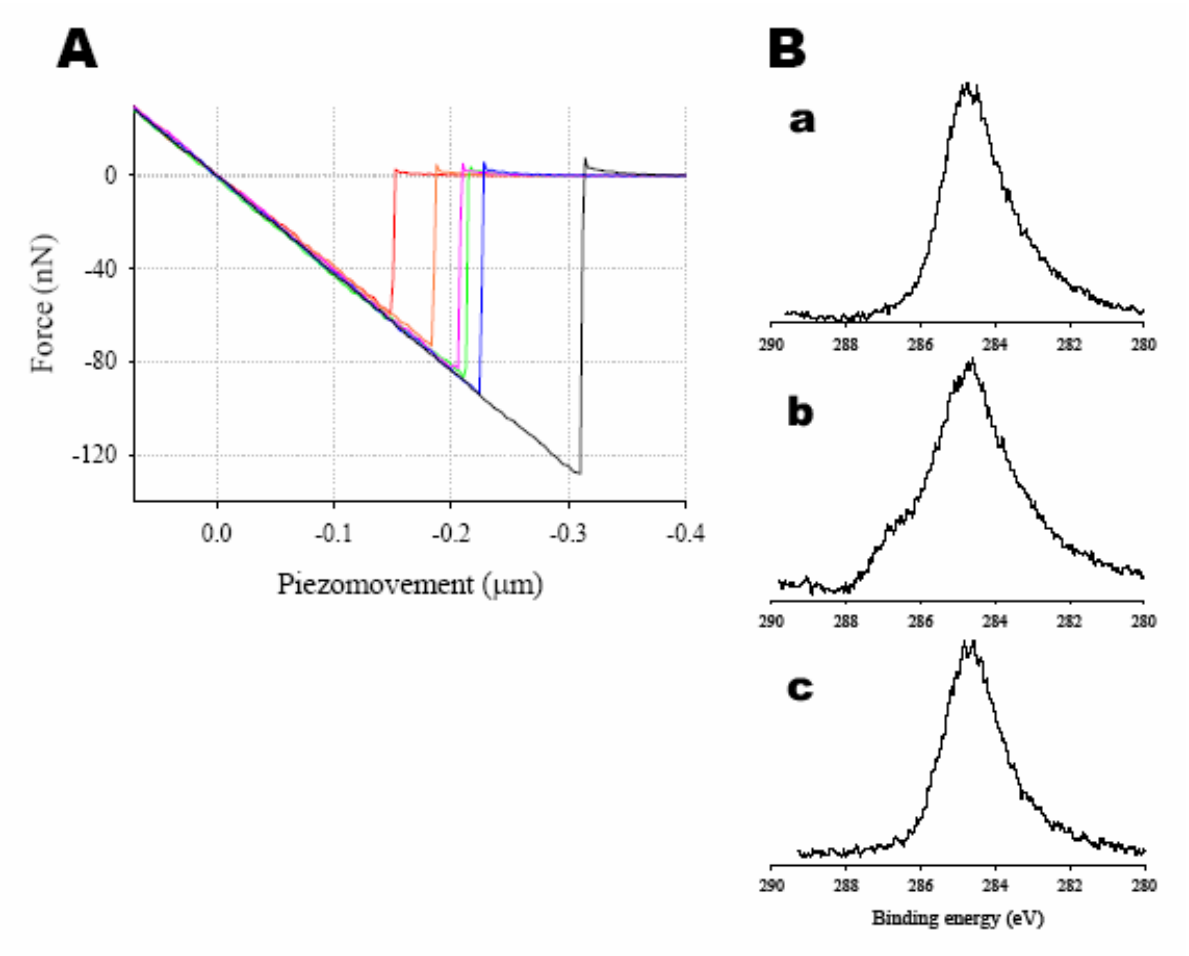

Figure 6-7. Wet adhesion of p(MEA)-coated gecko.
A. Adhesion of p(MEA)-coated pillar array to Si_3N_4 in water (5 pillar contact, 400nm pillar diameter, d=1μm and θ =45^o). A significant decay in adhesion was observed with successive contacts. The force traces shown in the figure represent every 10th cycle: 1(127.9 nN, black); 11(93.8 nN, blue), 21(86.6 nN, green), 31(82.7 nN, pink), 41(73.1 nN, orange), and 51(59.3 nN, red). B. Carbon 1s high resolution XPS spectra of bare PDMS (panel a), p(MEA)-coated PDMS (panel b), and p(MEA)-PDMS after incubation in water at room temperature for 18 hrs (panel c).

6.4 Conclusions

The geckel nanoadhesive was shown to be highly effective at adhering reversibly to surfaces under water, and with functional performance resembling that of a sticky note. Although we must be cautious in extrapolating our results to larger areas because of the challenges associated with maintaining equal load sharing among a large number of posts, in its current form (400 nm pillar diameter and 1 μm spacing) a 1 cm^2 surface area of geckel adhesive would transmit 9 N of force under water (90 kPa). It is interesting to note that this value is similar to estimates for the strength of gecko dry adhesion(*41, 43, 44*), suggesting that under wet conditions our hybrid geckel adhesive may perform as well as gecko adhesives do under dry conditions. Further refinement of the pillar geometry and spacing, the pillar material, and mussel mimetic polymer may lead to even greater improvements in performance of this nanostructured adhesive. The results of this study should be of relevance to the design of wet temporary adhesives for medical, industrial, consumer and military settings.

Chapter 7: Summary and Perspectives

7.1 Summary and Future Directions of Thesis Work

7.1.1 Cooperativity in mussel adhesion

Adhesives are essential to life - cyanoacrylates, epoxy resins, Velcro™, and other commercial adhesives are readily available, and we use them almost everyday. Adhesives are also used in industry; many products including even sophisticated semiconductors increasingly require adhesives to bond materials together. Despite our tremendous dependence on adhesives, most become completely nonfunctional upon exposure to water because the presence of water plays an interfering role in the boundary layer at interfaces. Furthermore, all types of intermolecular forces are dramatically decreased in aqueous environments. In addition, the hydrophilic nature of many adhesive polymers often results in solublization and/or diffusion into

an aquesous medium. Considering potential medical and industrial applications of water-resistant adhesives, understanding interfacial interactions in the presence of water is of utmost importance in development of effective adhesives.

In the sea, mussels are found to form a strong holdfast on surfaces of various materials in which the mussel adhesive proteins are secreted from so-called mussel foot, a process that is functionally equivalent to an injection molding. Measurement of adhesive strength of the attached mussel pads has been a difficult task which is largely due to cohesive failure by the strong pad and surface adhesion. The adhesive force measurement at a single-molecule level described in Chapter 3 (700-800 pN for TiO_2, ~ 2 nN for amine-presenting organic surfaces, ~400 pN for mucous layer and Au) revealed multiple adhesion mechanisms such as coordination, covalent, and pi-pi interactions depending upon the chemical nature of opposing substrates. The single-molecule information is expected to contribute on designing and understanding the adhesion mechanism of DOPA-containing adhesives in the future.

Interesting yet unexplored topic is cooperative adhesion. DOPA is the most abundant amino acid found in Mefp-3,5 (20 - 27 %) (*11, 15*), so that in a randomly distributed protein the average distance between DOPA is about 2 nm (the coutour length of amino acid in proteins is ~ 0.4 nm; 5 amino acids x 0.4 = 2 nm). Such close proximity of neighboring DOPA might result in cooperative effects, allowing for mussels to survive even large forces in the harsh seashore environment. It is expected that only 2 – 3 DOPA residues are strong enough to be equivalent to a covalent bond under a cooperative adhesive condition. This mechanism may explain, at least in part, the observation of cohesive failure of byssal threads when pulling a mussel body rather than adhesive failure at the interface between substrate and adhesive pad.

7.1.2 Characterization of polydopamine coating mechanisms

The DOPA-Lys motif in the amino acid sequence of Mefp-3,5 was demonstrated as an essential component for material-independent adhesion that has been observed in mussel adhesion (Chapter 4). Inspired by the chemical functionality of DOPA-Lys, dopamine, a bi-functional catecholamine molecule, was identified as a precursor for material-independent coatings. This polydopamine coating chemistry is unique due to the intrinsic latent chemical reactivity toward amine and thiol groups, providing a convenient route for bio- and polymeric-conjugation on any type of material surface.

Detailed characterization of the oxidative polymerization mechanism of dopamine, which is reminiscent to the formation of biopigment of melanin, and biocompatibility of the coating, remain as topics for future study. The use of structural analogues of dopamine such as epinephrine, norepinephrine, and pyrogallol as well as isotope labeling (^{13}C and ^{15}N) will provide better understanding of the polymerization mechanism. Other phenomena during oxidative dopamine polymerization are also interesting topics to study which include the formation of organic thin film at the air-water interface and nano- and micro-particles.

7.1.3 Improvement of gecko mimetic adhesives

In chapter 2, artificial gecko adhesives were reviewed and a new gecko-mussel hybrid adhesive called ‘Geckel’ was introduced in chapter 6. However, the gecko mimetic adhesives still do not match the properties exhibited by natural gecko adhesive. One possible reason is an oversimplified geometrical design of artificial adhesive pillar arrays in which the natural gecko hairs are approximated by a simple cylindrical shape, which is in contrast to the natural system consisting of a spatular shape whose diameter is larger than that of the supporting pillar. Force measurement in microscale hair mimics showed significant influence on the terminal shape of artificial adhesive pillars. Pillars terminated by spatulalike structures performed far better in

adhesion than flat, concave, and spherical terminal geometries (*51*). However, no experiments (adhesion vs. tip geometry) have been reported for nanoscale pillars, which are the dimensions of natural adhesives.

Another challenge is a large-area fabrication of nanopillar arrays for practical uses such as wall-, ceiling-walking robots. Photolithography has been the method of choice for mass production of semiconductors and microelectronic circuits, which requires a photomask with desired patterns. Fabrication of a feature size about 200 nm with wafer-scale throughtput is not a trivial task in academia. There are a few available lithographic techniques: phase-shift lithography (*138*), projection lithography (*139*), and interference lithography (*140, 141*). The phase difference controlled by varying the optical path length of the light passing throught vicinal structures results in constructive and destructive interference, which improves the contrast of light intensity on the surface of photoresist. However, it is difficult to create high aspect ratio patterns similar to the nano-structures found in setae and spetulae of gecko's hair. Projection lithography is the method used today in industrial production, in which a picture in the photomask is projected onto a wafer by an optical system located between the photomask and photoresist. This approach is simple to create the array of gecko hair but the equipment for projection lithography is not often available in academia. Finally, interference lithography is a relatively new technique which uses fringe-to-fringe spacing (or period) generated by interference of splitted monochromatic two-beam. This method is suitable to create a large area pattern that exhibits a certain symmetry such as circle, retangle, and hexagon.

REFERENCES

(1) K. A. Daltorio, S. N. Gorb, A. Peressadko, A. D. Horchler, T. E. Wei, R. E. Ritzmann, and Quinn, R. D. (2007) Microstructured polymer adhesive feet for climbing robots. *MRS Bulletin 32*, 504-508.

(2) T. Tang, C.-Y. Hui, and Glassmaker., N. J. (2005) Can a fibrillar interface be stronger and tougher than a non-fibrillar one? *J. Roy. Soc. Interface 2*, 505-516.

(3) J. Israelachvili (1985) *Intermolecular and Surface Forces*, Academic Press, London.

(4) J. H. Waite. (1983) Evidence for a repeating 3,4-dihydroxyphenylalanine- and hydroxyproline-containing decapeptide in the adhesive protein of the Mussel, Mytilus edulis L. *J. Biol. Chem. 258*, 2911-2915.

(5) J. H. Waite, T. J. Housley, and Tanzer., M. L. (1985) Peptide repeats in a mussel glue protein: theme and variations. *Biochemistry 24*, 5010-5014.

(6) S. W. Taylor, J. H. Waite, M. M. Ross, J. Shabanowitz, and D. F. Hunt. (1994) Trans-2,3-cis-3,4-dihydroxyproline, a new naturally occurring amino acid, is the six residue in the tandemly repeated consensus decapeptides of an adhesive protein from Mytilus edulis. *J. Am. Chem. Soc. 116*, 10803-10804.

(7) K. E. Anderson, and Waite., J. H. (2000) Immunolocalization of Dpfp-1, a byssal protein of the zebra mussel (Dreissena polymorpha). *J. Exp. Biol. 203*, 3065-3076.

(8) M. P. Olivieri, R. M. Wollman, and J. L. Alderfer. (1997) Nuclear magnetic resonance spectroscopy of mussel adhesive protein repeating peptide segment,. *J. Peptide, Res. 50*, 436-442.

(9) M. Kanyalkar, S. Srivastava, and E. Coutinho. (2002) Conformation of a model peptide of the tandem repeat decapeptide in mussel adhesive protein by NMR and MD simulations. *Biomaterials 23*, 389-396.

(10) N. Holten-Andersen, G. E. Fantner, S. Hohlbauch, J. H. Waite, and Zok., F. W. (2007) Protective coatings on extensible biofibres. *Nat. Mater. In press*.

(11) M. Yu, J. Hwang, and Deming, T. J. (1999) Role of L-3,4,-dihydroxyphenylalanine in mussel adhesive proteins. *J. Am. Chem. Soc. 121*, 5825-5826.

(12) T. V. Diamond. (1999), University of Delaware, Newark.

(13) V. V. Papov, T. V. Diamond, K. Biemann, and J. H. Waite. (1995) Hydroxyarginine-containing polyphenolic proteins in the adhesive plaques of the marine mussel Mytilus edulis,. *J. Biol. Chem. 270*, 20183-20192.

(14) Q. Lin, D. Gourdon, C. Sun, N. Holten-Andersen, T. H. Anderson, J. H. Waite, and Israelachvili, J. N. (2007) Adhesion mechanisms of the mussel foot proteins mfp-1 and mfp-3. *Proc. Nat. Acad. Sci. USA 104*, 3782-3786.

(15) J. H. Waite, and X. X. Qin. (2001) Polyphenolic phosphoprotein from the adhesive pads of the common mussel. *Biochemistry 40*, 2887-2893.

(16) G. Falini, S. Albeck, S. Weiner, and L .Addadi. (1996) Control of aragonite or calcite polymorphism by mollusk shell macromolecules,. *Science 271*, 67-69.

(17) J. Weaver. (1998) Isolation, purification and partial characterization of a mussel byssal precursor protein, Mytilus edulis foot protein-4. *Master Thesis, University of Delaware*.

(18) L. M. Rzepecki, K. M. Hansen, and J. H. Waite. (1992) Characterization of a cysteine rich polyphenolic protein from the blue mussel Mytilus edulis L. *Biol. Bull. 183*, 123-137.

(19) K. Inoue, Y. Takeuchi, D. Miki, and Odo, S. (1995) Mussel adhesive plaque protein gene is a novel member of Epidermal Growth Factor-like gene family. *J. Biol. Chem. 270*, 6698-6701.

(20) H. Zhao, and Waite., J. H. (2006) Linking adhesive and structural proteins in the attachment plauque of mytilus californianus. *J. Biol. Chem. 281*, 26150-26158.

(21) D. S. Hwang, H. J. Yoo, J. H. Jun, W. K. Moon, and H. J. Cha. (2004) Expression of functional recombinant mussel adhesive protein Mgfp-5 in Escherichia coli. *App. Environ. Microbiol. 70*, 3352-3359.

(22) D. S. Hwang, S. B. Sim, and Cha, H. J. (2007) Cell adhesion biomaterial based on mussel adhesive protein fused with RGD peptide. *Biomaterials 28*, 4039-4046.

(23) D. S. Hwang, Y. Gim, H. J. Yoo, and Cha, H. J. (2007) Practical recombinant hybrid mussel bioadhesive fp-151. *Biomaterials 28*, 3560-3568.

(24) L. M. McDowell, L. A. Burzio, J. H. Waite, and Schaefer., J. (1999) REDOR detection of cross-links formed in mussel byssus under high flow stress. *J. Biol. Chem. 274*, 20293-20295.

(25) L. A. Burzio, and J. H. Waite. (2000) Cross-linking in adhesive quinoproteins: studies with model decapeptides. *Biochemistry 39*, 11147-11153.

(26) F. Hook, B. Kasemo, T. Nylander, C. Fant, K. Sott, and H. Elwing. (2001) Variations in coupled water, viscoelastic properties and film thickness of a mefp-1 protein film during adsorption and cross-linking: A quartz crystal microbalance with dissipation monitoring, ellipsometry, and surface plasmon resonance study. *Anal. Chem. 74*, 5796-5804.

(27) F. L. Florin, V. T. Moy, and Gaub, H. E. (1994) Adhesion forces between individual ligand-receptor pairs. *Science 264*, 415-417.

(28) G. U. Lee, D. A. Kidwell, and Colton, R. J. (1994) Sensing discrete streptavidin-biotin interactions with atomic force microscopy. *Langmuir 10*, 354-357.

(29) O. H. Wilemsen, M. M. E. Snel, K. O. van der Werf, B. G. de Grooth, J. Greve, P. Hinterdorfer, H. J. Gruber, H. Schindler, Y. van Kooyk, and Figdor., C. G. (1998) Simultaneous height and adhesion imaging of antibody-antigen interactions by atomic force microsopy. *Biophys. J. 75*, 2220-2228.

(30) U. Dammer, M. Hegner, D. Anselmetti, P. Wagner, M. Dreier, W. Huber, and Guntherodt., H. J. (1996) Specific antigen/antibody interactions measured by force microscopy. *Biophys. J. 70*, 2437-2441.

(31) R. Ros, F. Schwesinger, D. Anselmetti, M. Kubon, R. Schafer, A. Pluckthun, and Rozsnyai., L. F. (1998) Antigen binding forces of individually addressed single-chain Fv antibody molecules. *Proc. Nat. Acad. Sci. USA 95*, 7402-7405.

(32) P. Hinterdorfer, W. Baumgartner, H. J. Gruber, K. Schilcher, and Schindler., H. (1996) Detection and localization of individual antibody-antigen recognition events by atomic force microscopy. *Proc. Nat. Acad. Sci. USA 93*, 3477-3481.

(33) M. Rief, M. Gautel, F. Oesterhelt, J. M. Fernandez, and Gaub., H. E. (1997) Reversible unfolding of individual titin Ig-domain by AFM. *Science 276*, 1109-1112.

(34) M. Rief, J. Pascual, M. Saraste, and Gaub., H. E. (1999) Single molecule force spectroscopy of spectrin repeats: low unfolding forces in helix bundles. *J. Mol. Biol. 286*, 553-561.

(35) F. Kienberger, G. Kada, H. J. Gruber, V. P. Pastushenko, C. K. Riener, M. Trieb, H. G. Knaus, H. Schindler, and Hinterdorfer, P. (2000) Recognition force spectroscopy studies of the NTA-His6 bond. *Single. Mol. 1*, 59.

(36) M. Conti, G. Falini, and Samori, B. (2000) How strong is the coordination bond between a histidine tag and Ni-Nitrilotriacetate? An experiment of mechanochemistry on single molecules. *Angew. Chem. Int. Ed. 39*, 215.

(37) L. Schmitt, M .Ludwig, and Gaub, H. E. (2000) A metal-chelating microscopy tip as a new toolbox for single-molecule experiments by atomic force microscopy. *Biophys. J. 78*, 3275-3285.

(38) M. Grandbois, M. Beyer, M. Rief, H. Clausen-Schaumann, and Gaub, H. E. (1999) How strong is a covalent bond? *Science 283*, 1727-1730.

(39) R. Ruibal, and Ernst., V. (1965) The structure of the digital setae of lizards. *J. Morphol. 117*, 271-294.

(40) E. E. Williams, and J. A. Peterson. (1982) Convergent and alternative designs in the digital adhesive pads of scincid lizards. *Science 215*, 1509-1511.

(41) K. Autumn, Y. A. Liang, S. T. Hsieh, W. Zesch, W. P. Chan, T. W. Kenny, R. Fearing, and Full, R. J. (2000) Adhesive force of a single gecko foot-hair. *Nature 405*, 681-685.

(42) W. Sun, P. Neuzil, T. S. Kustandi, S. Oh, and V. D. Samper. (2005) The nature of the gecko lizard adhesive force. *Biophys. J. 89*, L14-16.

(43) G. Huber, H. Mantz, R. Spolenak, K. Mecke, K. Jacobs, S. N. Borb, and Arzt., E. (2005) Evidence for capillary contributions to gecko adhesion from single spatula nanomechanical measurements. *Proc. Nat. Acad. Sci. USA 102*, 16293-16296.

(44) K. Autumn, M. Sitti, Y. A. Liang, A. M. Peattie, W. R. Hansen, S. Sponberg, T. W. Kenny, R. Fearing, J. N. Israelachvili, and Full, R. J. (2002) Evidence for van der Waals adhesion in gecko setae. *Proc. Nat. Acad. Sci. USA 99*, 12252-12256.

(45) K. Autumn, A. Dittmore, D. Santos, M. Spenko, and Cutkosky., M. (2006) Frictional adhesion: a new angle on gecko attachment. *J. Exp. Biol. 209*, 3569-3579.

(46) A. K. Geim, S. V. Dubonos, I. V. Grigorieva, K. S. Novoselov, A. A. Zhukov, and Shapoval., S. Y. (2003) Microfabricated adhesive mimicking gecko foot-hair. *Nat. Materials 2*, 461-463.

(47) A. Peressadko, and S. N. Gorb. (2004) When less is more: Experimental evidence for tenacity enhancement by division of contact area. *J. Adhesion 80*, 1-5.

(48) A. J. Crosby, M. Hageman, and A. Duncan. (2005) Controlling polymer adhesion with "Pancakes". *Langmuir 21*, 11738-11743.

(49) L. Ge, S. Sethl, L Cl, P. M. Ajayan, and Dhinojwala., A. (2007) Carbon nanotube-based synthetic gecko taptes. *Proc. Nat. Acad. Sci. USA 104*, 10792-10795.

(50) M. Jin, X. Feng, L. Feng, T. Sun, J. Zhai, T. Li, and Jiang., L. (2005) Superhydrophobic alighed polystyrene nanotube films with high adhesive force. *Adv. Mater. 17*, 1977-1981.

(51) A. del. Campo, C. Creiner, I. Alvarez, and Arzt., E. (2007) Patterned surfaces with pillars with controlled 3D tip geometry mimicking bioattachment devices. *Adv. Mater. 19*, 1973-1977.

(52) J. R. M. Chisholm, and Kelley, R. (2001) Worms start the reef-building process. *Nature 409*, 152.

(53) J. H. Waite. (2002) Adhesion a la moule. *Integ. & Comp. Biol. 42*, 1172-1180.

(54) J. H. Waite, M. L. T. (1981) Polyphenolic substance of mytilus edulis: novel adhesive containing L-Dopa and hydroxyproline. *Science 212*, 1038-1040.

(55) D. J. Crisp, G. Walker, G. A. Young, and Yule, A. B. (1985) Adhesion and substrate choice in mussels and barnacles. *J. Coll. Inter. Sci. 104*, 40-50.

(56) J. H. Waite. (1999) Reverse engineering of bioadhesion in marine mussels. *Ann. NY Acad. Sci. 875*, 301-309.

(57) S. Haemers, G. J. M. Koper, and Frens, G. (2003) Effect of oxidation rate on cross-linking of mussel adhesive proteins. *Biomacromolecules 4*, 632-640.

(58) J. Monahan, and Wilker, J. J. (2004) Cross-Linking the protein precursor of marine mussel adhesives: Bulk measurements and reagents for curing. *Langmuir 20*, 3724-3729.

(59) G. A. Young, and D. J. Crisp (1982) *Marine animals and adhesion.*, Applied Science Publishers Ltd.

(60) M. Yu, and T. J. Deming. (1998) Synthetic polypeptide mimics of marine adhesives. *Macromolecules 31*, 4739-4745.

(61) B. P. Frank, and G. Belfort. (2002) Adhesion of Mytilus edulis foot protein 1 on silica: ionic effects on biofouling. *Biotech. Prog. 18*, 580-586.

(62) P. Hinterdorfer, W. Baumgartner, H. J. Gruber, K. Schilcher, and Schindler., H. (1996) Detection and localization of individual antibody-antigen recognition events by atomic force microscopy. *Proc. Nat. Acad. Sci. USA 93*, 3477-3481.

(63) H. O. Pierson (1992) *Handbook of chemical vapor deposition.*, Noyes Pub., New Sersey.

(64) J. L. Hutter, and Bechhoefer., J. (1993) Calibration of atomic force microscopy. *Rev. Sci. Instr. 64*, 1868-1873.

(65) J. Liphardt, B. Onoa, S. B. Smith, J. I. Tinacio, and Bustamante, C. (2001) Reversible unfolding of single RNA molecules by mechanical force. *Science 292*, 733-737.

(66) R. Merkel, P. Nassoy, A. Leung, K. Ritchie, and E. Evans. (1999) Energy landscapes of receptor-ligand bonds explored with dynamic force spectroscopy. *Nature 397*, 50-53.

(67) M. Vega-Arroyo, P. R. LeBreton, T. Rajh, P. Zapol, and L. A. Curtiss. (2005) Density functional study of the TiO_2-dopamine complex. *Chem. Phys. Lett. 406*, 306-311.

(68) H. Zhao, C. Sun, R. J. Stewart, and Waite, J. H. (2005) Cement proteins of the tube-building polychaete Phragmatopoma californica. *J. Biol. Chem. 280*, 42938-42944.

(69) R. Rodriguez, M. A. Blesa, and A. E. Regazzoni. (1996) Surface complexation at the TiO2(anatase)/aqueous solution interface: chemisorption of catechol. *J. Col. Inter. Sci. 177*, 122-131.

(70) A. Y. Fadeev, and T. J. McCarthy. (2000) Self-Assembly is not the only reaction possible between alkyltrichlorosilanes and surfaces: monomolecular and oligomeric covalently attached layers of dichloro- and trichloroalkylsilanes on silicon. *Langmuir 16*, 7268-7274.

(71) U. Dammer, O. Popescu, P. Wagner, D. Anselmetti, H. -J. Guntherodt, and Misevic., G. N. (1995) Binding strength between cell adhesion proteoglycans measured by atomic force microscopy. *Science 267*, 1173-1175.

(72) N. D. Catron, H. Lee, and Messersmith., P. B. (2006) Enhancement of poly(ethylene glycol) mucoadsorption by biomimetic endgroup functionalization. *Biointerphases 1*, 134-141.

(73) T. Paunesku, T. Rajh, G. Wiederrecht, J. Maser, S. Vogt, M. Stojicevic, M. Protic, B. Lai, J. Oryhon, M. Thurnauer, and Woloschak., G. (2003) Biology of TiO_2-oligonucleotide nanocomposites. *Nat. Mater. 2*, 343-346.

(74) A. R. Statz, R. J. Meagher, A. E. Barron, and Messersmith, P. B. (2005) New peptidomimetic polymers for antifouling surfaces. *J. Am. Chem. Soc. 127*, 7972-7973.

(75) J. L. Dalsin, B.-H. Hu, B. P. Lee, and P. B. Messersmith. (2003) Mussel adhesive protein mimetic polymers for the preparation of nonfouling surfaces. *J. Am. Chem. Soc. 125*, 4253-4258.

(76) T. A. Sulchek, R. W. Friddle, K. Langry, E. Y. Lau, H. Albrecht, T. V. Ratto, S. J. DeNardo, M. E. Colvin, and Noy., A. (2005) Dynamic force microscopy of parallel individual Mucin-1-antibody bonds. *Proc. Nat. Acad. Sci. USA 102*, 16638-16643.

(77) T. A. Sulchek, R. W. Friddle, and Noy., A. (2006) Strength of multiple parallel biological bonds. *Biophys. J. 90*, 4686-4691.

(78) B. D. Ratner, and A. S. Hoffman (2004) *Biomaterials science: an introduction to materials in medicine*, Elsevier Academic Press, San Diego.

(79) J-A. Ahn, H-S. Kim, K. J. Lee, S. Jeon, S. J. Kang, Y. Sun, R. G. Nuzzo, and Rogers., J. A. (2006) Heteroneneous three-deminsional electronics by use of printed semiconductor nanomaterials. *Science 314*, 1754-1757.

(80) P. Alivisatos. (2004) The use of nanocrystals in biological detection. *Nat. Biotech. 22*, 47-52.

(81) R. Langer. (2001) Perspectives: drug delivery - drugs on target. *Science 293*, 58-59.

(82) J. C. Love, L. A. Estroff, J. K. Kriebel, R. G. Nuzzo, and Whitesides., G. M. (2005) Self-assembled monolayers of thiolates on metals as a form of nanotechnology. *Chem. Rev. 105*, 1103-1196.

(83) G. Decher. (1997) Fuzzy nanoassemblies: toward layered polymeric multicomposites. *Science 277*, 1232-1237.

(84) G. Roberts (1990) *Langmuir-Blodgett films*, Kluwer Acad., Norwell, MA.

(85) S. R. Whaley, D, S., English,, E. L. Hu, P. F. Barbara, and Belcher, A. M. (2000) Selection of peptides with semiconductor binding specificity for directed nanocrystal assembly. *Nature 405*, 665-8.

(86) C. Tamerler, and M. Sarikaya. (2007) Molecular biomimetics: Utilizing nature's molecular ways in practical engineering *Acta Biomaterialia 3*, 289-299.

(87) D.Y. Ryu, K. Shin, E. Drockenmuller, C.J. Hawker, and Russell., T. P. (2005) A generalized approach to the modification of solid surfaces. *Science 308*, 236-239.

(88) M.J. Sever, J. T. Weisser, J. Monahan, S. Srinivasan, and Wilker, J. J. (2004) Metal-mediated cross-linking in the generation of a marine-mussel adhesive. *Angew. Chem. Int. Ed. 43*, 448-50.

(89) H. Lee, N. F. Scherer, and Messersmith, P. B. (2006) Single molecule mechanics of mussel adhesion. *Proc. Nat. Acad. Sci. USA 103*, 12999-13003.

(90) C. Xu, K. Xu, H. Gu, R. Zheng, H. Liu, X. Zhang, Z. Guo, and B. Xu. (2004) Dopamine as a robust anchor to immobilize functional molecules on the iron oxide shell of magnetic nanoparticles. *J. Am. Chem. Soc. 126*, 9938-9939.

(91) S. Zuercher, D. Waeckerlin, Y. Bethuel, B. Malisova, M. Textor, S. Tosatti, and K. Gademann. (2006) Biomimetic Surface Modifications Based on the Cyanobacterial Iron Chelator Anachelin. *J. Am. Chem. Soc. 128*, 1064-1065.

(92) Y. Li, M. Liu, C. Xiang, Q. Xie, and Yao, S. (2006) Electrochemical quartz crystal microbalance study on growth and property of the polymer deposit at gold electrodes during oxidation of dopamine in aqueous solutions. *Thin Solid Films 497*, 270-278.

(93) X. Qu, D. Wu, L. Mets, and Scherer., N. F. (2004) Nanometer-localized multiple single-moleucle fluorescence microscopy. *Proc. Natl. Acad. Sci. USA 101*, 11298-11303.

(94) H. Lee, S. H. Choi, and Park, T. G. (2006) Direct visualization of hyaluronic acid polymer chain by self-assembled one-dimensional array of gold nanoparticles. *Macromolecules **39***, 23-25.

(95) T. W. Jensen, B.-H. Hu, S. M. Dellatore, A. S. Garcia, P. B. Messersmith, and Miller, W. M. (2004) Lipopeptides incorporated into supported phospholipid monolayers have high specific activity at low incorporation levels. *J. Am. Chem. Soc. 126*, 15223-15230.

(96) W. Montagna, and Prota., G. (1993) *Black skin: structure and function*, Academic Press, San Diego.

(97) C. G. Pierpont, and Lange., C. W. (1994) The chemistry of transition metal complexes containing catechol and semiquinone ligands. *Prog. Inorg. Chem. 41*, 331-442.

(98) M. Charbonnier, M. Romand, G. Stremsdoerfer, and Fares-Karam., A. (1999) *Rec. Res. Devel. Macromol. Res. 4*, 27-43.

(99) M.J. LaVoie, B.L. Ostaszewski, A.Weihofen, M.G. Scholssmacher, and Selkoe., D. J. (2005) Dopamine covalently modifies and functionally inactivates parkin. *Nature Med. 11*, 1214-1221.

(100) P. E. Laibinis, G. M. Whitesides, D. L. Allara, Y. T. Tao, A. N. Parikh, and Nuzzo., R. G. (1991) Comparison of the structures and wetting properties of self-assembled monolayers of n-alkanethiols on the coinage metal surfaces, copper, silver, and gold. *J. Am. Chem. Soc. 113*, 7152-7167.

(101) K. L. Prime, and Whitesides., G. M. (1993) Adsorption of proteins onto surfaces containing end-attached oligo(ethylene oxide): a model system using self-assembled monolayers. *J. Am. Chem. Soc. 115*.

(102) D. N. Haylock, and Nilsson., S. K. (2006) The role of hyaluronic acid in hemopoietic stem cell biology. *Reg. Med. 1*, 437-445.

(103) B. P. Toole. (2004) Hyaluronan: from extracellular glue to pericellular cue. *Nat. Rev. Cancer 4*, 528-539.

(104) G. Decher, and J. D. Hong. (1991) *Makromol. Chem. Macromol. Symp. 46*, 321.

(105) J. L. Lutkenhaus, K. D. Hrabak, K. MccEnnis, and Hammond, P. T. (2005) Elastomeric flexible free-standing hydrogen-bonded nanoscale assemblies. *J. Am. Chem. Soc. 127*, 17228-17234.

(106) P. T. Hammond. (2004) Form and function in multilayer assembly: new applications at the nanoscale. *Adv. Mater. 16*, 1271-1293.

(107) Z. Tang, Y. Wang, P. Podsiadlo, and Kotov, N. A. (2006) Biomedical applications of layer-by-layer assembly: from biomimetics to tissue engineering. *Adv. Mat. 18*, 3203-3224.

(108) D. E. Bergbreiter. (1994) Polyethylene surface chemistry. *Prog. Polym. Sci. 19*, 529-560.

(109) M. Raposo, R. S. Pontes, L. H. C. Mattoso, and Oliveira, O. N. (1997) Kinetics of adsorption of poly(o-methoxyaniline) self-assembled films. *Macromolecules 30*, 6095-6101.

(110) M. C. Hsieh, R. J. Farris, and McCarthy, T. J. (1997) Surface "priming" for layer-by-layer deposition: polyelectrolyte multilayer formation on allylamine plasma-modified poly(tetrafluoroethylene). *Macromolecules 30*, 8453-8458.

(111) G. Price, F. Keen, and Clifton, A. A. (1996) *Macromolecules 29*, 5664-5670.

(112) H. Zhao, P. Yang, J. Deng, L. Liu, J. Zhu, Y. Sui, J. Lu, and Yang, W. (2007) Fabrication of a molecular-level multilayer film on organic polymer surfaces via chemical bonding assembly. *Langmuir 23*, 1810-1814.

(113) A. Delcorte, P. Bertrand, E. Wischerhoff, and Laschewsky, A. (1997) Adsorption of polyelectcrolyte multilayer on polymer surfaces. *Langmuir 13*, 5125-5136.

(114) A. Khademhosseini, S. Jon, K. Y. Suh, T. -N. T. Tran, G. Eng, J. Yeh, J. Seong, and Langer, R. (2003) Direct patterning of protein- and cell-resistant polymeric monolayers and microstructures. *Adv. Mater. 15*, 1995-2000.

(115) C. Boura, P. Menu, E. Payan, C. Picart, J. C. Voegel, S. Muller, and Stoltz, J. F. (2003) Endothelial cells grown on thin polyelectrolyte mutlilayered films: an evaluation of a new versatile surface modification. *Biomaterials 24*, 3521-3530.

(116) J. H. Waite, N. H. Andersen, S. Jewhurst, and Sun., C. (2005) Mussel adhesion: finding the tricks worth mimicking. *J. Adhesion 81*, 1-21.

(117) C. Picart, Ph. Lavalle, P. Hubert, F. J. G. Cuisinier, G. Decher, P. Schaaf, and Voegel, J. C. (2001) Buildup mechanism for poly(l-lysine)/hyaluronic acid films onto a solid surface. *Langmuir 17*, 7414-7424.

(118) B. Thierry, F. M. Winnik, Y. Merhi, and Tabrizian, M. (2003) Nanocoatings onto arteries via layer-by-layer deposition: Toward the in vivo repair of demaged blood vessels. *J. Am. Chem. Soc. 125*, 7494-7495.

(119) J. Vicente, R. Ramirez-Camacho, A. Trinidad, J. R. Garcia-Berrocal, D. Lobo, and Pinilla, M. (2006) Anti-adhesive properties of polytetrafluoroethylene (Gore-Tex) in middle ear surgery. An experimental study. *Acta Oto-Laryngol. 126*, 144-148.

(120) V. Pardo-Yissar, E. Katz, O. Lioubashevski, and Willner., I. (2001) Layered polyelectrolyte films on Au electrodes: characterization of electron-transfer features at the charged polymer interface and application for selective redox reactions. *Langmuir 17*, 1110-1118.

(121) H. Lee, B. P. Lee, and Messersmith, P. B. (2007) A reversible wet/dry adhesive inspired by mussels and geckos. *Nature 448*, 338-341.

(122) P. Podsiadlo, Z. Liu, D. Paterson, P. B. Messersmith, and Kotov, N. A. (2007) Fusion of seashell nacre and marine bioadhesive analogs: high-strength nanocomposite by layer-by-layer assembly of clay and-3,4-Dihydroxyphenylalanine Polymer. *Adv. Mater. 19*, 949-955.

(123) H. Lee, S. M. Dellatore, W. M. Miller, and Messersmith, P. B. (2007) Mussel-inspired surface chemistry for multifunctional coatings. *Science 318*, 426-430.

(124) B. J. Murray, Q. Li, J. T. Newberg, E. J. Menke, J. C. Hemminger, and Penner., R. M. (2005) Shape- and size-selective electrochemical synthesis of dispersed silver(I) oxide colloids. *Nano Lett 5*, 2319-2324.

(125) C. H. Ho, J. Tobis, C. Sprich, R. Thomann, and J. C. Tiller. (2004) Nanoseparated polymeric networks with multiple antimicrobial properties. *Adv. Mat. 16*, 957-961.

(126) M. T. Northen, and K. L. Turner. (2005) A batch fabricated biomimetic dry adhesive. *Nanotechnology 16*, 1159-1166.

(127) M. Sitti, and R. Fearing. (2003) Synthetic gecko foot-hair micro/nano-structures as dry adhesives. *J. Adhes. Sci. Technol. 17*, 1055-1073.

(128) B. Yurdumakan, N. R. Raravikar, P. M. Ajayan, and A. Dhinojwala. (2005) Synthetic gecko foot-hairs from multiwalled carbon nanotubes. *Chem. Commun. 30*, 3799-3801.

(129) M. T. Northen, and K. L. Turner. (2006) Meso-scale adhesion testing of integrated micro- and nano-scale structures. . *Sensors and Actuators A 130-131*, 583-587.

(130) G. Huber, S. N. Gorb, R. Spolenak, and E. Arzt. (2005) Resolving the nanoscale adhesion of individual gecko spatulae by atomic force microscopy. *Biology Lett. 1*, 2.

(131) E. Arzt, S. Gorb, and R. Spolenak. (2003) From micro to nano contacts in biological attachment devices. *Proc. Nat. Acad. Sci. USA 100*, 10603-10606.

(132) E. Arzt. (2006) Biological and artificial attachment devices: Lessons for materials scientists from flies and geckos. *Materials Sci. and Eng. C: Biomimetic and Supramol. Systems 26*, 1245-1250.

(133) R. Spolenak, S. N. Gorb, and E. Arzt. (2005) Adhesion design maps for bio-inspired attachment systems. *Acta biomaterialia 1*, 5-13.

(134) J. H. Waite. (1987) Nature's underwater adhesive specialist. *Chemtech. 17*, 692-697.

(135) J. H. Waite, and M. L. Tanzer. (1981) Polyphenolic substance of Mytilus edulis: novel adhesive containing L-DOPA and hydroxyproline. *Science 212*, 1038-1040.

(136) B. P. Lee, C.-Y. Chao, F. N. Nunalee, E. Motan, K. R. Shull, and P. B. Messersmith. (2006) Rapid Gel Formation and Adhesion in Photocurable and Biodegradable Block Copolymers with High DOPA Content. *Macromolecules 39*, 1740-1748.

(137) G. M. Whitesides. (2006) The origins and the future of microfluidics. *Nature 442*, 368-373.

(138) E. S. Kwak, J. Henzie, S. H. Chang, S. K. Gray, G. C. Schatz, and Odom, T. W. (2005) Surface plasmon standing waves in large-area subwavelength hole arrays. *Nano Lett 5*, 1963.

(139) E. Yablonovitch, and Vrijen, R. B. (1999) Optical projection lithography at half the Rayleigh resolution limit by two-photon exposure. *Optical Engineering 38*, 334-338.

(140) H. I. Smith, S. D. Hector, M. L. Schattenburg, and Anderson, E. H. (1991) A new approach to high fidelity e-beam lithography based on an in-situ, global fiducial grid. *J. Adhes. Sci. Technol. B 9*, 2992-2995.

(141) C. A. Ross, H. I. Smith, T. Savas, M. Schattenburg, M. Farhoud, M. Hwang, M. Walsh, M. C. Abraham, and Ram, R. J. (1999) Fabrication of patterned media for high density magnetic storage. *J. Vac. Sci. Technol. B 17*, 3168-3176.

Haeshin Lee Curriculum Vitae

Biomedical Engineering Department
Northwestern University
2145 Sheridan Rd. E262
Evanston, IL 60208
e-mail: hlee73@northwestern.edu

Education

Ph.D. Biomedical Engineering, Northwestern University, Sep. 2003 – Mar. 2008
B.S. Biological Sciences, Korea Advanced Institute of Science & Technology (KAIST), Mar. 1993 – Feb. 1997.

Research Experiences

Researcher, Department of Biochemistry and Molecular Biology, The University of Chicago, Feb. 2002 – Aug. 2003
Researcher, Department of Biological Sciences, Korea Advanced Institute of Science & Technology May 2000 – Jan. 2002; Oct. 1997 – Apr. 1998

Other Experiences

Mandatory military service. Apr. 1998 – Feb. 2000.

Book Chapter

Haeshin Lee, Phillip B. Messersmith, 'Bio-inspired nano-materials for a new generation of medicine' Edited by Tuan Vo-Dinh in Nanotechnology in Biology and Medicine, Chapter 3, CRC Press, ISBN 0849329493, 2007 (Jan. 24th)

Awards and Honors

1. Top 100 Science Stories, *Discover Magazine*, 2008, January
2. Scientists of the year 2007, The Ministry of Science and Technology, Korea Government
3. Graduate Student Award, Materials Research Society Meeting, Boston, 2007
4. Richard W. Jones best poster award, 2007, BME, Northwestern University

Patents

1. Phillip B. Messersmith, **Haeshin Lee**, Bruce P. Lee "Wet/Dry gecko-mussel (Geckel) hybrid na nomaterial adhesive" US patent application filed
2. Phillip B. Messersmith, **Haeshin Lee** Yuhan Lee "Substrate-independent polymer primers for la yer-by-layer and other coatings" US patent application filed
3. Phillip B. Messersmith, **Haeshin Lee** "Poly(dopamine) coating: versatile surface modification in spired by mussel adhesion" US patent application filed
4. Tae Gwan Park, **Haeshin Lee** "Conjugate of Epidermal Growth Factor and Poly(ethylene glycol)

and preparation methods", Korea patent No.550206, Feb 1, 2006

Publications

1. **Haeshin Lee**, Yuhan Lee, Andrea R. Statz, Junsung Rho, Tae Gwan Park, **Phillip B. Messersmith**. "Surface-independent Layer-by-Layer Assembly Using Mussel Adhesive Inspired Polymers" ***Adv. Mater.*** 2008 In press
2. **Haeshin Lee**, Shara M. Dellatore, William M. Miller, **Phillip B. Messersmith**. "Mussel-inspired Surface Chemistry for Multifunctional Coatings" ***Science*** 2007, 318, 426-430.
3. **Haeshin Lee**, Bruce P. Lee, **Phillip B. Messersmith**. "A reversible wet/dry adhesive inspired by mussel and gecko adhesion" ***Nature*** 2007, 448, 338-341. **(Cover Paper)**
4. **Haeshin Lee**, Norbert F. Scherer, **Phillip B. Messersmith**. "Single molecule mechanics of mussel adhesion" ***Proc. Natl. Acad. Sci. USA***. 2006, 103, 12999-13003.
5. Jason M. Zhao, **Haeshin Lee**, Rene Nome, Sophia Majid, Norbert F. Scherer, **Wouter D. Hoff**. "Single-molecule detection of structural change during PAS domain activation" ***Proc. Natl. Acad. Sci. USA***. 2006, 103, 11561-11566
6. Nathaniel D. Catron, **Haeshin Lee**, **Phillip B. Messersmith**. "Enhancement of poly(ethylene glycol) mucoadsorption by biomimetic endgroup functionalization" ***Biointerphases*** 2006, 1, 134-141
7. **Haeshin Lee**, Seung Ho Choi, **Tae Gwan Park**. "Direct visualization of hyaluronic acid polymer chain by self-assembled one-dimensional array of gold nanoparticles" ***Macromolecules*** 2006, 39, 23-25
8. **Haeshin Lee**, **Tae Gwan Park** "A novel method for identifying PEGylation sites using streptavidin and biotin interaction" ***J. Pharm. Sci***. 2003, 92, 97-103
9. Seung Ho Choi, **Haeshin Lee**, and **Tae Gwan Park** "PEGylation of G-CSF using cleavable oligo-lactic acid linkage" ***J. Controlled Rel***. 2003, 89, 271-284.
10. **Haeshin Lee**, Il Ho Chang, Sung Ho Ryo, **Tae Gwan Park** "N-terminal site-specific mono-PEGylation of Epidermal Growth Factor" ***Pharm. Res.*** 2003, 20, 818-825.
11. **Haeshin Lee**, **Tae Gwan Park** "Preparation and Characterization of PEGylated Epidermal Growth Factor: Evaluation of *In Vitro* Biological Activity" ***Pharm. Res***. 2002, 19, 845-851 **(Cover Paper)**.
12. **Haeshin Lee**, Tae Hyoung Kim, and **Tae Gwan Park** "Receptor-mediated Gene Delivery System Using Streptavidin and Biotin-derivatized and Pegylated Epidermal Growth Factor" ***J. Controlled Rel.*** 2002, 83, 109-119.
13. **Haeshin Lee**, Ji Hoon Jeong, **Tae Gwan Park** "PEG grafted polylysine with fusogenic peptide for gene delivery: high transfection efficiency with low cytotoxicity" ***J. Controlled Rel.*** 2002, 79, 283-291.
14. Tae Hyoung Kim, **Haeshin Lee**, **Tae Gwan Park** "PEGylated Recombinant Human Epidermal Growth Factor for Sustained Release from Biodegradable PLGA Microspheres" ***Biomaterials*** 2002, 23, 2311-2317.
15. **Haeshin Lee**, Ji Hoon Jeong, **Tae Gwan Park** "A New Gene Delivery Formulation of Polyethylenimine/DNA Complexes Coated with PEG Conjugated Fusogenic Peptide" ***J. Controlled Rel.*** 2001, 76, 183-192.
16. **Haeshin Lee**, Ji Hoon Jeong, Jee Hoon Lee, **Tae Gwan Park** "Enhancing Transfection Efficiency Using Polyethylene Glycol Grafted Polyethylenimine and Fusogenic Peptide" ***Biotech. & Bio process Eng.*** 2001, 6, 269-273.
17. Ji Hoon Jeong, Soon Ho Song, Dong Woo Lim, **Haeshin Lee**, **Tae Gwan Park** "DNA Transfection Using Linear Poly(ethylenimine) Prepared by Controlled Acid Hydrolysis of Poly(2-ethyl-2-oxazoline)" ***J. Controlled Rel.*** 2001, 73, 391-399.

18. **Haeshin Lee**, **Tae Gwan Park** "Conjugation of Trypsin by Temperature-Sensitive Polymer s Containing a Carbohydrate Moiety: Thermal Modulation of Enzyme Activity" ***Biotechnol. Pro g***. 1998, 14, 508-516.
19. **Haeshin Lee**, **Tae Gwan Park** "Reduction/Oxidation Induced Cleavable/Crosslinkable Temper ature-Sensitive Hydrogel Network Containing Disulfide Linkages" ***Polymer Journal*** 1998, 30, 9 76-980.

Manuscript in preparation and review

20. Yuhan Lee, **Haeshin Lee**, Taeghwan Hyeon, Phillip B. Messersmith, Tae Gwan Park "Bio-inspi red Surface Immobilization of Hyaluronic Acid on Monodisperse Magnetite Nanocrystals for Ta rgeted Cancer Imaging" Submitted to *Angew. Chem. Int. Ed*.
21. **Haeshin Lee,** Junsung Rho, Kyle Holmberg, Phillip B. Messersmith "Mussel-inspired preparatio n of non-hydrolyzable, reactive surfaces for bioconjugation" Manuscript in preparation
22. Joseph R. Knab, **Haeshin Lee**, Wouter D. Hoff, Andrea G. Markelz "Changes in picosecond dyn amics during protein photocycling" Manuscript in preparation

Research Areas

Bio-inspired Materials and Interfaces

Mussel Adhesive Protein

- Development of new biomedical wet-resistant adhesives
- Developing material-independent (marine) surface chemistry

Gecko Adhesive

- Development of reversible nanoadhesives using nano-fabrication techniques
- Protein Biochemistry and Biophysics.

Single-molecule Biophysics

- Single molecule force measurement using Atomic Force Microscopy (AFM)

Protein folding

- Structural dynamics study of photoactive yellow protein (PYP).

Drug Delivery Systems

PEGylation of Therapeutic Proteins

- Protein-PEGylation (rhEGF, G-CSF, and Interferon)

Mucoadhesive polymer development

Polymeric gene delivery carriers and microsphere formulations

- Fusogenic peptides and polyethylene glycol (PEG).
- Formulation of PLGA microspheres.

Protein conjugations and hydrogels for protein delivery

- Development of a novel glycoconjugated activity-modulated enzyme.
- Design a cleavable/crosslinkable temperature-sensitive hydrogel.

Media Interviews and Highlights (selected from total 35 medial exposures)

1. Super sticky coating has 'mussel' (by Tracy Staedter) **Discovery Channel**, Oct. 18th, 2007, http://dsc.discovery.com/news/2007/10/18/glue-mussel-sticky.html
2. Mussels mighty grip inspires dopamine-based glue (by John Roach) **National Geographic News**. Oct. 18th, 2007, http://news.nationalgeographic.com/news/2007/10/071018-mussels-stick.html
3. Tree frog inspires new easy-off stickies. (by JR Minkel), **Scientific American**, Oct. 11th, 2007 http://www.sciam.com/article.cfm?chanId=sa003&articleId=913F4091-E7F2-99DF-319205DF5501B1CC&modsrc=latest_news
4. Design by gecko, glue by mussel, yield a powerful adhesive. (by Kenneth Chang) **New York Times**. July, 24th, 2007. http://www.nytimes.com/2007/07/24/science/24geck.html?_r=1&ref=science&oref=slogin
5. Gecko, mussel powers combined in new sticky adhesive **National Geographic News**. (by John Roach), July 18th, 2007 http://news.nationalgeographic.com/news/2007/07/070718-geckel-glue.html
6. Scientists design new superadhesive called 'geckel' **CBC news**, July 19th, 2007. http://www.cbc.ca/technology/story/2007/07/19/geckel.html
7. Geckos inspire a new breed of glue, **MSNBC**, July 18th, 2007 http://www.msnbc.msn.com/id/19832570/
8. Gecko glue comes with mussel power, **The Times**, July 19, 2007 (by Mark Henderson), http://www.timesonline.co.uk/tol/news/uk/science/article2100023.ece
9. Gecko glue exploits mussel power, **BBC News**, July 18, 2007, (by Jonathan Fildes), http://news.bbc.co.uk/2/hi/science/nature/6904175.stm
10. Animal adaptations inspire possible wound-care method, **Chicago Tribune**, July 30, 2007, (by Jon Van). http://www.chicagotribune.com/business/chi-mon_notebook_0730jul30,0,1483365.story
11. Physorg.com, http://www.physorg.com/news103980911.html & Nanotechweb.org, http://nanotechweb.org/articles/news/6/7/19/1
12. (Korea Media) [New Technology] Sticky Things, (by Young-Wan Lee), **Chosun**, 2007, July, 18th, http://news.chosun.com/site/data/html_dir/2007/07/18/2007071801656.html
13. (Korea Media) Strong Holdfast of Mussel Adhesion,(by Young-Wan Lee), **Chosun**, 2006, Aug. 31th, http://news.chosun.com/site/data/html_dir/2006/08/31/2006083170025.html
14. Unlocking the secrets of stickiness, (by Carolyn Y. Johnson), **Boston Globe**, Aug. 28th, 2006.
15. Mussel power makes better glue, (by Hannah Devlin), **The Times**, Aug, 15th, 2006.
16. Revealed: the secrets of mussels' superglue, (by Anna Gosline), **New Scientist**, Aug, 14th, 2006 (http://www.newscientist.com/article/dn9742-revealed-the-secrets-of-)

Highlights in peer-review journals (selected)

17. Mussel muscle, (by Andrew Mitchinson), **Nature**, 2006, 442, 877 (highlighted publication #4)
18. Mussel power, (by Constance Holden), **Science**, 2006, 313, 1025 (highlighted publication #4)
19. Natural stickness inspires synthetic solutions, **Materials Today**, 2007, 10, 15 (highlighted publication #1)
20. Mussel power **Nature Materials**, 2008, 7, 8-9 (highlighted the publication #1)

Conference Presentation

1. Haeshin Lee, Phillip B. Messersmith. "Geckel: A dry/wet adhesive inspired by mussel and gecko adhesion" Oral presentation, Material Research Society Meeting. Boston, Nov., 2007
2. Haeshin Lee, Phillip B. Messersmith. "Geckel: A dry/wet adhesive inspired by mussel and gecko adhesion" Self-Assembling Peptide Systems Workshop. Crete, Greece. July, 2007
3. Haeshin Lee, Phillip B. Messersmith. "DOPAminylation: versatile mussel-inspired surface modif ication chemistry" Material Research Society Meeting. San Francisco. April, 2007
4. Haeshin Lee, Phillip B. Messersmith. "Dry/Wet nanoadhesive inspired by mussel and gecko adhe sion" Oral presentation, ACS annual meeting, Chicago, March, 2007
5. Haeshin Lee, Nathaniel D. Catron, Phillip B. Messersmith. "Biomimetic end-group functionalizat ion for mucoadhesive polymers" 13th International Symposium on Recent Advances in Drug Deli very Systems. Utah, Feb. 2007
6. Haeshin Lee, Phillip B. Messersmith. "DOPAminylation: versatile mussel-inspired surface modif ication chemistry" Gordon Research Conference (Biointerfaces), Les Diableret, Switzerland, Oct ober, 2006
7. Haeshin Lee, Phillip B. Messersmith. "Single molecule mussel mechanics: probing iron-DOPA i nteractions" Material Research Society Meeting. San Francisco. April, 2006
8. Haeshin Lee, Norbert F. Scherer, Phillip B. Messersmith. Organic Thin film Gordon Research C onference July, 2005
9. Haeshin Lee, Phillip B. Messersmith. "Probing interfacial roles of DOPA" Society for Biomateri als Meeting, Memphis, 2005
10. Haeshin Lee, Phillip B. Merrersmith. "Single molecule force measurement of DOPA" Material R esearch Society Meeting. Boston. November, 2004
11. Haeshin Lee, Wouter D. Hoff "apo Photoactive Yellow Protein: a molten globule with an active s ite for chromophore attachment" *Biophys. J*. Sup. 84, 340a, 2003.
12. Haeshin Lee, Tae Gwan Park "Preparation and characterization of mono-PEGylated epidermal gr owth factor: evaluation of *in vitro* biological activity" Proceedings of the 29th International Sym posium on Controlled Release of Bioactive Materials, Seoul, Korea, July 2002. Oral Presentation No. 183.
13. Haeshin Lee, Tae Hyoung Kim, Tae Gwan Park "Receptor-mediated gene delivery system using streptavidin and biotin-derivatized and PEGylated epidermal growth factor" Proceedings of the 2 9th International Symposium on Controlled Release of Bioactive Materials, Seoul, Korea. June 2 002. Poster presentation No. 752.
14. Hong Ki Kim, Haeshin Lee, Tae Gwan Park "Chracterization of acylated human growth hormon e by degradation produces of microspheres" Proceedings of the 29th International Symposium on Controlled Release of Bioactive Materials, Seoul, Korea. June 2002. Poster presentation.
15. Haeshin Lee, Ji Hoon Jeong, and Tae Gwan Park "A new formulation approach of PEG grafted polylysine with fusogenic peptide for gene delivery" Proceedings of the 28th International Symp osium on Controlled Release of Bioactive Materials, San Diego, California, USA June 2001. Post er presentation.
16. Haeshin Lee, Ji Hoon Jeong, and Tae Gwan Park "A new formulation approach of cationic poly meric gene delivery system" 10th International Symposium on Recent Advances in Drug Deliver y Systems, Utah, USA. February 2001. Abstracts, p166
17. Ji Hoon Jeong, Soon Ho Song, Dong Woo Lim, Haeshin Lee and Tae Gwan Park "DNA Transfe ction Using Linear Poly(ethylenimine) Prepared by Controlled Acid Hydrolysis of Poly(2-ethyl-2-oxazoline)" 10th International Symposium on Recent Advances in Drug Delivery Systems, Uta h, USA. February 2001. Abstracts, p168

18. Haeshin Lee, Tae Hyoung Kim, Tae Gwan Park "Receptor-mediated Gene Delivery System Using Streptavidin and Biotin-derivatized and Pegylated Epidermal Growth Factor" KAIST-TIT joint symposium for young scientists. KAIST, Taejon. September 5, 2001. Abstract No. 12.